New insights into the nanoscaled structure of stratum corneum lipid model membranes applying specifically deuterated lipids in neutron diffraction studies

DISSERTATION

zur Erlangung des

Doktorgrades der Naturwissenschaften (Dr. rer. nat.)

der

Naturwissenschaftlichen Fakultät I – Biowissenschaften

der Martin-Luther-Universität

Halle-Wittenberg,

vorgelegt

von

Frau Adina Eichner

Durchgeführt am:	Institut für Pharmazie, Arbeitsgruppe Biopharmazie, Martin-Luther-Universität Halle-Wittenberg, Halle, Deutschland
Gutachter:	**Prof. Dr. Dr. h.c. Reinhard Neubert**, Institut für angewandte Dermatopharmazie, Aninstitut der Martin-Luther-Universität Halle-Wittenberg, Halle, Deutschland
Zweitgutachter:	**Prof. Dr. Bodo Dobner**, Institut für Pharmazie, Martin-Luther-Universität Halle-Wittenberg, Halle, Deutschland
Drittgutachter:	**Prof. Dr. Gerald Brezesinski**, Max-Planck-Institut für Kolloid- und Grenzflächenforschung, Potsdam, Deutschland

Halle (Saale), 24.08.2017

Tag der Verteidigung: 29.11.2017

For my life and my love

TABLE OF CONTENTS

p.

FIGURE INDEX

INDEX OF TABLES

ABBREVIATIONS AND SYMBOLS

Å	Angstrom; 1 Å = 0.1 nm
a.u.	arbitrary units
BA	behenic acid
b_{coh}	coherent neutron scattering length
CER	ceramide
CER[AP]-C18	ceramide N-(α-hydroxyoctadecanoyl)-phytosphingosine
CER[AP]-C18-d_3	ceramide N-(α-hydroxyoctadecanoyl)-phytosphingosine-C18 with three terminal ^{1}H/*d* exchanges
CER[EOSl	ceramide ω-hydroxy sphingosine esterified with linoleic acid
CER[EOS]-br	ceramide ω-hydroxy sphingosine esterified with C10-methyl- branched palmitic acid
CER[EOS]-d_3	ceramide ω-hydroxy sphingosine esterified with C10-methyl-branched palmitic acid with three deuterium labels at C10 methyl group
CHOL	cholesterol
ChS	cholesterol sulfate
°C	degree centigrade
d/^{2}H	deuterium
d	d spacing (lamellar repeat distance), Å
Equ.	equation
F_h	structure factor, SF
FFA	free fatty acid
Fig.	figure
FWHM	full width at half maximum
h	lamellar order
h	Planck constant
^{1}H	hydrogen
HZB	Helmholtz-Zentrum für Materialien und Energie Berlin, Germany
IPM	isopropyl myristate
IPM-d_3	isopropyl myristate with three terminal ^{1}H/*d* exchanges
IR	infrared spectrometry
K	Kelvin
LPP	long-periodicity phase
MLZ	Heinz Meier-Leibnitz Zentrum, Garching, Germany
MW	mega watt
MD	molecular dynamics
NSLD	neutron scattering length density
ω	omega
p.	page
PA	palmitic acid
%	percent
PMT	photomultiplier counts
RH	relative humidity, %
SANS	small-angle neutron scattering
SAXS	small-angle X-ray scattering

SC	stratum corneum
SF	structure factor, F_h
SPP	short-periodicity phase
θ	theta; scattering angle, °
T	temperature, °C
Tbl.	table
TEWL	trans-epidermal water loss
u	atomic units
(V/V)	volume ratio, %
wt%	mass ratio, %

1 INTRODUCTION

The stratum corneum (SC) represents the outermost layer of mammalian skin and exhibits the main protection barrier [1]. Simultaneously, the skin represents a great opportunity as it offers a large surface to which substances can be applied. For therapeutic or cosmetic reasons it is often necessary to overcome its protecting layer. Since the barrier function is attributed to the intercellular lipids, which form continuous multilamellar organized membranes, surrounding dead cornified cells (corneocytes) [2], it is indispensable to expand the knowledge of the lipid arrangement on a molecular level and identify the high-ordered structure. As a consequence, the ratio between therapeutic substance transfer and intact SC barrier function could be optimized.

The major lipid classes extracted from the SC lipid matrix are ceramides (CER), cholesterol (CHOL), and free fatty acids (FFA) [2-4]. The very heterogeneous group of the CER is known to play a fundamental role for the structural arrangement as well as for the maintenance of the skin barrier function [5]. Due to their immense influence on the SC lipid structure, ceramides are the point of interest in many studies concerning their quantitative ratios in native material [6-10] and their molecular arrangement [11-13].

A special feature for investigations in the field of structural SC lipid arrangements is represented by neutron diffraction experiments. They offer a wide range of advantages over X-rays, e.g. their deep interactions with biological materials or their varying coherent scattering lengths for deuterium (^{2}H) and hydrogen (^{1}H) [14-17]. Therefore, neutron diffraction is a versatile technique in order to investigate SC lipid lamellae as performed before in numerous works [18-24]. The application of SC lipid model membranes is essential because native lipid mixtures are very heterogeneous and consequently too complex to receive detailed information about the single lipid arrangement. Especially, deuterated lipids enable the determination of their position within the membranes in these experiments due to a H/D exchange.

Furthermore, there are two lamellar phases described, in which the SC lipids can be assembled, differing in their unit cell scale. In detail, a short-periodicity phase (SPP) with an approximated distance of 60 Å and a long-periodicity phase (LPP) with a repeat interval of 130 Å were described in native material [25-27]. Whereas the SPP is known to be dependent on long-chain CERs as [AP] or [NP] [28, 29], the LPP presence is highly related to the appearance of ultra-long-chain CERs as [EOS] or [EOH] [30-35]. As the SPP is well defined by neutron diffraction studies on SC lipid model membranes [21, 28], its longer pendant is still in focus of discussion [12, 19, 22, 36-38].

In the present work, for the first time the specifically labelled CER[AP]-C18 and a methyl-branched CER[EOS] variant were applied for closer insights into the nanoscaled structure of SC lipid model membranes. Therefore, SC lipid model membranes were prepared, containing one or two CER species besides cholesterol and a free fatty acid. Beginning with CER[AP]-C18, a well-known SC lipid model membrane [39] was investigated under the usage of the partially deuterated CER variation. Furthermore, in chapter 4.1 the position of the long-chain CER within the lipid lamellae was determined. In a second approach (see chapter 4.2), the methyl-branched variation of ultra-long-chain CER[EOS] was applied in addition to CER[AP]-C18. Moreover, the effect of the lipophilic penetration enhancer isopropyl myristate (IPM) on the LPP forming SC lipid model membrane was investigated in chapter 4.3 as well as the thermotropic phase behavior of the lipid matrix.

A discussion of the received results is presented in chapter 5, together with an outlook and perspectives which arose from this thesis. A final summary will conclude this work (see chapter 6).

2 BASIC PRINCIPLES AND FUNDAMENTAL CONCEPTS

This chapter includes the theoretical background of the thesis and explains basic concepts. First of all, information about the human skin and its structure will be addressed, followed by more detailed implementations relating to the SC and its composition.

Later on, the chosen technique of neutron scattering and the respective data treatment, that was used to obtain the presented results, will the described.

2.1 The mammalian skin

The skin, with a total surface of about 1.5- 2 m^2, is the largest and most functional organ of human beings. Due to its complex structure, it delimits the body to external as well as internal influences and signals. Equally, it serves as multifunctional interface between the body and its environment. Its natural structure enables a classification in several layers with different thicknesses and characteristic properties for the body´s balanced supply. Apart from this, due to the evaporation or sweating of water, the skin is highly involved in the regulation of temperature and water economy.

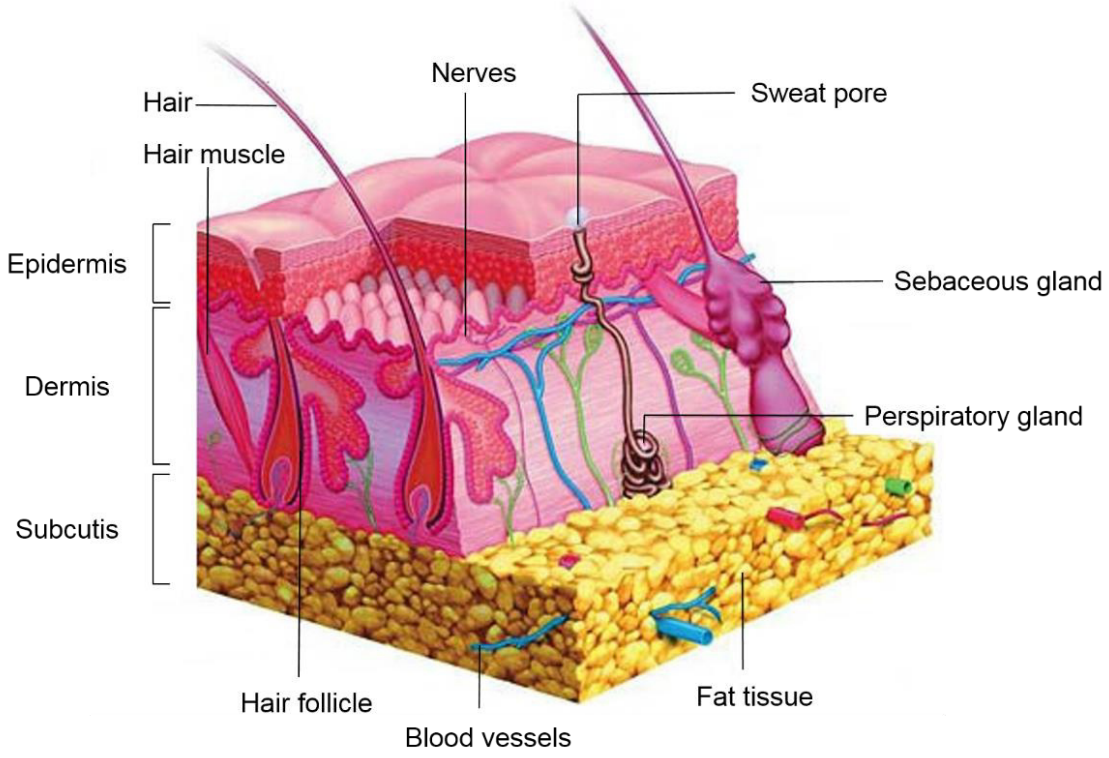

Fig. (1): The human skin. A schematic cross section is presented, adapted and modified from [40].

As Fig. (1) indicates, the skin is classified in epidermis, dermis and subcutis, as its main parts, which structures are highly differentiated. The subcutis, for example, is the fat storage and

accommodative part. Its function is described as isolating, pressure protecting and energy reserve, based on the fat depot [41]. The dermis is the largest layer and mostly represented by protein structures interfused by smaller blood vessels. Here, the endings of nerves and skin appendices, as hair muscles and follicles, sebaceous glands or perspiratory glands are located. The high number of several proteins realizes the dermis stability and simultaneously its elasticity [42, 43]. In detail, these are fibroblasts or structure proteins, like collagen and elastin [44]. The third main layer is the epidermis, which is itself split up into several strati, in detail: stratum basale, stratum spinosum, stratum granulosum and the outermost one, the stratum corneum (SC). The epidermis is mostly represented by cells, called keratinocytes, which develop and differentiate during their passage through the epidermis. Their division starts in the stratum basale, their further formation happens in the stratum spinosum and granulosum and finally their dying and flattening in the SC. Reaching the SC, these cell bodies are named as corneocytes or horny cells, consisting of the structure protein keratin.

After the basic facts corresponding to the skin structure, a more detailed view to its uppermost layer is mandatory in order to explain the structure-function relationship of the SC components.

2.1.1 The SC and its function as penetration barrier

The unique structure of the SC is known to play the fundamental role in the proper barrier function of mammalian skin [45]. Thereby, the SC thickness differs depending on the place of sampling mainly from ten to 20 µm [46].

Corresponding to first ideas, in 1983 Elias presented his vision of the SC structure as “Brick and Mortar Model“ [2]. In that conception, the SC is built as a brick wall with keratin-filled corneocytes (“bricks”), which are embedded into a complex lipid matrix (“mortar”). In total, a number of 15-30 cell layers is described [46-50], being twice as much as the living epidermis [47]. This is explainable due to the substantial smaller volume of the dead flattened corneocytes compared to the cells in the layers beneath. In their final formation, corneocytes are surrounded by the so-called cornified envelope (CE) [51, 52], a cross-linked protein covering, to which some ceramides are covalently linked forming a monolayer. The horny cells themselves are connected by corneodesmosomes, which increase the stability of the SC substantially [53] (see Fig. (2)).

In general, there are two pathways known for the penetration of substances: transepidermal and transappendageal [54]. Thereby the latter plays only a minor role, due to the small surface and number of glands (transglandular) and hair follicles (transfollicular) compared to the complete epidermal area [55]. Consequently, most of the agents directly overcome the epidermis. Here, it can be differentiated between the way across the “bricks and mortar”, the

so-called transcellular route and the intercellular pathway along the lipid matrix [56, 57] (see Fig. (2)).

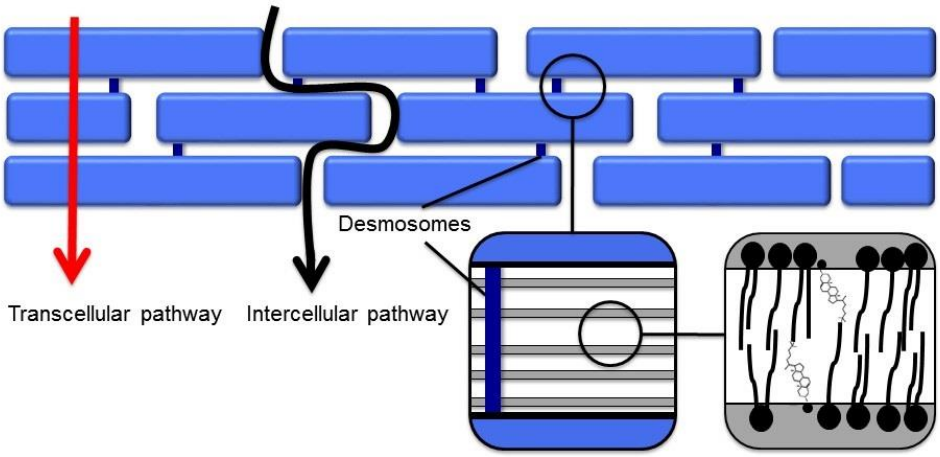

Fig. (2): The human SC, adapted from [58]. The corneocytes (blue "bricks") are surrounded by the white lipid "mortar", which is arranged in multilamellar layers. Both main penetration routes are given. For the transcellular pathway (red) substances need to overcome cells and lipid layers. Substances, which prefer the intercellular route (black), penetrate across the lipid route.

The quantitative substance transfer across the transcellular route is highly limited due to the alternating lipophilic (mortar) and hydrophilic (protein structure of corneocytes and cornified envelope) areas. Therefore, the preferred pathway is represented by the intercellular route [56, 59]. However, the SC barrier function is highly connected to the lipid domains [60]. Thus, it is not surprising, that the penetration rate across the SC is rather small, as the favorite pathway represents the main barrier properties as well.

As direct interface between the human body and its environment, the SC protection properties against external influences also include the prevention of dehydration [61]. The mechanism is described as a hydrogen bond network between water and the hydroxy groups of the present sphingolipids [62], which minimizes the trans-epidermal water loss (TEWL).

2.1.2 SC lipids and their molecular structure

The SC lipids form continuous membranes (see Fig. (2)), varying by their intra- and interindividual composition [63]. The multilamellar system is built in the stratum granulosum, where lamellar bodies are modeled in multilayered stacks [52, 64]. At the central interface to the SC, the exocytosis of the lamellar bodies enables the formation of the crystalline lamellar structures parallel to the skin surface [65, 66]. The SC lipid compounds are mainly free fatty acids, cholesterol, and the very heterogeneous group of ceramides in a nearly equimolar ratio [5, 67, 68].

Ceramides

The group of CERs generates the main part of the matrix ingredients [63, 69, 70]. However, depending on the investigated native skin areas, possible morbidity and the analytical methods, the CER ratio in several studies differs between 13.6 and 70.0 wt%. [71, 72].

CERs consist of a polar head group region (blue circle) and elongated hydrophobic alkyl chains, as presented in Fig. (3):

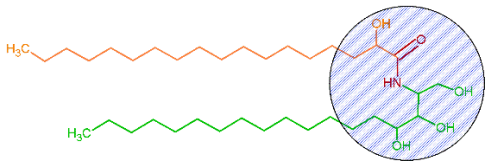

Fig. (3): CER[AP]-C18 as an CER example. In general, a sphingoid base (green) is amide linked (red) to a fatty acid (orange).

In total, an immense amount of 342 individual CER compounds was lately described [73]. To this day, a classification into 19 classes was suggested involving all subspecies [73-76] as shown in Fig. (4). The high number of subclasses is predicated on the five described N-acylated sphingoid bases as well as on the high number of present fatty acids. Thus, a unique name system was necessary to differentiate between CER subclasses. In the beginning, there was a numbering system, first relating to the chromatographic retention of the CERs (CER 1-8) [77] and afterwards, based on their chronological publication (CER 9-12) [78]. Later on in 1993, Motta et al. developed a letter nomenclature system [79], which was further complemented by Robson [80], t´ Kindt [76] and Rabionet [75].

Implementing a minimum two letter code, typical chemical CER characteristics are included, whereby the first letter stands for the present fatty acid, i.e. **A** for an **α**-hydroxy fatty acid and **N** indicates a **n**on-hydroxy fatty acid. A further letter was added for **e**sterified fatty acids (**E**). The corresponding sphingoid bases phytosphingosine (**P**), sphingosine (**S**), dihydrosphingosin (**DS**), 6-hydroxy-sphingosine (**H**), and dihydroxy-dihydrosphingosine (**T**), as the latest detection [76], are then added as the last letter. But it has to be pointed out, that t´Kindt and co-workers, who described the **T**-base for the first time, were not able to determine the exact positions of both additional hydroxy groups to this day. Furthermore, CER[ODS] was not yet detected but proposed in the literature [76].

Within the total number of different CER subclasses, another differentiation between free and bounded CERs is possible. The latter are covalently linked to the insoluble protein structures of the cornified envelope via their **o**mega-positioned hydroxy fatty acid (**O**), which is simultaneously the binding site for esterification in ultra-long-chain CERs [52].

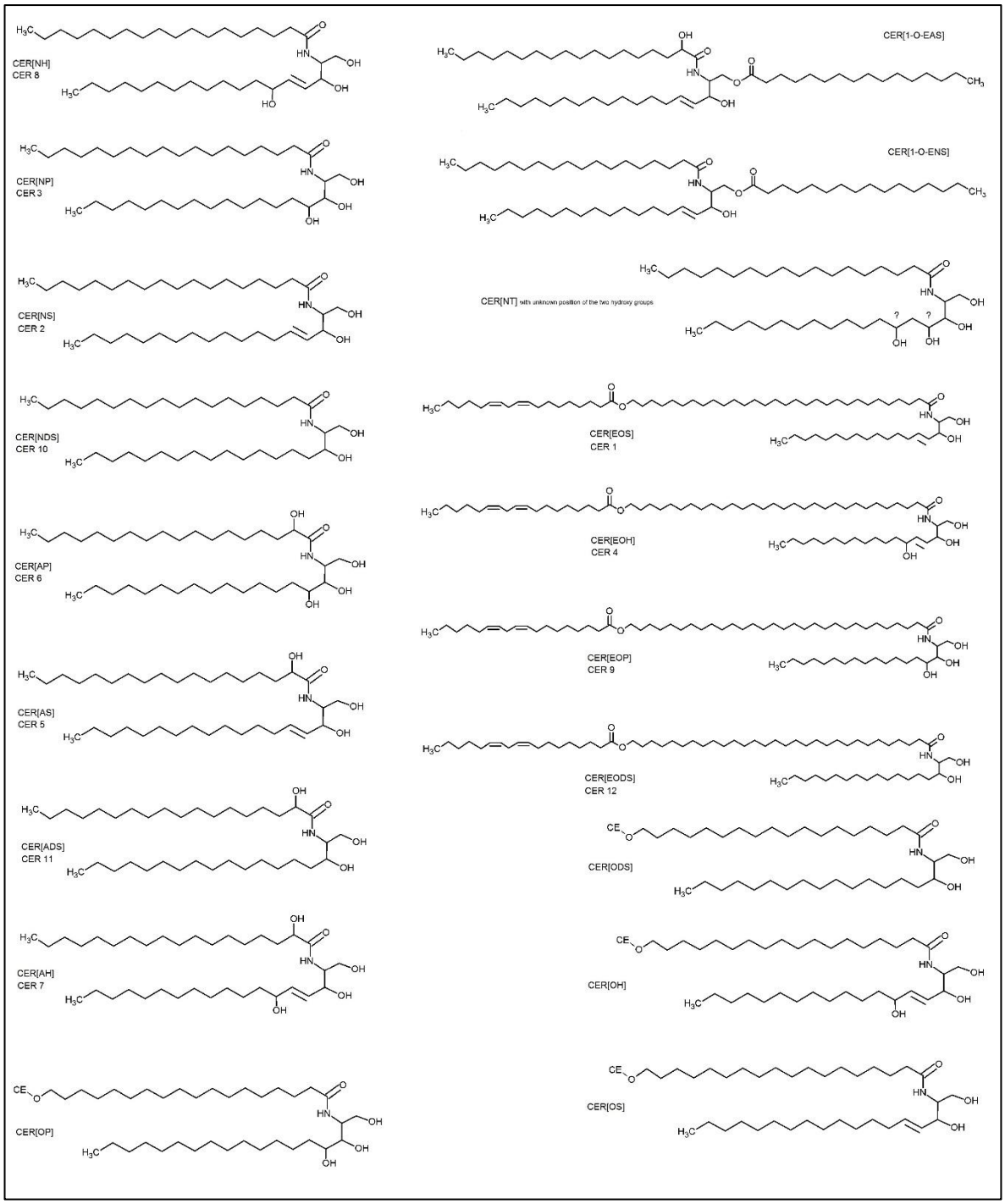

Fig. (4): Presentation of all known native CER species to this day. In addition to the letter code, the numbers of the CER species are given.

In addition to the kind of sphingoid bases and amide-linked fatty acids, the alkyl chain lengths of the CERs vary between C18-C22 or C18-C26 [68, 81]. Longer chain lengths correspond to esterified ω-acyl CER species, as CER[EOS] or [EODS], where the number of carbon atoms of the ultra-long N-acyl chains is mostly between 30 and 32 [68, 73, 81]. Effects of the chain length to the physiological state of the SC were found by Mojumdar et al., who described a reduced barrier function due to decreasing chain length distributions [82].

The CERs, which were applied within this thesis, are the synthetically derived long-chain CER[AP]-C18 and a modified CER variant based on ultra-long-chain ω-acyl CER[EOS]-C30-C18:2. In native SC, CER[AP] is available with about 8.8 wt% [76]. Former neutron diffraction studies revealed its key role in the assembling process of SC model membranes [19, 20, 39]. For this thesis, the long-chain CER variant with a defined chain length of 18 carbon atoms was chosen, in order to confirm the results to former neutron diffraction studies [38, 39]. With 6.5 wt%, native CER[EOS] is the most prevalent ultra-long-chain CER species [76]. It is described to be mandatory for the SC barrier function [83]. This is in accordance with several diseases, where the skin protection shield is decreased [84, 85]. For example in psoriasis, the CER[EOS] level can decline about 40 % [79]. Furthermore, this ultra-long-chain CER is discussed to be indispensable for the body´s water retention [85] and for the SC lipid organization as well [32, 86, 87]. The ultra-long-chain CER[EOS] variant, applied in the presented experiments, is called CER[EOS]-br. There, the saturated palmitic acid was esterified. It had a methyl-branching at C10, which facilitated the deuterium insertion at this position and thus, enabled the comparison to a former experiment on that topic [38].

Cholesterol

Cholesterol is one of the most present sterols in biological membranes and in native SC, it is even the only one [88]. On average, a cholesterol amount of 25 wt% to 32 wt% is described [69, 89]. But, concerning abnormal variations of native skin, the amount of cholesterol can vary between 13.1 wt% and 37.5 wt% [90, 91]. Its special constitution, with the four voluminous cycloalkane rings and the small polar head, realized by a hydroxy group, generates only a marginal head-to-tail polarity. In the lipid multilayers, the ring system is located in the lipophilic area and the head group within the polar region [18, 92]. The necessity of CHOL for the lamellar arrangement and a proper barrier function was described before [93, 94] and moreover, there is a minimum level, which is required for the CER arrangement (*unpublished data*; [95]). Further experiments, based on molecular dynamic (MD) simulations, could figure out its smoothing effect on the rigid and highly ordered bilayers of FFA [96]. In a comparable way, the influence of this sterol on the membrane thickness is discussed: SAXS and SANS studies demonstrated a decreasing d spacing with an increasing content of CHOL [97]. This was discussed as a rising tilting or disordering effect of CHOL on the alkyl chains of the CER[AP] based SC model system.

In the systems probed within this thesis, the surplus percentage of CHOL, which could not be integrated into the membranes, is visible as separated crystalline cholesterol peak. But its presence is neither affecting the d spacing of the lamellar structures [98] nor the performed data treatment.

Free fatty acids

The total amount of fatty acids can vary between 17.0 wt%. and 64.1 wt%. in healthy, but different areas of human skin [71, 99]. On average, a ratio of 20 wt%. is supposed [70]. Most of the FFAs are saturated and have more than 18 carbon atoms [100]. The most abundant chain lengths are between C24-C28 [70, 76, 81, 101]. Compared to CERs, the FFAs can arrange themselves in nonflexible multilayers without any support by CHOL. That can be explained by their single alkyl chain connected to the small hydrophilic head group. Therefore, their assembling process is very fast and the resulting structure is highly ordered [59]. Corresponding to earlier studies, in the present thesis together with CER[AP]-C18 stearic acid (SA) was chosen for a chain lengths match [39]. In the SC lipid model membranes containing CER[EOS]-br, behenic acid (BA) was selected [19, 38].

2.1.3 SC lipid model systems and the presence of SPP and LPP

Since the description of the main components of the very thin SC, an important question is, how the lipids in between the corneocytes are arranged in order to get more detailed information related to its efficient barrier properties. In 1973, for the first time lamellar phases were described in human SC [102]. Later on, also using an electron microscopy technique, Madison et al. were able to determine a lamellar phase with a repeat distance of 130 Å [25, 103]. These first discoveries were verified by X-ray scattering studies, where comparable spacings were found in human [27] as well as in murine [26, 104] and porcine SC [105]. Simultaneously, Bouwstra et al. presented the lipid arrangement in this large unit cell, referred to as long-periodicity phase (LPP) [27]. They implemented a three-lipid layer unit cell, interrupted by polar head group regions [106]. Thereby, the larger outer lipid areas (~ 46 Å) are supposed to be predominately crystalline and the smaller inner one (~ 24 Å) is more liquid [107]. This model is known as ´sandwich model´ [106, 108]. However, within the large unit cell, other sublattice spacings were discussed as well [34, 108-110]. The latest of these model ideas, the ´asymmetry model` was introduced by the group of Norlén [110]. There, the stacked lipid bilayers were mainly constituted by *fully extended* ceramides, which could be the main reason for the SC barrier properties, as the authors suggested. In detail, repeat distances of about 110 Å were found with two sublattice spacings of 45 Å and 65 Å.

Although a LPP was also detected in other human structures, like vernix caseosa [111], its presence in SC lipid models is still a matter of debate. Numerous studies were focused on SC lipid models, which simplified the complex native mixture and enabled the determination of single influences of each lipid subspecies to the membrane assembling process. For example, the role of the ultra-long-chain ω-acyl CERs, as CER[EOS], and their impact to the LPP appearance as well as to the barrier function were proven [30, 32, 34]. Even a direct

dependence of the CER[EOS] level to the LPP formation was verified [112, 113]. Furthermore, the kind of the esterified ω-acyl fatty acid of the ultra-long-chain CERs has an influence on the LPP formation. Since the unsaturated oleic and linoleic acid esterified in CER[EOS] causes a LPP, a CER[EOS] variation esterified with steric acid could not show comparable results [11]. However, CER[EOS] is not able to form a LPP on its own, as Groen et al. figured out the necessary stabilizing effect of cholesterol for that purpose [37]. Additionally, Kessner et al. could establish that CER[EOS] forms a LPP only under high humidity, while the ultra-long-chain CER of the phytosphingosine type was not able to act simultaneously [12]. Comparable results were received due to an exchange of CER[EOS] by CER[EOP in a SC lipid model system, where the LPP assembly was highly supported by the sphingosine type, but not by the phytosphingosine [114]. Recent neutron diffraction studies of the group of Bouwstra on SC lipid model membranes were able to determine the LPP in model membranes for the first time using perdeuterated molecules. Besides CER[NS], CHOL, and lignoceric acid even CER[EOS] was localized within the large unit cell [36, 115]. In contrast to that, former neutron diffraction studies of our group were not able to detect a LPP neither under the presence of CER[EOS] [19] nor a methyl-branched CER[EOS] variation [38]. These experiments revealed only the presence of the shorter pendant of the LPP, referred to as short periodicity phase (SPP).

The SPP was described and verified in numerous neutron diffraction studies in SC lipid model membranes [18, 39, 92, 116]. Especially, the influence of long-chain ceramides as CER[AP] and CER[NP] to the lipid assembling procedure in a SPP was the point of interest in several works [21, 28, 118]. But due to the selected CER chain length distribution (e.g. C18 to C24) often a shorter unit cell scale was received than described in native SC. However, experiments on human [27] and mouse SC [119] revealed a repeat distance of approximately 60 Å for the coexisting SPP. Fig.(5) and Fig. (6) show sketches of the lipid arrangement within both unit cells.

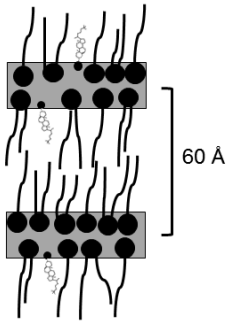

Fig. (5): Scheme of a SPP with a spacing of ~60 Å. A possible arrangement under the presence of long- chain CERs, FFA and CHOL is presented [18, 21, 92, 116, 117].

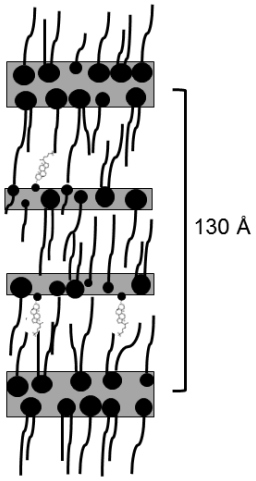

Fig. (6): Scheme of a LPP with a spacing of ~130 Å. A possible arrangement of FFA and CHOL under the presence of long-chain and ultra-long-chain CERs is presented. Compared to the SPP, a three-layer unit cell is described [36, 106, 115].

Till now, the exact localization of long-chain CER[AP] within the SPP could not be ascertained. But there were first results concerning CER[NS]-C24, received in a neutron diffraction study [117]. The authors determined the CER subspecies with both alkyl chains directed towards the center of the symmetric membrane, as presented in Fig. (5). This conformational state is referred to as *hairpin* conformation. Its counterpart, with both alkyl chains pointing in opposite directions, is called *fully extended* version (see Fig. (7)).

CERs are able to change between their typical conformations [120], which is an important property for the integrity of the lipid membrane and its barrier function. Kiselev et al. verified, that this so-called *chain flip* is mainly depending on the water content of the lipids [23]. For CER[AP]-C18 they proved under high hydration the *hairpin* conformation as energetically more stable. Moreover, the chain length of the ceramides seems to be a regulating factor as well. As Školová et al. demonstrated, a CER[NS]-C24 variation was present in its splayed conformation, whereas the shorter CER[NS]-C16 became apparent as *hairpin* version [121]. The authors explained the contradictorily outcomes compared to the former study on CER[NS]-C24 [117] as limiting effect of neutron diffraction experiments. Due to the alternating directions of the CER, the average neutron scattering length density (NSLD) profile would be the same for a centrosymmetric and asymmetric arrangement within the SPP unit.

Fig. (7): The conformational states of ceramides. The left picture presents the *fully extended* version. In the middle, the *hairpin* conformation is given, next to the V-shaped state on the right hand side [24, 120].

A third conformational state is referred to as V-shape [122], which was observed in SPP forming SC lipid model membranes containing single CER component [AP] [24] and in mixture with CER[NP] [28, 118]. A recent study figured out, that CER[AP]-C18 prefers the V-shaped conformation at high temperatures [123]. However, it is not discussed, which enantiomer of the applied racemic mixture could be responsible for that finding. This is of high importance, as only the D-form is existing in native SC and for both enantiomers, different properties, e.g. concerning their phase behavior, their favorite conformational state, or their chromatographic retention are known [124].

2.2 Cosmetically relevant penetration accelerator IPM

In cutaneous formulations with therapeutic or cosmetic relevance, active ingredients have to overcome the SC barrier to have their intended effects. If their own chemical properties impede the passage through the SC, additives are applied for an optimized substance flux. Hydrophilic penetration enhancers such as urea and taurine [125] as well as lipophilic ones such as oleic acid (OA) and isopropyl myristate (IPM) [126-129] were checked lately for that purpose. Especially lipophilic penetration enhancers are known to interact with the present lipids and produce a decreased lamellar order. As a consequence, the penetration of active ingredients along the intercellular pathway is facilitated.

However, the exact mode of action of penetration enhancers is still a matter of discussion. In particular, the liquid wax IPM was focused in numerous studies with varying outcomes. This may be reasoned in the chemical structure of the molecule with an ester group next to a short branched and a longer extended alkyl chain (see Fig. (8)).

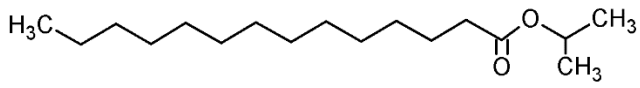

Fig. (8): The chemical structure of IPM. Myristic acid is esterified with isopropanol.

Compared to other lipophilic molecules, there is no clear head-to-tail polarity, due to the non-polar parts which frame the small polar group. This is of high profit for the molecule function as enhancer. While the lipophilic part interacts with the alkyl chains of the SC lipid membranes [130], the ester group was localized in the polar areas of the bilayer [131], stabilizing the molecule. This was also proven in an earlier neutron diffraction study on a SC lipid model membrane based on CER[AP] [132]. Additionally, Engelbrecht et al., even described a complete incorporation of partially deuterated IPM inside the bilayer. Especially, its minimal head-to-tail polarity was meant to be the reason for this phenomenon.

However, the effects of IPM to the lipid lamellae are ambivalent: The intensive interaction between IPM and the alkyl chains causes a higher flexibility of the rigid lipid arrangement [133, 134], which is profitable for higher penetration rates [135, 136]. This interaction also features the accumulation of IPM in the SC [137], which is problematic, as the disordering effect has to be reversible in order to regenerate the intact barrier properties afterwards.

2.3 Basic principles of neutron scattering

2.3.1 The neutron and its properties

In 1932, James Chadwick verified the existence of neutrons and their basic properties [138]. He established his discovery on earlier experiments from the married couple Joliot Curie on Beryllium´s irradiation with α-particles. Together with the protons, neutrons form the atomic nucleus. They are in a neutral charge and possess a mass of 1.00866492 atomic units (~1 au) equal to 1.67495 * 10^{-27} kg [139], whereby their energy depends on their velocities and masses [140]. Due to their electronically neutral properties, they can penetrate deeply into the investigated material without destroying it [14]. Furthermore, neutrons have a very low energy with wavelengths correlating to the interatomic distances of biological matter. The interaction of neutrons with the atomic nucleus is very profitable due to the low atomic number of typical atoms within biological systems [15]. Therefore, neutrons are very versatile and powerful tools for investigations on biological membrane nanostructures.

Especially, the high number of hydrogen in biological samples offers an important advantage of neutrons over X-rays. While hydrogen is nearly invisible for X-rays, neutrons can even differentiate between isotopes based on the varying coherent scattering length density b_{coh} for hydrogen (^{1}H b_{coh}: -0.37406 × 10^{-12} cm) and deuterium (^{2}H b_{coh}: 0.6671 × 10^{-12} cm) [14-17, 141] (see Fig. (9)). This enables the determination of deuterium labelled molecules by the special feature of contrast matching [142, 143]. Numerous fields of biological neutron science profited from that property [144-147].

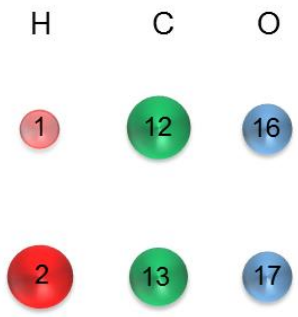

Fig. (9): Neutron scattering lengths of elements and their isotopes. The isotopes are marked with their masses [140]. The scattering length (SL) for hydrogen is strongly depending on the isotope, as for ^{2}H the SL is positive (red ball) while for ^{1}H the SL is negative (pale red ball). For carbon and oxygen only slight differences in the SL of the isotopes are known.

Moreover, neutrons can act either as a wave or particles. The wave properties are mandatory for neutron diffraction experiments, whereby their particle properties are necessary, dealing with their production and detection. It is common, to express the neutron wavelength in Angstrom (Å) with 1 Å ≅ 0.1 nm. Based on their masses m_n and velocities v, neutrons have different energies E depending on their post-production treatment. For example, a cold source decreases the neutron velocity and wavelength λ. Due to this correlation, the neutron energy and wavelength are always quoted with the appropriate velocity.

This relationship is estimated through the de Broglie equation [148] as:

$$\lambda = \frac{h}{m_n v} \qquad \textbf{Equ. (1)}$$

with h as Planck´s constant. The product $m_n v$ is equivalent to the neutron momentum $\vec{p}$. Hence, $\vec{p}$ can also be calculated by:

$$\vec{p} = \frac{h}{\lambda} \qquad \textbf{Equ. (2)}$$

Based on the equality of the neutron kinetic energy E with $\frac{1}{2} m_n v^2$, E is also indicated as:

$$E = \frac{h^2}{2 m_n v^2} \qquad \textbf{Equ. (3)}$$

2.3.2 Neutron diffraction - Bragg´s law

To understand the diffraction process, it is important to go into detail about the neutron momentum, which is an essential property and which can be expressed as:

$$\vec{p} = \hbar \cdot \vec{k} \qquad \textbf{Equ. (4)}$$

including the reduction of Planck´s constant h to $\hbar = \frac{h}{2\pi}$., with $\vec{k}$ defined as the neutron wave vector, which is further given by $|\vec{k}| = \frac{2\pi}{\lambda}$.

During a diffraction experiment on multilamellar lipid membranes, the samples are exposed to a monochromatic and collimated incoming neutron beam. Thereby, the neutrons are scattered, while their momentum is changing. Additionally, a change of the neutrons direction can be registered. This phenomenon is known as diffraction and primary described by Bragg´s law:

$$n\,\lambda = 2d \cdot \sin\theta \qquad \textbf{Equ. (5)}$$

where n is the diffraction order, d represents the spacing between the lattice planes of the lipid membranes and θ is the angle between the incident beam and the planes (see Fig. (10)).

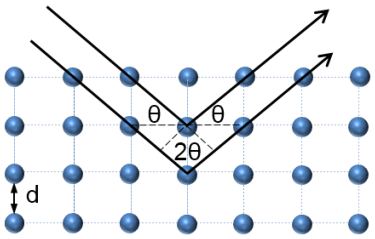

Fig. (10): Neutron scattering process, according to Bragg ´s law [14]. The incoming neutrons with a defined wavelength λ penetrate into the sample and are scattered by the ordered array of the nuclei of the atoms. Thereby the horizontal planes are separated by the interatomic distance *d*. The resulting angle between the incident and scattered beams, with respect to the lattice, is *2θ*.

Moreover, the change of the neutron momentum is demonstrated by the scattering vector Q. The relationship between Q, the scattering angle $2\,\theta$, and the wavelength λ is explained geometrical in Fig. (11). The incident neutron beam, described by $\overrightarrow{k_i}$, is scattered at the sample to the final wave vector $\overrightarrow{k_f}$ resulting in the scattering vector Q with $Q = k_f - k_i$. The scattering angle between $\overrightarrow{k_i}$, and $\overrightarrow{k_f}$ is $2\,\theta$.

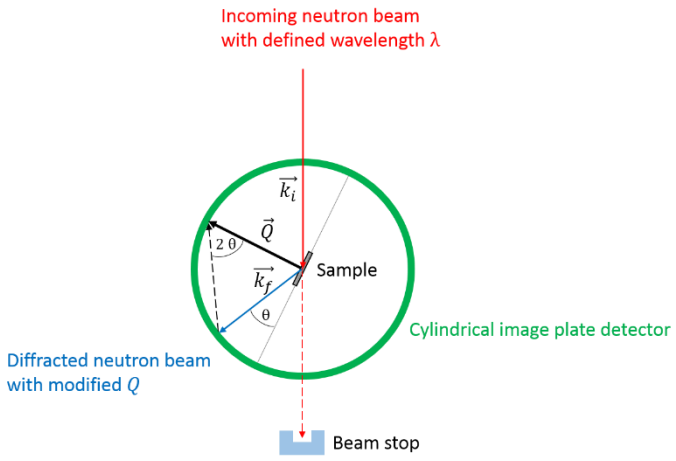

Fig. (11): The correlation of Q presented at neutron diffraction instrument BIODIFF at MLZ.

Assuming the scattering effect is processed without any loss of energy ($\Delta E = 0$), the following equation can be applied

$$|k_i| = |k_f| = k \qquad \textbf{Equ. (6)}$$

realizing the elastic scattering of the neutrons. The absolute value of the scattering vector Q is given by the equation

$$|Q^2| = |k_i|^2 + |k_f|^2 - 2\,|k_i||k_f|\,\cos 2\,\theta. \qquad \textbf{Equ. (7)}$$

Reduced, Equ. (7). can be estimated to

$$Q = 2\,k\,\sin\theta. \qquad \textbf{Equ. (8)}$$

Due to $|\vec{k}| = \frac{2\,\pi}{\lambda}$, the final consolidation to the scattering context can be achieved by

$$Q = \frac{4\,\pi}{\lambda}\,\sin\theta. \qquad \textbf{Equ. (9)}$$

Summarizing, the peculiarity of diffraction can be outlined as scattering process in ordered materials, e.g. the lamellar lipid phases. Thereby the process is described by certain physical functions for further basic analyses and fundamental data reduction.

2.3.3 General data treatment

During the neutron diffraction experiments, the detectors register the intensity I of the scattered neutrons as a function of the scattering angle $2\,\theta$. From the position Q_n of a series of equidistant peaks (see Fig. (13)), the periodicity (d spacing) of the lamellar phases, as shown in Fig. (12) can be calculated using

$$d = \frac{2\,n\,\pi}{Q_n} \qquad \textbf{Equ. (10)}$$

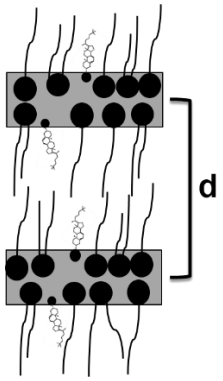

Fig. (12): The lamellar repeat distance of the bilayer structure. Due to the calculation of d the lipid interval can be identified.

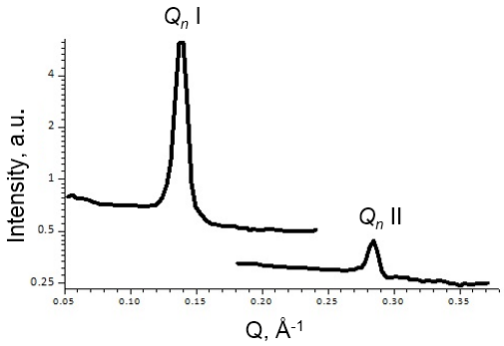

Fig. (13): The scattering pattern of a lipid model membrane. From the pattern, the position of the equidistant peaks (Q_n) and their intensities I [$a.u.$] can be identified. Additionally, the lamellar orders are labeled with Roman numerals, indicating the 1st and the 2nd diffraction order.

The peak positions and intensities are determined by fitting Gaussian functions using the software package IGOR Pro Version 6.34A (WaveMetrics Inc., Portland, OR, USA). So, the particular analysis of the integrated peak intensity I_h of the h^{th} order is performed [149]. Using I_h, the absolute values of their correlating form factors F_h are calculated by

$$F_h = \sqrt{h \cdot A_h \cdot I_h} \qquad \textbf{Equ. (11)}$$

with A_h as absorption correction and h as Lorentz factor, which is related to the data collection geometry [150].

The determination of the phase factor of F_h is realized by contrast variation, which assumes only "+" or "-" for centrosymmetric bilayers like the lamellar lipid phases [149, 151]. For that purpose, the samples are measured at least at three different D_2O/H_2O ratios, which provide a linear correlation between the $|F_h|$ value and D_2O content. More details concerning the mentioned procedure and neutron diffraction data evaluation are described elsewhere [152, 153].

The application of partially deuterated lipids in neutron diffraction experiments for the investigation of SC lipid membrane structures is well established [18, 92, 132, 154]. The final localization of the labelled molecules requires the determination of the structure factors F_{h_deut} from the deuterated sample as well as the corresponding factors F_{h_prot} from the protonated sample. The difference F_{h_diff} of both structure factors is calculated by

$$F_{h\_diff} = F_{h\_deut} - F_{h\_prot} \qquad \textbf{Equ. (12)}$$

Finally, to infer conclusions from the data to the nanoscaled membrane structure, the neutron scattering length density (NSLD) profiles $\rho_s(x)_{diff}$ are calculated. They are determined, using Fourier transformation of the structure factors F_{h_diff} according to [153]:

$$\rho_s(x)_{diff} = a + b\,\frac{2}{d}\sum_{h=1}^{h_{max}} F_{h_{diff}}\,cos\left(\frac{2\pi hx}{d}\right) \qquad \textbf{Equ. (13)}$$

with a and b as unknown coefficients for relative normalization of $\rho_s(x)_{diff}$, h as diffraction order of the associated structure factor F_{h_diff} and d describes the lamellar repeat distance. The resulting NSLD profiles $\rho_s(x)_{diff}$ represent the deuterium distribution across the lipid bilayer and enable the determination of the labelled lipid positions.

3 PRACTICAL IMPLEMENTATION OF THE NEUTRON DIFFRACTION EXPERIMENTS

The present thesis focusses on the lamellar arrangement of SC lipids, as they are known to play a crucial role for the SC barrier function. Therefore, simple model membranes without corneocytes were prepared, in order to investigate the lipid interactions without any interferences with the horny cells. Hence, synthetically derived lipids were applied. The defined chain lengths and head group structures of the lipids enabled their reproducible assembling process with final conclusions about their basic impact on each other [155, 156]. Native SC lipid mixtures are too complex and heterogeneous to reveal individual influences between the compounds. Thus, quaternary lipid mixtures were used with the focus on one or two CER subclasses. All samples and a list of the applied chemicals and materials are given in the appendix. In addition to samples containing the deuterated label, always a protonated reference sample was necessary.

3.1 Preparation of the SC lipid model membranes

In order to receive well oriented multilamellar lipid layers, the SC lipid model membranes were prepared by following a known procedure [157].

First, the lipids were dissolved separately in a chloroform/ methanol mixture (2:1; v/v) with a final concentration of 10 mg/mL. Afterwards, they were merged to the final lipid solutions in the suitable ratios. The solutions containing the ultra-long-chain CER[EOS]-br were transmitted by a Hamilton pipette, whereby the samples without CER[EOS]-br were sprayed with an airbrush pistol on the quartz wafer. For each sample, 1.2 mL of the lipid mixture were used. Furthermore, in both cases, the wafers were located on a heating plate with an inert surface, realizing a constant temperature (see Fig. (14)).

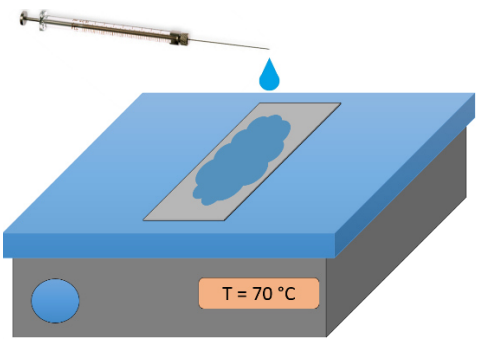

Fig. (14): Sample preparation. The quartz wafer was positioned on a heating plate, where the lipid solutions with CER[EOS]-br were placed by a Hamilton pipette. For the samples without CER[EOS]-br, an airbrush pistol was applied for that purpose.

Due to the heat treatment, a fast and efficient removal of the organic solvent was induced. After the cooldown to room temperature, the samples were stored in a desiccator under

vacuum for twelve hours, in order to eliminate solvent rests. The subsequent annealing procedure enabled the final assembling process of the lipid membranes. During the heating period the samples were able to equilibrate under a water-saturated environment in the oven. The alternating heating-cooling treatment caused opaque lipid films indicating a final lipid arrangement in highly ordered multiple stacks. More details about the respective samples and their preparation can be found in the accepted publications, presented in chapter 4.

It was described before, that the state of order increases with the annealing process [152] and furthermore it is known, that a decreasing bilayer orientation results in a proportional lower number of structure factors [151]. The annealing procedure is well-established in neutron scattering experiments based on higher peak intensities followed by an enormous benefit for the data analysis [141, 151].

3.2 Appropriated neutron diffraction instrument V1 at HZB

Most of the performed neutron diffraction studies were performed by means of the membrane diffractometer V1. The instrument is located at the Helmholtz-Zentrum für Materialien und Energie (HZB, Berlin, Germany), which run the cold source research reactor BER II. The pyrolytic graphite monochromator generated a defined wavelength λ of 4.57 Å. The sample-to-detector distances were 1022.4 mm and 1025.7 mm, respectively. The scattered neutrons were recorded by the two-dimensional position-sensitive ^{3}He detector. It had a detection area of 200 x 200 mm^2 with a spatial resolution of 1.5 x 1.5 mm^2. For all measurements, the reflection mode was selected. During the scans, the samples were stored in lockable aluminum chambers, which enabled a constant sample environment. The samples were mounted by Huber goniometers, which enabled an exact alignment of the samples with respect to the incident neutron beam. The measurements were either performed as continuous θ-2θ scans or as rocking scans. In both cases, changing positions of the detector enabled an optimal recording of the intensity. A detailed description of the experimental setup can be found elsewhere [39].

3.3 Appropriated neutron diffraction instrument BIODIFF at MLZ

The Forschungs- Neutronenquelle FRM II of Heinz Maier-Leibnitz Zentrum (MLZ) in Garching (Germany) is a cold neutron source. The resident diffractometer BIODIFF was especially designed for the characterization of biological single crystals, for example protein structure investigation [158-161]. For an experimental part of this thesis, BIODIFF was used for the first time for studies of SC lipid model membranes.

A new installed sample environment enabled the required conditions during the measurements (see Fig. (15)).

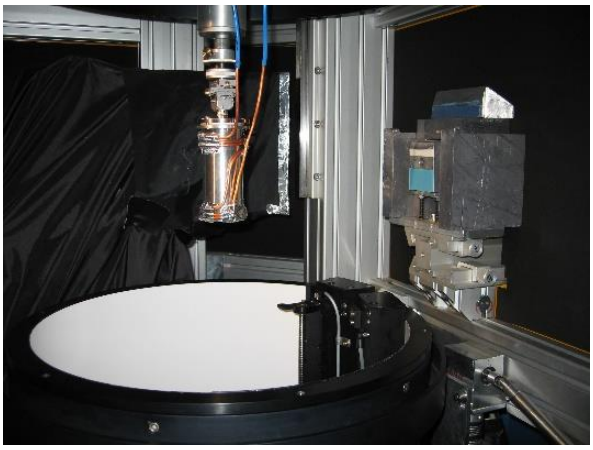

Fig. (15): View into the detector area of BIODIFF. The image plate detector is in the down position. The samples were mounted on a Huber goniometer to align them with respect to the incoming beam (from the right-hand side). The new installed sample environment at BIODIFF was constituted by a cylindrically aluminum chamber (100 x 50 mm). Cupper tubes surrounded the cell in the upper and lower area, realizing the temperature regulation. So an interference with the neutron beam was prevented. To gain the aspired temperature, a Julabo F20 was used.

The variable pyrolytic graphite monochromator PG (002) in combination with the velocity selector ($\lambda/2$ filter) [162] realized a wavelength of 4.72 Å. The detector was a cylindrical image plate. Its dimensions were 400 mm in diameter and 450 mm in height [163], realizing an angular range of ± 152° horizontal and ± 48° vertical [162] with a high resolution of 250 µm^2 (pixel size). Compared to V1 at HZB, here only the centered sample was rotated. During the measurement, the scattered neutrons were recorded as photomultiplier counts (PMT) by the image plate´s reaction of $BaFBr:Eu^{2+}$ + Gd_2O_3 [135]. The direct correlation between the number of PMT and the neutrons was determined as conversion factor of 25.

3.4 Environmental conditions of the samples during the neutron diffraction studies

During all experiments, the samples were equilibrated at certain temperatures (T) and well-defined relative humidity (RH). To simulate *in vivo* conditions, the samples were measured at skin temperature (32 °C). For the investigation of the thermotropic phase behavior of several samples, further temperatures were applied (50 °C, 70 °C, 75 °C). The samples were measured at a K_2SO_4 associated RH of 98% or a NaBr generated RH of 57%. Therefore, saturated solutions of the respective salt in D_2O/ H_2O were used. At least, all samples were measured at three different D_2O/ H_2O ratios (100/0, 50/50 and 8/92 % (mol/mol). As mentioned above, the phase signs of the SFs were determined by this so-called contrast variation. After every change of RH, contrast or temperature, the samples were equilibrated for a time of six to eight hours [19, 28, 38].

4 RESULTS INTRODUCED BY SCIENTIFIC PUBLICATIONS

The following chapter includes the experimental results of the performed neutron diffraction studies as they were published as papers in international journals.

The first intention of this thesis was the confirmation of an earlier proposed idea of CER[AP]-C18 arrangement within a SC lipid model membrane [39]. For that purpose, a partially deuterated variant of the CER was applied in a neutron diffraction study on a SC lipid system together with CHOL, SA and cholesterol sulfate (ChS), which enabled an insight into the nanoscaled bilayer structure. The second intention of this work included the application of CER[EOS]-br, which was introduced in a former neutron diffraction approach [38]. Now, its specifically deuterated variant should reveal its position within the lamellar structures of a membrane based on CER[AP]-C18, CHOL and BA. In the last part of this work, the lipophilic penetration enhancer IPM was added to the SC lipid model system, which was investigated before. Here, the effect of the enhancer on the special features of the lipid membrane and the thermotropic phase behavior were the points of interest.

4.1 Synthesis of specifically deuterated ceramide [AP]-C18 and its biophysical characterization using neutron diffraction

Stefan Sonnenberger[1], Adina Eichner[1], Thomas Hauß, Annett Schroeter, Reinhard H. H. Neubert, Bodo Dobner, *Chemistry and Physics of Lipids* (2017) **204** p.15-24

[1]These authors contributed equally to this work.

Online version: http://dx.doi.org/10.1016/j.chemphyslip.2017.02.001

Chemistry and Physics of Lipids 204 (2017) 15–24

Contents lists available at ScienceDirect

Chemistry and Physics of Lipids

journal homepage: www.elsevier.com/locate/chemphyslip

Synthesis of specifically deuterated ceramide [AP]-C18 and its biophysical characterization using neutron diffraction

Stefan Sonnenberger[a,1], Adina Eichner[a,1], Thomas Hauß[b], Annett Schroeter[a], Reinhard H.H. Neubert[a,c,*], Bodo Dobner[a]

[a] Institute of Pharmacy, Martin Luther University Halle-Wittenberg, 06120 Halle/Saale, Germany
[b] Institute of Soft Matter and Functional Materials, Helmholtz-Zentrum Berlin für Materialien und Energie, 14109 Berlin, Germany
[c] Institute of Applied Dermatopharmacy at the Martin Luther University Halle-Wittenberg, 06120 Halle/Saale, Germany

ARTICLE INFO

Article history:
Received 24 November 2016
Received in revised form 13 January 2017
Accepted 3 February 2017
Available online 12 February 2017

Keywords:
Ceramides
CER[AP]
Synthesis
Specific deuteration
Neutron diffraction

ABSTRACT

The very heterogeneous group of ceramides is known to be mandatory for proper barrier functions of the outermost layer of mammalian skin, referred to as stratum corneum (SC). The synthesis of a specifically deuterated ceramide [AP]-C18 variant is described. The synthesized ceramide contains the racemic forms of the α hydroxy fatty acid. For the biophysical implementation, the received diastereomeric ceramide was applied in a neutron diffraction experiment. Therefore, a SC lipid model membrane was prepared containing the described ceramide (CER), cholesterol (CHOL), stearic acid (SA), and cholesterol sulfate (ChS) in a ratio of 55/25/15/5 wt%. Thus, we were able to localize the deuterated molecule part within the bilayers. In the process, a short-periodicity phase (SPP) was observed with a unit cell scale of about 44 Å. For the first time, we were able to confirm former ideas concerning the arrangement of the CER within this quaternary lipid model membrane.

1. Introduction

The outermost layer of mammalian epidermis represents the main barrier function of the skin (Scheuplin, 1976; Wertz and van den Bergh, 1998). This very thin but complex structure, referred to as stratum corneum (SC), delimits the penetration flux through the skin. Thus, it prevents transepidermal water loss (TEWL) as well as the penetration of xenobiotics into the skin. In detail, these properties are highly connected to the unique SC structure meaning dead corneocytes embedded into a complex multi-lamellar lipid matrix (Elias, 1983). The lamellar lipid arrangement in the matrix is responsible for the SC barrier function (Wertz and van den Bergh, 1998). There are three lipid classes most abundant in the SC: ceramides (CER), cholesterol (CHOL) and free fatty acids (FFA) (Elias, 1983; Gray and Yardley, 1975; Yardley and Summerly, 1981). The ceramides are the most heterogeneous group and important for the lipid assembling process. Based on that issue, ceramides are of high interest referring to their molecular arrangement (de Sousa Neto et al., 2011; Groen et al., 2009; Kessner et al., 2010). There are two lamellar phases described, which SC lipids are able to form: a short-periodicity phase (SPP), meaning a lamellar spacing of about 60 Å and a long-periodicity phase (LPP) with a spacing of about 130 Å (Bouwstra et al., 1991; Madison et al., 1987; White et al., 1988). For the SPP formation, particularly long-chain ceramides such as CER[AP] or CER[NP] are mandatory, as several studies on SC lipid model membranes revealed (de Jager et al., 2003; Engelbrecht et al., 2012b; Schroeter, 2010; Schroeter et al., 2009c). Model systems containing synthetically derived lipids are versatile devices for investigations on SC lipids, as they overcome the complexity of native material. With their defined chain lengths and head group structures, these lipids enable a more detailed insight concerning their interactions and lamellar arrangement on a molecular scale. Neutron diffraction offers a wide range of advantages for the investigation of such samples. For example, neutrons differ in their coherent scattering length b_{coh} for hydrogen H^1 (-0.374×10^{-12} cm) and its isotope deuterium D (0.667×10^{-12} cm) (Sears, 1992). Therefore, the localization of deuterium-labelled molecule parts is possible as performed in numerous studies before (Eichner et al., 2016;

Abbreviations: CER, ceramide; CER[AP]-C18, *N*-(α-hydroxyoctadecanoyl)-phytosphingosine; CHOL, cholesterol; ChS, cholesterol sulfate; FFA, free fatty acid; RH, relative humidity; SC, stratum corneum; SA, stearic acid.

* Corresponding author at: Institute of Pharmacy, Martin Luther University Halle-Wittenberg, 06120 Halle/Saale, Germany.
E-mail addresses: stefan.sonnenberger@pharmazie.uni-halle.de (S. Sonnenberger), adina.eichner@pharmazie.uni-halle.de (A. Eichner), reinhard.neubert@pharmazie.uni-halle.de (R.H.H. Neubert).

[1] These authors contributed equally to this work.

http://dx.doi.org/10.1016/j.chemphyslip.2017.02.001
0009-3084/

Engelbrecht et al., 2012a, 2011; Kessner et al., 2008; Mojumdar et al., 2015, 2016, 2013; Schroeter et al., 2009b).

With a ratio of 8.8% of the SC CER fraction (t'Kindt et al., 2012), the polar CER[AP] is still of high interest in studies, concerning its impact on the molecular lipid lattice (Gruzinov et al., 2017; Kiselev et al., 2007, 2005; Raudenkolb et al., 2005). Its chain lengths distribution varies from C32 to C52 (t'Kindt et al., 2012). The CER [AP] variant we applied has a defined chain length of C18/18 (C36 in total). This molecule is known to be highly involved in the membrane assembling process of certain SC lipid model membranes (Ruettinger et al., 2008; Schroeter et al., 2009a). Ruettinger et al. presented two coexisting SPP with lamellar spacings of 46.3 Å and 45.3 Å in a neutron diffraction experiment on a CER[AP]-C18 based SC lipid model membrane (CER[AP]-C18_CHOL_SA_ChS (55/25/15/5%wt)). They proposed the CER in its hairpin conformation within the bilayer structures. In order to verify this assumption, the objectives of the present study were the synthesis of a specifically deuterated CER[AP]-C18 and its application in the SC lipid model system of Ruettinger et al. in a neutron diffraction experiment. Therefore, the synthesis of an α hydroxy stearic acid with terminal CD_3 group was the main objective, followed by the synthesis of the specifically deuterated DL-CER[AP] and the corresponding neutron scattering experiment.

2. Materials and methods

2.1. Materials

Fig. 1 presents the chemical structures of the applied SC lipids. The racemic DL-CER[AP]-C18 (*N*-(α-hydroxyoctadecanoyl)-phytosphingosine) with a purity of 98% was a generous gift of Evonik Industries AG (Essen, Germany) and used as received. The synthesis of DL-CER[AP]-C18-*d3* is described below. Cholesterol (CHOL), cholesterol sulfate (ChS) and stearic acid (SA) were purchased from Sigma Aldrich (St. Louis, USA) and used as received. Lithium aluminium deuteride was purchased from ARMAR (Europe) GmbH (Leipzig, Germany). PyBOP® was obtained from Carbolution Chemicals GmbH (Saarbrücken, Germany). Phytosphingosine was received from Evonik Goldschmidt GmbH (Essen, Germany). Silica gel 60 (0.063–0.200 mm) for column chromatography was obtained from Merck (Darmstadt, Germany). For TLC were used pre-coated aluminium sheets ALUGRAM® Xtra SIL G/UV_{254} from Macherey-Nagel (Düren, Germany). For detection of the TLC plates, bromothymol blue solution was used. Other materials and solvents were purchased from Sigma-Aldrich (St. Louis, USA). The solvents were dried and distilled before using.

Mass spectrometry data were obtained on a Finnigan MAT 710C (Thermoseparation Products, San Jose, CA) for ESI-MS and on a LTQ-Orbitrap XL hybrid mass spectrometer (Thermo Fisher Scientific, Bremen, Germany) for HR-MS (high resolution mass spectrometry). For GC–MS the samples were separated with HP 5890 II followed by injection in a MS 5971 A (Hewlett-Packard). Melting points were determined on Boetius apparatus and were not corrected. ^{1}H NMR and ^{13}C NMR data were recorded on Varian Gemini 2000 and Varian Inova 500 instruments. As solvents for the NMR $CDCl_3$, CD_3OD and THF-D_8 were used. Elemental analyses data were obtained on a CHNS-932 (Leco Corporation, St. Joseph, MI). An HP 1200 Agilent (Agilent Technologies, Waldbronn, Germany) was used for HPLC with an ELSD 2000 Alltech detector (Grace Davison, Columbia, MD, USA) and a Nucleodur 100-5 125 × 2 column from Macherey-Nagel (Düren, Germany). Quartz slides (Spectrosil 2000, 25 × 65 × 0.3 mm^3) for the neutron diffraction experiments were purchased from Saint-Gobain (Wiesbaden, Germany). For the deposition of the lipids onto the quartz surface, an airbrush instrument produced by Harder & Steenbeck (Norderstedt, Germany) was employed. Chloroform and methanol (GC-grade) were used as solvents for preparation of the lipid solution and received from Merck (Darmstadt, Germany).

2.2. Synthesis of 1-bromohexadecane-16,16,16-d_3 (**5**)

2.2.1. Synthesis of methyl 16-hydroxyhexadecanoate (**2**)

A solution of 16-hexadecanolide (**1**) (53.4 g, 0.21 mol) and catalytic amounts of PTSA in methanol (1500 mL) was refluxed for 24 h. For working up, water (700 mL) was added and the formed white precipitate was extracted three times with chloroform (500 mL). The combined organic layer was washed two times with saturated aqueous $NaHCO_3$ solution (500 mL), two times with brine (500 mL), dried over Na_2SO_4 and concentrated to dryness under reduced pressure. The residue was recrystallized from

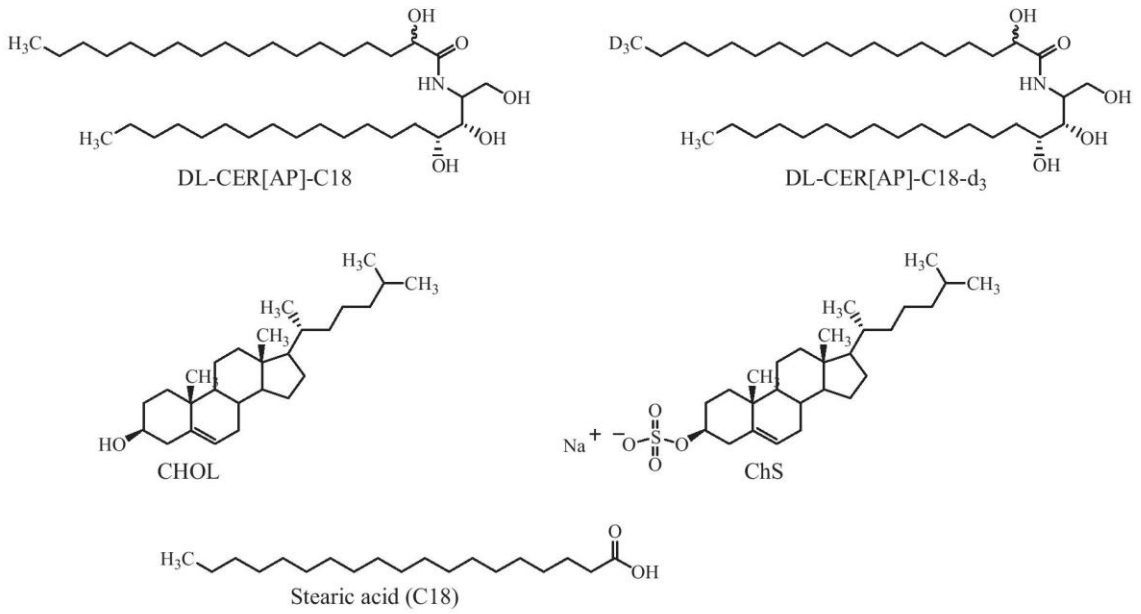

Fig. 1. Chemical structures of the lipids, applied in the SC lipid model membranes.

heptane to give 56.8 g (yield 94%) of compound **2** as a white crystalline solid: m.p. 53 °C; R_f = 0.41 ($CHCl_3$/Et_2O 8/2); ^{1}H NMR (400 MHz, $CDCl_3$, 27 °C): δ = 1.25–1.40 (m, 22H, HO(CH_2)$_2$(CH_2)$_{11}$–), 1.53–1.65 (m, 4H, HOCH$_2$C***H***$_2$–; –C***H***$_2$CH$_2$COO–), 2.30 (t, ^3J = 7.6 Hz, 2H, –C***H***$_2$COO–), 3.63 (t, ^3J = 6.7 Hz, 2H, HOC***H***$_2$–) 3.66 ppm (s, 3H, –C***H***$_3$); ^{13}C NMR (100 MHz, $CDCl_3$, 27 °C): δ = 25.11, 25.89, 29.30, 29.40, 29.58, 29.72, 29.75, 29.76, 29.78, 32.97, 34.27, 51.57, 63.24, 174.50 ppm; ESI MS: *m*/*z*: 287.2 [M+H]$^+$, 309.3 [M+Na]$^+$; elemental analysis calcd: (%) for $C_{17}H_{34}O_3$: C 71.28, H 11.97; found: C 71.23, H 11.89. Spectroscopic data correspond with the literature (Sui et al., 2010).

*2.2.2. Synthesis of methyl 16-[(tetrahydro-2H-pyran-2-yl)oxy] hexadecanoate (**3**)*

A solution of compound **2** (56.8 g, 0.2 mol), fresh distilled dihydropyran (29.4 g, 0.35 mol, 31.7 mL, 1.75 eq), catalytic amounts of PPTS in dry methylene chloride (300 mL) was stirred for 24 h at r. t. For working up the mixture was washed three times with water (50 mL), dried over Na_2SO_4 and concentrated to dryness under reduced pressure. The crude residue was recrystallized from a small amount of heptane to give 61.8 g (yield 87%) of compound **3** as white waxy substance: m.p. = 40 °C; R_f = 0.48 ($CHCl_3$); ^{1}H NMR (400 MHz, $CDCl_3$, 27 °C): δ = 1.25–1.37 (m, 22H, –(C***H***$_2$)$_{11}$(CH$_2$)$_2$COO–), 1.49–1.63 (m, 8H, –OCH$_2$C***H***$_2$(CH$_2$)$_{11}$C***H***$_2$CH$_2$ COO–; –(C***H***$_2$)$_2$CH$_2$CH–O–), 1.69–1.75 (m, 1H, –C***H***H'CH–O–), 1.79–1.90 (m, 1H, –CH***H'***CH–O–), 2.30 (t, $^3J_{H,H}$ = 7.5 Hz, 2H, –C***H***$_2$COO–), 3.38 (dt, $^2J_{H,H}$ = 9.5 Hz, $^3J_{H,H}$ = 6.7 Hz, 1H, –OC***H***H'(CH$_2$)$_{14}$–), 3.47–3.52 (m, 1H, –C***H***H'(CH$_2$)$_3$CH–O–), 3.68 (s, 3H, –C***H***$_3$), 3.73 (dt, $^2J_{H,H}$ = 9.5 Hz, $^3J_{H,H}$ = 6.9 Hz, 1H, –OCH***H'***(CH$_2$)$_{14}$–), 3.85–3.90 (m, 1H, –CH***H'***(CH$_2$)$_3$CH–O–), 4.57–4.58 ppm (m, 1H, –OC***H***–O–); ^{13}C NMR (100 MHz, $CDCl_3$, 27 °C): δ = 19.87, 25.13, 25.69, 26.41, 29.32, 29.41, 29.61, 29.66, 29.75, 29.76, 29.77, 29.80, 29.81, 29.93, 30.97, 34.29, 51.57,62.50, 67.86, 99.00, 174.48 ppm; ESI MS: *m*/*z*: 393.2 [M+Na]$^+$; elemental analysis calcd: (%) for $C_{22}H_{42}O_4$: C 71.30, H 11.43; found: C 71.39, H 11.65.

*2.2.3. Synthesis of 2-(hexadecyl-16,16,16-d_3-oxy)tetrahydro-2H-pyran (**4**)*

In a round-bottomed flask under argon atmosphere a solution of compound **3** (26.0 g, 0.07 mol) in abs. diethyl ether (100 mL) was dropped slowly to a stirred suspension of $LiAlD_4$ (3.53 g, 0.084 mol) in abs. diethyl ether (120 mL). After adding, the mixture was heated under reflux for 6 h. For working up, the mixture was cooled down to 0 °C and D_2O (5 mL) was added carefully dropwise under strong stirring. Afterwards the reaction was stirred at r.t. for 2 h. The precipitate was removed from the ether solution by suction with a frit and was washed three times with ether (20 mL). The combined ether solutions were washed twice with aqua dest. (50 mL), brine (50 mL), dried over Na_2SO_4 and concentrated to dryness under reduced pressure. Additionally the evaporated double deuterated alcohol was dried over P_2O_5.

The dried alcohol and triethylamine (6.50 mL, 0.084 mol) were dissolved in chloroform (250 mL) under argon atmosphere. The mixture was cooled down to 0 °C and under strong stirring was added dropwise a solution of methanesulfonyl chloride (11.6 mL, 0.084 mol) in chloroform (100 mL). After adding, the mixture was stirred at 0 °C for 2 before the mixture was allowed to warm up to room temperature. The stirring was continued for further 12 h. Triethylamine (3.25 mL, 0.042 mol) and ice (100 g) were added and the mixture was stirred for 2 h at r.t. The chloroform phase was separated and the water layer was extracted two times with chloroform (50 mL). The combined chloroform phases were washed twice with aqua dest. (50 mL), dried over Na_2SO_4, concentrated to dryness under reduced pressure and dried over P_2O_5. The obtained mesylate was reduced without further purification.

In a round-bottomed flask a solution of the dried mesylate in abs. diethyl ether (100 mL) was dropped slowly to a stirred suspension of $LiAlD_4$ (1.68 g, 0.04 mol) in abs. diethyl ether (100 mL). After adding the mixture was heated under reflux for 6 h. For working up, the mixture was cooled down to 0 °C and aqua dest. (5 mL) was added carefully dropwise under strong stirring. The reaction was stirred at r.t. for further 2 h. The precipitate was removed from the ether solution by suction with a frit and was washed three times with ether (20 mL). The combined ether solutions were washed two times with aqua dest. (50 mL), brine (50 mL), dried over Na_2SO_4, and concentrated to dryness under reduced pressure. The obtained crude residue was purified by column chromatography using a gradient technique with heptane/diethyl ether/triethylamine eluent to give 14.2 g (yield 61%) of compound **4** as a white waxy substance: R_f = 0.61 ($CHCl_3$); ^{1}H NMR (500 MHz, $CDCl_3$, 27 °C): δ = 1.25–1.35 (m, 26H, D_3C(C***H***$_2$)$_{13}$), 1.49–1.61 (m, 6H, –C***H***$_2$CH$_2$OCH–CH$_2$(C***H***$_2$)$_2$–), 1.68–1.73 (m, 1H, –C***H***H'CH–O–), 1.79–1.86 (m, 1H, –CH***H'***CH–O–), 3.37 (dt, $^2J_{H,H}$ = 9.6 Hz, $^3J_{H,H}$ = 6.7 Hz, 1H, –OC***H***H'(CH$_2$)$_{14}$–), 3.47–3.51 (m, 1H, –C***H***H'(CH$_2$)$_3$CH–O–), 3.72 (dt, $^2J_{H,H}$ = 9.6 Hz, $^3J_{H,H}$ = 6.9 Hz, 1H, –OCH***H'***(CH$_2$)$_{14}$–), 3.84–3.89 (m, 1H, –CH***H'***(CH$_2$)$_3$CH–O–), 4.56–4.58 ppm (m, 1H, –OC***H***–O–); ^{13}C NMR (125 MHz, $CDCl_3$, 27 °C): δ = 19.85, 22.57, 25.68, 26.40, 29.53, 29.65, 29.76, 29.77, 29.81, 29.83, 29.85, 29.92, 30.95, 32.00, 62.45, 67.84, 98.97 ppm; ESI MS: *m*/*z*: 352.3 [M+Na]$^+$.

*2.2.4. Synthesis of 1-bromohexadecane-16,16,16-d_3 (**5**)*

Triphenylphosphine (17.31 g, 0.066 mol) was dissolved in methylene chloride (100 mL). The mixture was cooled down to 0 °C and a solution of bromine (3.38 mL, 0.066 mol) in methylene chloride (10 mL) was added dropwise without an increase of the temperature over 5 °C and without a yellow coloration of the mixture. Afterwards a solution of compound **4** (10.81 g, 0.03 mol) in methylene chloride (15 mL) was added and the mixture was stirred for 12 h at r.t. For working up, the dark coloured methylene chloride phase was washed two times with aqua dest. (50 mL), dried over Na_2SO_4 and concentrated to dryness under reduced pressure. The obtained residue was absorbed on silica gel before purification by column chromatography using a gradient technique with heptane/diethyl ether eluent to give 8.37 g (yield 90%) of compound **5** as colourless oily liquid: R_f = 0.74 ($CHCl_3$/heptane 4/6); ^{1}H NMR (400 MHz, $CDCl_3$, 27 °C): δ = 1.26–1.32 (m, 24H, D_3C(C***H***$_2$)$_{12}$–), 1.39–1.46 (m, 2H, –C***H***$_2$(CH$_2$)$_2$Br), 1.82–1.89 (m, 2H, –C***H***$_2$CH$_2$Br), 3.40 ppm (t, $^3J_{H,H}$ = 6.9 Hz, 2H, –C***H***$_2$Br); ^{13}C NMR (100 MHz, $CDCl_3$, 27 °C): δ = 22.59, 28.36, 28.95, 29.55, 29.62, 29.72, 29.79, 29.83, 29.85, 29.86, 29.87, 32.01, 33.03, 34.04 ppm; EI MS: *m*/*z*: 307/309 [M]$^+$.

2.3. Synthesis of (2RS)-2-hydroxyoctadecanoic acid-d_3

*2.3.1. Synthesis of (2RS)-2-aminooctadecanoic acid-18,18,18-d_3 (**7**)*

To a solution of diethyl acetamidomalonate (**6**) (8.14 g, 37.5 mmol) in abs. ethanol (20 mL) was added dropwise a solution of sodium ethanolate (0.80 g, 35 mmol sodium in 20 mL ethanol) and was afterwards stirred for 30 min. After adding a solution of compound **5** (7.63 g, 25 mmol) in ethanol (10 mL) the mixture was refluxed for 18 h. The reaction was followed by TLC (R_f = 0,16 ($CHCl_3$:Heptan 6:4)) For working up, aqua dest. (50 mL) was added. The mixture was extracted three times with diethyl ether (100 mL). The combined ether phases were dried over Na_2SO_4 and concentrated to dryness under reduced pressure. The compound was used without a further purification.

To the residue conc. HCl (27 mL) and DMF (3 mL) were added, and then refluxed for 24 h. After adding of 32% ammonia solution (18.9 mL) the mixture was stirred for 1 h at r.t. and the formed precipitate was filtered by suction with a frit, washed with aqua

dest. (10 mL), methanol (10 mL) and diethyl ether (10 mL) to obtain 7.14 g (yield 95%) of compound **7**. The amino acid was used without further characterisation and purification.

*2.3.2. Synthesis of methyl (2RS)-2-hydroxyoctadecanoate-18,18,18-d_3 (**8**)*

To a stirred solution of compound **7** (2.12 g, 7 mmol) in 2 N-H_2SO_4 (15 mL) a solution of $NaNO_2$ (1.14 g, 16.5 mmol) in aqua dest. (13 mL) was added dropwise over 1 h at a temperature of 80 °C. The mixture was stirred for additionally 8 h at 80 °C. Afterwards the layer was extracted three times with diethyl ether (50 mL). The combined ether phases was dried over Na_2SO_4 and concentrated to dryness under reduced pressure.

To the obtained crude hydroxy acid methanol (10 mL), toluene (20 mL) and three drops conc. HCl were added. The mixture was refluxed for 4 h. For working up, brine (10 mL) was added and the mixture was extracted three times with diethyl ether (25 mL). The combined ether phases were washed with brine (25 mL), dried over Na_2SO_4 and concentrated to dryness under reduced pressure. The obtained residue was purified by column chromatography using a gradient technique with heptane/diethyl ether eluent to give 0.98 g (yield 44%) of compound **8** as a white solid: m.p. = 58 °C; R_f = 0.43 ($CHCl_3$); ^{1}H NMR (500 MHz, $CDCl_3$, 27 °C): δ = 1.26–1.48 (m, 28H, $D_3C(CH_2)_{14}$–), 1.59–1.67 (m, 1H, –C***H***'CHOH–), 1.75–1.81 (m, 1H, –CH***H***'CHOH–), 3.79 (s, 3H, $–CH_3$), 4.18 ppm (dd, $^3J_{H,H}$ = 7.4 Hz, $^3J_{H,H}$ = 4.2 Hz, 1H, –C***H***OH–); ^{13}C NMR (125 MHz, $CDCl_3$, 27 °C): δ = 22.58, 24.90, 29.47, 29.53, 29.62, 29.71, 29.79, 29.82, 29.84, 29.85, 29.86, 32.00, 34.60, 52.60, 70.64, 176.01 ppm; ESI MS: *m/z*: 340.3 $[M+Na]^+$, 657.1 $[2M+Na]^+$.

*2.3.3. Synthesis of (2RS)-2-hydroxyoctadecanoic acid-18,18,18-d_3 (**9**)*

A solution of compound **8** (0.87 g, 2.7 mmol) and KOH (0.23 g, 4.1 mmol) in 30 mL 96% ethanol was refluxed for 2 h. The solvent was evaporated and the crude was taken up in 2 N-HCl (20 mL). The aqueous layer was extracted three times with diethyl ether (20 mL). The combined ether phases were washed with brine (30 mL), dried over Na_2SO_4 and concentrated to dryness under reduced pressure. The residue was recrystallized from heptane/acetone (8:1) to give 0.74 g (yield 89%) of compound **9** as a white crystalline solid: m.p. = 87 °C; R_f = 0.26 ($CHCl_3$/MeOH 9/1); ^{1}H NMR (400 MHz, $CDCl_3$, 27 °C): δ = 1.11–1.35 (m, 26H, $D_3C(CH_2)_{13}$–), 1.40–1.52 (m, 2H, –C***H***$_2$CH$_2$CHOH–), 1.60–1.75 (m, 1H, –C***H***H'CHOH–), 1.82–1.90 (m, 1H, –CH***H***'CHOH–), 4.28 ppm (dd, $^3J_{H,H}$ = 7.5 Hz, $^3J_{H,H}$ = 4.2 Hz, 1H, –C***H***OH–); ^{13}C NMR (125 MHz, THF-d_8, 27 °C): δ = 23.46, 26.19, 30.49, 30.59, 30.72, 30.76, 30.77, 30.80, 30.81, 32.95, 35.68, 71.00, 176.74 ppm; ESI MS: *m/z*: 302.8 $[M-H]^-$.

2.4. Synthesis of specific deuterated CER[AP]-C18-d_3

*2.4.1. Synthesis of (RS)-2-Acetoxyoctadecanoic acid-18,18,18-d_3 (**10**)*

To a solution of compound **9** (190 mg, 0.63 mmol) in methylene chloride (10 mL) acetic anhydride (0.95 mL, 10 mmol) and pyridine (1.57 mL, 19.4 mmol) were added. The mixture was stirred for 16 h at room temperature. Afterwards the reaction was quenched by saturated aqueous $NaHCO_3$ solution (10 mL). The mixture was extracted three times with chloroform (10 mL). The combined organic layers were washed with 0.5 M $NaHSO_4$ (25 mL), dried over Na_2SO_4 and concentrated to dryness under reduced pressure to give 206 mg (yield 95%) of compound **10** as a yellow solid: m.p. = 63 °C; R_f = 0.51 ($CHCl_3$/MeOH 9/1); ^{1}H NMR (500 MHz, $CDCl_3$, 27 °C): δ = 1.25–1.35 (m, 26H, $D_3C(CH_2)_{13}$–), 1.39–1.46 (m, 2H, –C***H***$_2$CH$_2$ CHOH–), 1.82–1.89 (m, 2H, –C***H***$_2$CHOH–), 2.14 (s, 3H, $–OOCCH_3$), 5,01 ppm (dd, $^3J_{H,H}$ = 7.3 Hz, $^3J_{H,H}$ = 5.4 Hz, 1H, –C***H***O–COO–); ^{13}C NMR (100 MHz, $CDCl_3$, 27 °C): δ = 20.75, 22.58, 25.26, 29.27, 29.50, 29.53, 29.68, 29.77, 29.81, 29.85, 29.86, 31.13, 32.00, 72.01, 170.77, 174.96 ppm; ESI MS: *m/z*: 344.5 $[M-H]^-$, 689.4 $[2M-H]^-$.

*2.4.2. Synthesis of [18,18,18-d_3-(2RS)-2-hydroxy-1-oxo-1-{[(3S,4R)-1,3,4-trihydroxyoctadec-(2S)-2-yl]amino}octadec-2-yl-]acetate (**11**)*

To a solution of compound **10** (206 mg, 0.6 mmol) and PyBOP® (359 mg, 0.69 mmol) in methylene chloride (5 mL) was added DIPEA (213 µL, 1.25 mmol). The reaction was stirred for 15 min. Afterwards phytosphingosine (219 mg, 0.69 mmol) was added to the clear solution. The mixture was stirred for 16 h at r.t. and was afterwards evaporated to dryness. The obtained residue was purified by column chromatography using gradient technique starting with chloroform to chloroform/methanol (98.5/1.5 V/V) eluent to give 281 mg (yield 73%) of compound **11** as a white waxy solid: m.p. = 98 °C; R_f = 0.30 ($CHCl_3$/MeOH/NH_3 90/10/1); ^{1}H NMR (500 MHz, $CDCl_3$, 27 °C): δ = 0.86 (t, $^3J_{H,H}$ = 7.0 Hz, 3H, $–CH_3$), 1.24–1.69 (m, 56H, $D_3C(CH_2)_{15}$–, $H_3C(CH_2)_{13}$–), 2.13 (s, 3H, $–OOCCH_3$), 3.58–3.66 (m, 3H, –C***H***OHC***H***OHCH–C***H***H'OH), 3.88 (dd, $^2J_{H,H}$ = 11.6 Hz, $^3J_{H,H}$ = 2.7 Hz, 1H, –CH***H***'OH), 4.05–4.10 (m, 1H, –C***H***–NH–), 5.08 (dt, $^3J_{H,H}$ = 7.2 Hz, $^3J_{H,H}$ = 4.9 Hz, 1H, –C***H***–CONH–), 6.87 ppm (d, $^3J_{H,H}$ = 8.6 Hz, 1H, –CON***H***–); ^{13}C NMR (100 MHz, $CDCl_3$, 27 °C): δ = 20.75, 22.58, 25.26, 29.27, 29.50, 29.53, 29.68, 29.77, 29.81, 29.85, 29.86, 31.13, 32.00, 72.01, 170.77, 174.96 ppm; ESI MS: *m/z*: 344.5 $[M-H]^-$, 689.4 $[2M-H]^-$.

*2.4.3. Synthesis of (2RS)-N-[(3S,4R)-1,3,4-trihydroxyoctadec-(2S)-2-yl]-2-hydroxyoctadecanamide-18,18,18-d_3 (**12**)*

To a solution of compound **11** (220 mg, 034 mmol) in a mixture of chloroform and methanol (4:1, 10 mL) catalytic amounts of K_2CO_3 was given. The mixture was stirred for 2 h at r.t. and was afterwards filtered. The filter was washed twice with a mixture of chloroform and methanol (5 mL, 4:1). The combined organic layers were concentrated to dryness. The obtained residue was absorbed on silica gel before purification by column chromatography using a gradient technique with chloroform/methanol/NH_3 eluent to give 190 mg (yield 92%) of compound **12** as a white waxy substance: m.p. = 130 °C; R_f = L-form 0.39, D-form 0.22 ($CHCl_3$/MeOH/NH_3 90/10/1); ^{1}H NMR (500 MHz, $CDCl_3$, 27 °C): δ = 0.88 (t, $^3J_{H,H}$ = 6.9 Hz, 3H, $–CH_3$), 1.26–1.85 (m, 56H, $D_3C(CH_2)_{15}$–, $H_3C(CH_2)_{13}$–), 3.61–3.66 (m, 2H, $–CH_2$ C***H***OHC***H***OH–), 3.79 (dd, $^2J_{H,H}$ = 11.5 Hz, $^3J_{H,H}$ = 5.3 Hz, 1H, –C***H***H'OH), 3.93–3.97 (m, 1H, –CH***H***'OH) 4.12–4.17 (m, 1H, –C***H***–NH–), 7.22 ppm(d, $^3J_{H,H}$ = 7.4, 1H, –CON***H***–); ^{13}C NMR (100 MHz, THF-d_8, 27 °C): δ = 14.60, 23.46, 23.73, 26.23, 26.29, 26.95, 26.97, 30.49, 30.75, 30.78, 30.80, 30.83, 30.84, 30.85, 30.86, 30.88, 30.93, 30.96, 31.04, 32.95, 33.04, 34.44, 34.61, 36.05, 36.07, 53.32, 53.37, 62.47, 62.50, 72.81, 72.87, 73.22, 73.32, 77.32, 77.34, 175.08, 175.14 ppm; ESI MS: *m/z*: 601.6 $[M-H]^-$, 637.5 $[2M-H]^-$; HRMS calcd for $C_{36}H_{71}D_3NO_5$ $[M+H]^+$ 603.5755; found 603.5750, HPLC L-form 56%, D-form 44%.

2.5. Sample preparation for the neutron scattering experiments

The sample composition was adapted from a former experiment on this quaternary system (Ruettinger et al., 2008), in order to check these results by the inserted deuteration. Stearic acid was chosen to be equal to the CER chain length to avoid mismatch. To differ between CD_3 and CH_3, two samples were prepared: the fully protonated reference sample_AP and sample_AP-d_3, containing

Table 1
Composition of the investigated SC lipid model systems.

SC lipid model membrane system	Ratio (wt%)	Designation
CER[AP]-C18/CHOL/SA/ChS	55/25/15/5	sample_AP
CER[AP]-C18-d_3/CHOL/SA/ChS	55/25/15/5	sample_AP-d_3

the d_3-label. Table 1 provides the several compositions of the investigated multilamellar systems.

The samples were prepared, referring to a known procedure (Seul and Sammon, 1990). The lipids were separately dissolved in a chloroform/methanol mixture (2:1, V/V) with a final concentration of 10 mg/mL. Defined volumes of the lipid solutions were mixed up to the aimed ratio. Using airbrush technique, a volume of 1.2 mL of each lipid solution was spread on a heated (80 °C) quartz wafer, covering an area of $4.5 \times 2.5\,cm^2$. The entirely removal of the solvent was effected by a vacuum storage for 12 h. The followed annealing procedure enabled a higher state of order of the lipid arrangement and is well-established in comparable neutron scattering experiments (Schroeter et al., 2009a; Takahashi et al., 1997; Wiener and White, 1991; Worchester and Franks, 1976). Here, in cycles the samples were heated up to 80 °C under a water-saturated atmosphere (60 min, 2×30 min) each followed by a cooldown to room temperature (30 min, 2×15 min). The peak intensity was even higher after a buffer treatment (see Fig. (a) in supplemental data), resulting in a better signal-to-noise ratio with a high benefit for the data treatment.

2.6. Neutron diffraction experiment

The neutron diffraction data were collected at the V1 Membrane Diffractometer at the Helmholtz-Zentrum für Materialien und Energie (HZB, Berlin, Germany). Compared to *in vivo* skin conditions, the samples were set to 32 °C. Moreover, a relative humidity (RH) of 57% was achieved, using a saturated salt solution of NaBr (Sigma-Aldrich, Steinheim, Germany) in the several D_2O/H_2O contrast (Young, 1967). The samples were equilibrated in closable aluminum cans, realizing a constant temperature and relative humidity. Former experiments revealed an equilibration time of 6–8 h for an optimized hydration level of SC lipid model membranes after every change of D_2O ratio (Engelbrecht et al., 2012b). Sample_AP-d_3 was measured at three different D_2O/H_2O contrasts (100/0, 50/50, 8/92 (V/V)), in order to differentiate the neutron scattering length density (NSLD) between water and the lipids (contrast matching). Moreover, the determination of the structure factors (SF) phase signs was done due to the contrast matching. As for sample_AP the SF phase signs were known from the former experiment (Ruettinger et al., 2008), only one scan at 8% D_2O and 57% RH was performed.

During the neutron diffraction runs, the pyrolytic graphite monochromator, generated a selected wavelength of 4.57 Å. The two −dimensional position- sensitive ^3He detector (area: $20 \times 20\,cm^2$, spatial resolution: $1.5 \times 1.5\,mm^2$) was in a distance of 102.24 cm to the sample. A more precise description of the experimental setup was described earlier (Ruettinger et al., 2008). The collected diffraction data were recorded as rocking scans (ω-scan), where the samples being rocked around the Bragg positions θ, while the detector was set to a fixed position 2θ. The detector registered the intensities I of the scattered neutrons as a function of the scattering angle 2θ. By means of equation $Q = (4\pi \sin\theta)/\lambda$, the scattering vector Q is defined with λ as the wavelength of the incoming neutrons. In lamellar membranes, the positions of Bragg peaks (Q_n) are equidistant in the diffraction pattern. The repeat distance d (d spacing) of the lamellar bilayers was calculated with $d = (2n\pi)/Q_n$, with n as Bragg peak order. The software package IGOR Pro Version 6.34A (WaveMetrics Inc., Portland, OR, USA) was used for the Gaussian fitting of the h^{th} Bragg peak orders intensities' I_h (Franks and Lieb, 1979). The calculation of the absolute values of the structure factors (SF;F_h) was done with Eq. (1)

$$F_h = \sqrt{h \cdot A_h(\theta) \cdot I_h} \tag{1}$$

where h was the Lorentz factor and $A_h(\theta)$ the absorption correction, referring to the geometry of the data collection (Cser, 2001). For the absorption correction, a sample thickness of 7 μm and a linear absorption coefficient of $6\,cm^{-1}$ were supposed. The SF phase signs were determined by contrast matching with a linear correlation between $|F_h|$ and the D_2O ratios. For centrosymmetric bilayers the phase signs are only "+" or "−" (Franks and Lieb, 1979; Wiener and White, 1991). Insights into the bilayer structure were received by the calculation of neutron scattering length density (NSLD) profiles $\rho_s(x)$ (a.u.). For that purpose, Fourier transformation of the SF's was performed with (Nagle and Tristam-Nagle, 2000):

$$\rho_s(x) = a + b\frac{2}{d}\sum_{n=1}^{h_{max}} F_h \cos\left(\frac{2\pi hx}{d}\right) \tag{2}$$

where a and b are constants for the relative normalization of $\rho_s(x)$.

F_{h_deut} and F_{h_prot} were used for the calculation of the particularly profiles $\rho_{deut}(x)$ and $\rho_{prot}(x)$. Subtracting both, the deuterium difference $\rho_{diff}(x)$ was calculated, using

$$\rho_{diff}(x) = \rho_{deut}(x) - \rho_{prot}(x) \tag{3}$$

Appearing maxima in $\rho_{diff}(x)$ were highly connected to the position of the d_3-label within the lipid bilayers.

3. Results and discussion

3.1. Synthesis

The synthesis of DL-CER[AP]-C18-d_3 is shown in Schemes 1 and 2. For the preparation of the specific deuterated α hydroxy stearic acid, a procedure described by Mori and Funaki was used. According to the literature, an α amino acid as intermediate was formed, before the conversion to the α hydroxy acid was fulfilled (Mori and Funaki, 1985). First, it was necessary to synthesize the ω-deuterated hexadecyl bromide **5**. Although this bromide **5** is commercially available the starting material for the synthesis of the terminal labelled hexadecyl bromide **5** (Scheme 1) was 16-hexadecanolide **1** to achieve the required amounts for the latter steps of synthesis.

The 16-hexadecanolide (**1**) was transferred by transesterification in the methyl 16-hydroxyhexadecanoate (**2**) (Cundy and Gurr, 2000). The hydroxyl group was protected by reaction with fresh distilled 3,4-dihydro-2*H*-pyran (DHP) (Miyashita et al., 1977) to yield compound **3**. For the introduction of the CD_3-group the methyl ester function was reduced by a three step reaction: First, the ester was reduced with $LiAlD_4$ to CD_2-alcohol, followed by an esterification of the alcohol function with MesCl yielding the

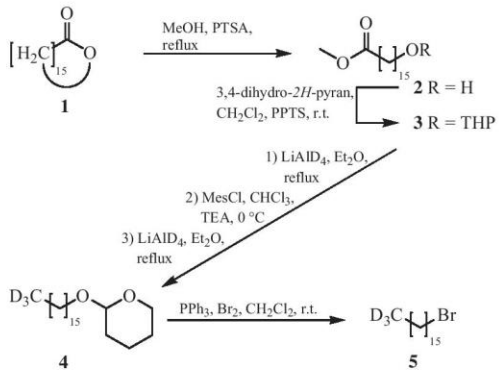

Scheme 1. Synthesis of the 1-bromohexadecane-16,16,16-D_3 5.

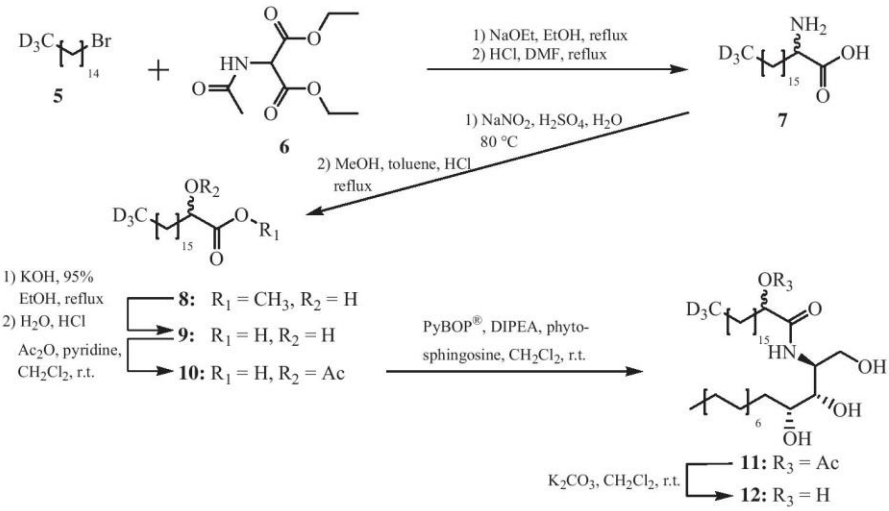

Scheme 2. Synthesis of the DL-CER[AP] 12 with a terminal deuterated α hydroxy stearic acid.

methansulfonate. In the third step the activated ester was reduced again via the use of $LiAlD_4$ to the terminal CD_3-group (Dobner and Nuhn, 1991; Tulloch, 1977). The obtained THP protected deuterated alkanol **4** was converted via bromine and triphenylphosphine to the hexadecyl bromide-16,16,16-d_3 (**5**) (Schwarz et al., 1975).

For the synthesis of the specifically deuterated DL-CER[AP] (Scheme 2) the diethyl acetaminomalonate (**6**) was alkylated with the alkyl bromide **5**, followed by acidic hydrolysis to form the α-amino acid **7** as a racemic mixture of both enantiomers. In the next step, the amino function was substituted by a hydroxy function by reaction with sodium nitrite and sulfuric acid (Mori and Funaki, 1985).

For a better purification, the obtained hydroxy acid was first esterified before purification. Afterwards the ester **8** was hydrolyzed under alkaline conditions to yield the acid **9** by common procedure. For the coupling to the ceramide, it was necessary to protect the free hydroxy group to avoid side reactions under the used conditions. Therefore we used a procedure described in the literature (Wisse et al., 2015). First, the hydroxy group was blocked as acetate ester **10**. The protected α hydroxy acid was bonded at phytosphingosine under usage of the coupling reagent PyBOP® (Coste et al., 1990; Sonnenberger et al., 2016). In a last step the acetylated ceramide **11** was deacetylated in order to obtain the DL-CER[AP]-C18-d_3. In spite of the difference of the R_f values, a separation of the diastereomers was not possible with the conducted column chromatography. The column was prepared using the wet method and the ceramide containing residue was adsorbed before chromatography. At a gradient of chloroform/methanol/ammonia (96/4/0.5 V/V/V) both diastereomers were eluted.

Additionally, a direct coupling reaction of the unprotected hydroxy acid **9** with the aminoalkohol phytosphingosine was tested because of the amino group is a better nucleophile than the hydroxy groups of the phytosphingosine. It resulted in the forming of the deuterated ceramide diastereomers and an additional product. This by-product has a slightly higher R_f than the L-diastereomer and a similar chromatographic behaviour like the L-form.

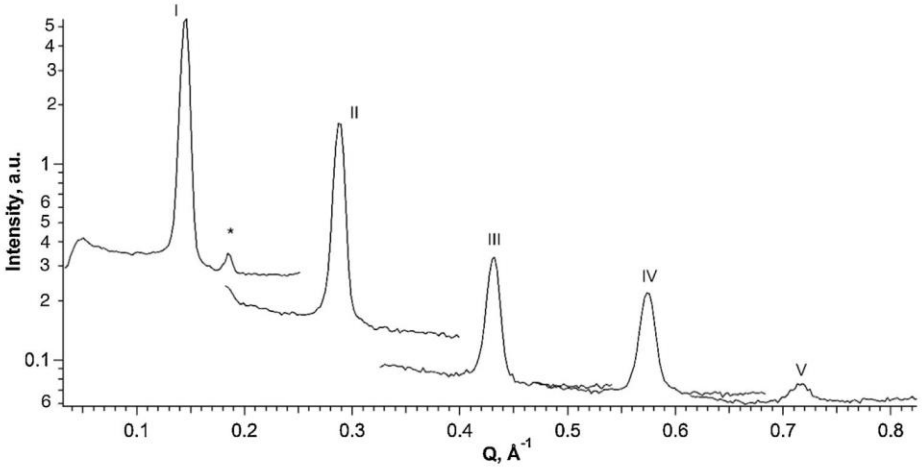

Fig. 2. Bragg peak pattern of sample_AP-d_3, received at 100% D_2O, 57% RH and 32 °C. The roman numbers indicate the 1st–5th Bragg peak orders. The asterisk marks the [010] diffraction peak of phase separated crystalline CHOL.

Via HPLC a diastereomer composition of 56% of the L-form and 44% of the D-form could be determined (see Fig. (d) in supplement data).

3.2. Neutron diffraction experiment

3.2.1. Discussion of the received SC lipid model membrane structure

The first approach of this study comprised the determination of the lamellar bilayer structure of the CER[AP]-C18-d_3 containing model membrane. As former experiments presented first ideas of the structural arrangement of a comparable lipid mixture (Ruettinger et al., 2008), the aim of the here presented study is to survey these previous results. Therefore, sample_AP-d_3 was prepared and measured next to sample_AP, which Ruettinger et al. (Ruettinger et al., 2008) used as a part of their study. Fig. 2 represents the neutron diffraction pattern of sample_AP-$d3$.

For both samples, a high-ordered system was obtained, up to the 5th diffraction order. The lamellar spacing was calculated with $d = 43.86 \pm 0.03$ Å. The small peak at $Q = 0.184$ Å indicated a surplus of crystalline cholesterol, which was not integrated in the lipid bilayers. But this was not affecting the lamellar lipid organization and further data treatment (Ali et al., 2006; de Jager et al., 2005). After the integration of the Bragg peak signals, the SFs were calculated following Eq. (1) and plotted against the D_2O ratios (see Fig. (b) in the supplemental data). The correlations between SFs and D_2O contrasts were nearly linear for all diffraction orders. With the expected positive or negative gains ($-+-+-$ for the first to the fifth order), the SF phase signs were used as received. The absolute SF values and Bragg peak positions are given in Table (a) in the supplemental data. By Fourier transformation (Eq. (2)), the NSLD profiles $\rho_s(x)$ for the D_2O contrasts were received (see Fig. 3). They are all centered at zero and have a relative scaling from the Fourier transformation. All $\rho_s(x)$ show comparable curves at the membrane center, where the alkyl chains of the lipids are located. The absent minima of the curves at x = 0 Å are highly connected to the presence of the deuterium labels in that area, referring to the positive b_{coh}. At both edges of the profiles, differences between the curves are visible. Due to the D_2O/H_2O exchange, we are able to localize water molecules within the bilayer. Calculating the water distribution function as difference between $\rho_s(x)_{100\%D2O}$ and $\rho_s(x)_{8\%D2O}$, the present maxima are highly connected to the presence of water, what we can educe from the function gains at both profile edges. In that area, the polar head groups of the lipids are located (Kiselev et al., 2005). In the middle of the membrane, the slightly fluctuation around zero suggests no presence of water alongside the alkyl chains. Based on the evaluation of the hydrophobic-hydrophilic boundary x_{HH} at 16.28 ± 0.03 Å (see Fig. (c) in the supplemental data), we can conclude, that the hydrophobic part of the bilayer is about 32.56 ± 0.06 Å and each polar part covers 5.65 ± 0.03 Å.

With a lamellar repeat distance of about 44 Å, the detected phase is smaller than the established short-periodicity phase with about 60 Å (Bouwstra et al., 1991) and even smaller than the spacings of sample_AP, Ruettinger et al. presented (46.3 Å and 45.3 Å). In native material, a more complex chain lengths distribution is given by the ceramides, resulting in a spacing of about 60 Å. Thus, the smaller d spacing is due to the presence of carbon chains with only 18 atoms. Nevertheless the application of CER[AP]-C18 as single ceramide component in this SC lipid model system induced the formation of a SPP. Smaller repeat distances were described elsewhere as well (Gruzinov et al., 2017; Kessner et al., 2008; Kiselev et al., 2005; Ruettinger et al., 2008; Ryabova et al., 2009, 2010). Furthermore, the profiles presented maxima within the hydrophobic area at ±12 Å, which Kiselev et al. connected to the position of integrated cholesterol.

3.2.2. Localization of deuterium label in CER[AP]-based SC lipid model membrane

The second approach of this neutron diffraction study, is the localization of the deuterium label of CER[AP]-C18 within the lipid membranes. Therefore, the NSLD profiles of the partially deuterated sample_AP-d_3 and non-deuterated reference sample_AP were calculated by Fourier transformation (Eq. (2)) using the normalized SFs. The profiles show distinct differences in the bilayer center (see Fig. 4). The NSLD profile $\rho_{prot}(x)$ of sample_AP has a distinct minimum representing the CH_3 groups (Kiselev et al., 2005). Moreover, the NSLD profile $\rho_{deut}(x)$ of the labelled sample_AP-d_3 has a significant maximum at the membrane center. Due to the positive values of b_{coh} for deuterium, this is a precious hint to the presence of CD_3.

According to Eq. (3), the deuterium difference $\rho_{diff}(x)$ was calculated. Thus, the maximum of $\rho_{diff}(x)$ at $x = 0$ Å represents the

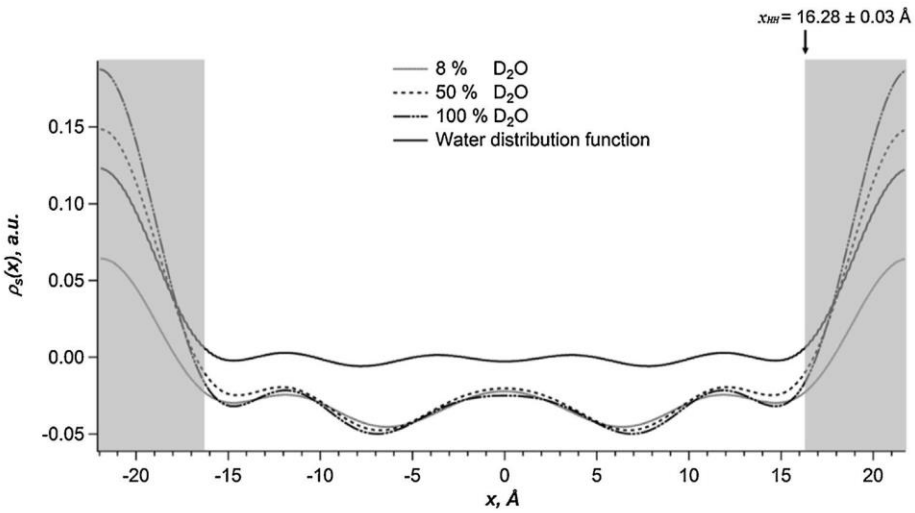

Fig. 3. NSLD profiles $\rho_s(x)$ across the bilayer of sample_AP-d_3 at 57% RH and 32 °C. The profiles received at all three D_2O ratios are given. The difference between $\rho_s(x)_{100\%D2O}$ and $\rho_s(x)_{8\%D2O}$ is the water distribution function. The grey boxes indicate the polar bilayer areas.

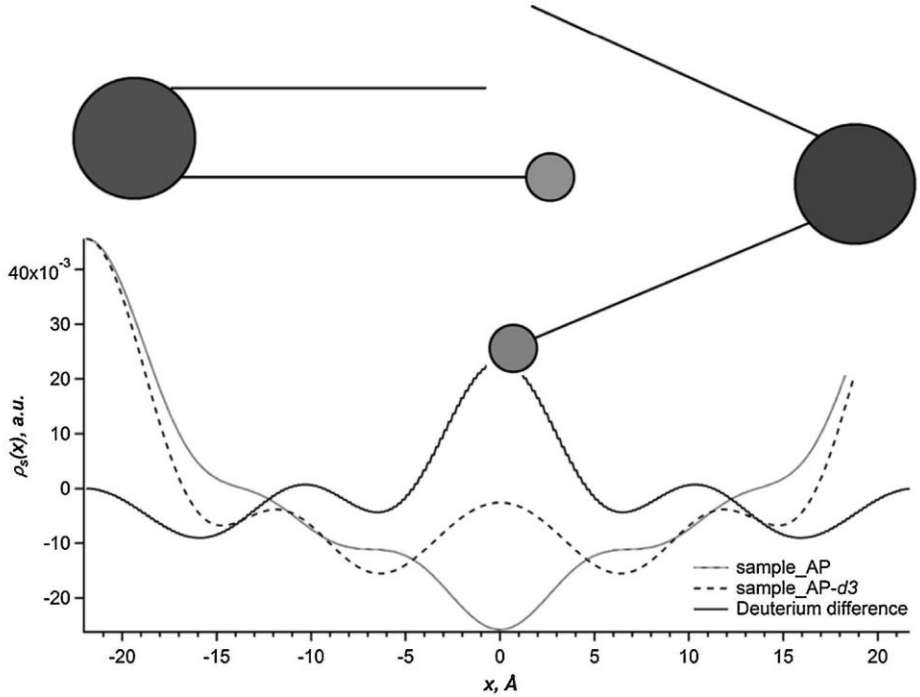

Fig. 4. NSLD profile $\rho_{diff}(x)$ (black line) as result of the difference of $\rho_{deut}(x)$ across the bilayer of sample_AP-d_3 (dotted line) and $\rho_{prot}(x)$ across the bilayer of sample_AP (grey line), received at 8% D_2O, 57% RH, and 32 °C. A possible position of CER[AP]-d_3 in its hairpin and V-shape conformation is presented.

high density of the appearing deuterium atoms. These results reveal the position of CD_3 groups clearly within the SC lipid model membranes. A proposed position of DL-CER[AP]-C18-d_3 is given in Fig. 4. The head groups are arranged in the polar membrane areas at both edges of the unit cell and the non-polar alkyl chains point towards the membrane center. Referring to a distance of 1.27 Å per all-*trans* C—C bonding (Petrache et al., 2000; Small, 1986), for the α hydroxy acid, a maximum chain length of 22.9 Å can be estimated. For a bilayer with two molecules arranged opposite each other, this would mean a spacing of about 46 Å, only for the alkyl chains. Including the spacing of the lipid head groups, the received repeat distance (~44 Å) is only explainable due to interdigitating CD_3 groups in the membrane center. But at this point, we are not able to determine the conformational states of the ceramide. The hairpin structure was assumed, as it is energetically more stable than the extended version (Kiselev et al., 2007). Moreover, we applied both enantiomers of CER[AP] and for them, different phase behaviors were described: The extended conformation is known to be dominantly for D-CER[AP], next to larger lamellar spacings (Raudenkolb et al., 2005). However, for L-CER[AP] a V-shape conformation was described together with smaller unit cell scales, (Raudenkolb et al., 2005). Due to the spacing of about 44 Å, a tilt of the CER is possible as well, as Fig. 4 presents. Nevertheless, the proposed CER[AP]-C18 position of Ruettinger et al. is reasonable.

In order to gain closer insights, further studies with separated diastereomers will be necessary. Therefore, the chemical synthesis of both of them is aimed in further studies.

As former comparable experiments of this and other groups introduced the location of fatty acids and cholesterol in SPPs in SC lipid model membrane (Kessner et al., 2008; Mojumdar et al., 2013; Schroeter et al., 2009b), the here presented results supplement the knowledge about the arrangement of CER[AP]-C18.

4. Conclusion

A diasteromer mixture of CER[AP] was synthesized with CD_3 group in the chain of the fatty acid. For the synthesis of the α hydroxy fatty acid a method described in the literature was used. Therefore, as intermediate, an α amino acid was formed by alkylation of a malonic acid derivate with a synthesized terminal deuterated alkyl bromide followed by conversion to the hydroxy acid. For the ceramide synthesis PyBOP® was used as coupling reagent. The diastereomer composition was determined by HPLC. The synthesized CER was characterized in a biophysical approach using neutron diffraction. Its application in a SC lipid model membrane enabled the localization of the deuterium label in the high-ordered lamellar structures, with a repeat distance of about 44 Å. The combination of the chosen technique and the complex synthesis of CER[AP]-d_3 enabled the molecular insight into the bilayer nano-structure.

Moreover, it is possible to use the deuterated CER as internal standard in LC–MS experiments as well as in infrared based techniques (Skolova et al., 2014, 2016) or ^2H NMR studies (Stahlberg et al., 2016, 2015).

Acknowledgements

The authors would like to thank the Helmholtz-Zentrum Berlin für Materialien und Energie (HZB, Berlin, Germany) for the allocation of beam time as well as the financial support. Evonik Industries AG (Essen, Germany) is gratefully acknowledged for the generous gift of DL-CER[AP]-C18. Moreover, the authors are thankful for the funding of the Deutsche Forschungsgemeinschaft (Projects: NE 427/30-1 and DO 463/6-1).

Appendix A. Supplementary data

Supplementary data associated with this article can be found, in the online version, at http://dx.doi.org/10.1016/j.chemphyslip.2017.02.001.

References

Ali, M.R., Cheng, K.H., Huang, J., 2006. Ceramide drives cholesterol out of the ordered lipid bilyer phase into the crystal phase in 1-palmitoyl-2-oleoyl-sn-glycero-3-phosphocholine/cholesterol/ceramide ternary mixtures. Biochemistry 45, 12629–12638.

Bouwstra, J.A., Gooris, G.S., van der Spek, J.A., Bras, W., 1991. Structural investigations of human stratum corneum by small-angle X-ray scattering. J. Invest. Dermatol. 97, 1005–1012.

Coste, J., Le-Nguyen, D., Castro, B., 1990. PyBOB: a new peptide coupling reagent devoid of toxic byproduct. Tetrahedron Lett. 31, 205–208.

Cser, F., 2001. About the Lorentz correction used in the interpretatin of small angle X-ray scattering data of semicrystalline polymers. J. Appl. Polym. Sci. 80, 2300–2308.

Cundy, D.J., Gurr, P.A., 2000. An improved synthesis of ± methyl eicosanoic acid. Org. Prep. Proced. Int. 32, 461–468.

de Jager, M.W., Gooris, G.S., Dolbnya, I.P., Bras, W., Ponec, M., Bouwstra, J.A., 2003. The phase behaviour of skin lipid mixtures based on synthetic ceramides. Chem. Phys. Lipids 125, 123–134.

de Jager, M.W., Gooris, G.S., Ponec, M., Bouwstra, J.A., 2005. Lipid mixtures prepared with well-defined synthetic ceramides closely mimic the unique stratum corneum lipid phase behavior. J. Lipid Res. 46, 2649–2656.

de Sousa Neto, D., Gorris, G., Bouwstra, J., 2011. Effect of the w-acylceramides on the lipid organization of stratum corneum model membranes evaluated by X-ray diffraction and FTIR studies. Chem. Phys. Lipids 164, 184–195.

Dobner, B., Nuhn, P., 1991. Syntheses of deuterium-labelled methyl branched fatty acids. Chem. Phys. Lipids 60, 21–28.

Eichner, A., Sonnenberger, S., Dobner, B., Hauß, T., Schroeter, A., Neubert, R.H.H., 2016. Localization of methyl-branched ceramide [EOS] species within the long-periodicity phase in stratum corneum lipid model membranes: a neutron diffraction study. Biochim. Biophys. Acta Biomembr. 1858, 2911–2922.

Elias, P.M., 1983. Epidermal lipids, barrier function and desquamation. J. Invest. Dermatol. 80, 44s–49s.

Engelbrecht, T.N., Schroeter, A., Hauss, T., Neubert, R.H.H., 2011. Lipophilic penetration enhancers and their impact to the bilayer structure of stratum corneum lipid model membranes: neutron diffraction studies based on the example Oleic Acid. Biochim. Biophys. Acta Biomembr. 1808, 2798–2806.

Engelbrecht, T.N., Demé, B., Dobner, B., Neubert, R.H.H., 2012a. Study of the influence of the penetration enhancer isopropyl myristate on the nanostructure of stratum corneum lipid model membranes using neutron diffraction and deuterium labelling. Skin Pharmacol. Physiol. 25, 200–207.

Engelbrecht, T.N., Schroeter, A., Hauß, T., Demé, B., Scheidt, H.A., Huster, D., Neubert, R.H.H., 2012b. The impact of ceramides NP and AP on the nanostructure of stratum corneum lipid bilayer: part I: neutron diffraction and ^{2}H NMR studies on multilamellar models based on ceramides with symmetric alkyl chain length distribution. Soft Matter 8, 2599–2607.

Franks, N.P., Lieb, W.R., 1979. The structure of lipid bilayers and the effects of general anaesthetics. J. Mol. Biol. 133, 469–500.

Gray, G.M., Yardley, H.J., 1975. Different populations of pig epidermal cells: isolation and lipid composition. J. Lipid Res. 16, 441–447.

Groen, D., Gooris, G.S., Bouwstra, J.A., 2009. New insights into the stratum corneum lipid organization by X-ray diffraction analysis. Biophys. J. 97, 2242–2249.

Gruzinov, A.Y., Zabelin, A.V., Kiselev, M.A., 2017. Short periodicity phase based on ceramide [AP] in the model lipid membranes of stratum corneum does not change during hydration. Chem. Phys. Lipids 202, 1–5.

Kessner, D., Kiselev, M.A., Hauss, T., Dante, S., Wartewig, S., Neubert, R.H.H., 2008. Localisation of partially deuterated cholesterol in quaternary SC lipid model membranes: a neutron diffraction study. Eur. Biophys. J. 37, 1051–1057.

Kessner, D., Brezesinski, G., Funari, S.S., Dobner, B., Neubert, R.H.H., 2010. Impact of long chain w-acylceramides on the stratum corneum lipid nanostructure: part 1: Thermotropic phase behaviour of CER[EOS] and CER[EOP] studied using X-ray powder diffraction and FT-Raman spectroscopy. Chem. Phys. Lipids 163, 42–50.

Kiselev, M.A., Ryabova, N.Y., Balagurov, A.M., Dante, S., Hauss, T., Zbytovska, J., Wartewig, S., Neubert, R.H.H., 2005. New insights into the structure and hydration of a stratum corneum lipid model membrane by neutron diffraction. Eur. Biophys. J. 34, 1030–1040.

Kiselev, M.A., Ermakova, E.V., Gruzinov, A.Y., Zabelin, A.V., 2007. Conformation of ceramide 6 molecules and chain-flip transitions in the lipid matrix of the outermost layer of mammalian skin, the Stratum corneum. Crystallogr. Rep. 52, 525–528.

Madison, K.C., Swartzendruber, D.C., Wertz, P.W., Downing, D.T., 1987. Presence of intact intercellular lipid lammellae in the upper layers of the stratum corneum. J. Invest. Dermatol. 88, 714–718.

Miyashita, N., Yoshikoshi, A., Grieco, P.A., 1977. Pyridinium p-toluenesulfonate: a mild and efficient catalyst for the tetrahydropyranylation of alcohols. J. Org. Chem. 42, 3772–3774.

Mojumdar, E.H., Groen, D., Gooris, G.S., Barlow, D.J., Lawrence, M.J., Demé, B., Bouwstra, J.A., 2013. Localization of cholesterol and fatty acid in a model lipid membrane: a neutron diffraction approach. Biophys. J. 105, 911–918.

Mojumdar, E.H., Gooris, G.S., Barlow, D.J., Lawrence, M.J., Demé, B., Bouwstra, J.A., 2015. Skin Lipids: localization of ceramide and fatty acid in the unit cell of the long periodicity phase. Biophys. J. 108, 2670–2679.

Mojumdar, E.H., Gooris, G.S., Groen, D., Barlow, D.J., Lawrence, M.J., Demé, B., Bouwstra, J.A., 2016. Stratum corneum lipid matrix: localization of acyl ceramide and cholesterol in the unit cell of the long periodicity phase. Biochim. Biophys. Acta Biomembr. 1858, 1926–1934.

Mori, K., Funaki, Y., 1985. Synthesis of (4E,8E,2S,3R,2'R)-N-2'-hydroxyhexadecanoyl-9-methyl-4,8-sphingadiemine, the ceramide portion of the fruiting-inducing cerebroside in a basidiomycete schizophyllum commune, and its (2R,3S)-isomer. Tetrahedron 41, 2369–2377.

Nagle, J.F., Tristam-Nagle, S., 2000. Structure of lipid bilayers. Biochim. Biophys. Acta 1469, 159–195.

Petrache, H.I., Dodd, S.W., Brown, M.F., 2000. Area per lipid and acyl length distribution in fluid phosphatidylcholines determined by ^{2}H NMR spectroscopy. Biophys. J. 79, 3172–3192.

Raudenkolb, S., Wartewig, S., Neubert, R.H.H., 2005. Polymorphism of ceramide 6: a vibrational spectroscopic and X-ray powder diffraction investigation of the diastereomers of *N*-(α-hydroxyoctadecanoyl)-phytosphingosine. Chem. Phys. Lipids 133, 89–102.

Ruettinger, A., Kiselev, M.A., Hauss, T., Dante, S., Balagurov, A.M., Neubert, R.H.H., 2008. Fatty acid interdigitation in stratum corneum model membranes: a neutron diffraction study. Eur. J. Dermatol.: EJD 37, 759–771.

Ryabova, N.Y., Kiselev, M.A., Balagurov, A.M., 2009. Transition processes in stratum corneum model lipid membranes with a mixture of free fatty acids. Biofizika 54, 852–862.

Ryabova, N.Y., Kiselev, M.A., Dante, S., Hauß, T., Balagurov, A.M., 2010. Investigation of stratum corneum lipid model membranes with free fatty acid composition by neutron diffraction. Eur. Biophys. J. 39, 1167–1176.

Scheuplin, R.J., 1976. Permeability of the skin: a review of major concepts and some new developments. J. Invest. Dermatol. 67, 672–676.

Schroeter, A., Kessner, D., Kiselev, M.A., Hauß, T., Dante, S., Neubert, R.H.H., 2009a. Basic nanostructure of stratum corneum lipid matrices based on ceramides [EOS] and [AP]: A neutron diffraction study. Biophys. J. 97, 1104–1114.

Schroeter, A., Kiselev, M.A., Hauß, T., Dante, S., Neubert, R.H.H., 2009b. Evidence of free fatty acid interdigitation in stratum conreum model membranes based in ceramide [AP] by deuterium labelling. Biochim. Biophys. Acta 1788, 2194–2203.

Schroeter, A., Kiselev, M.A., Hauß, T., Dante, S., Neubert, R.H.H., 2009c. Evidence of free fatty acid interdigitation in stratum corneum model membranes based in ceramide [AP] by deuterium labelling. Biochim. Biophys. Acta 1788, 2194–2203.

Schroeter, A., 2010. The Role of Ceramide (AP) for the Structural Assembly of Stratum Corneum Lipid Model Membranes. Institute of Pharmacy. Martin Luther University Halle-Wittenberg, Halle.

Schwarz, M., Oliver, J.E., Sonnet, P.E., 1975. Synthesis of 3,11-dimethyl-2-nonacosane, a sex pheromone of the german cockroach. J. Org. Chem. 40, 2410–2411.

Sears, V.F., 1992. Neutron scattering lengths and cross section. Neutron News 3, 26–37.

Seul, M., Sammon, M.J., 1990. Preparation of surfactant multilayer films on solid substrates by deposition from organic solution. Thin Solid Films 185, 287–305.

Skolova, B., Hudska, K., Pullmannova, P., Kovacik, A., Palat, K., Roh, J., Fleddermann, J., Estrela-Lopis, I., Vavrova, K., 2014. Different phase behavior and packing of ceramides with long (C16) and very long (C24) acyls in model membranes: infrared spectroscopy using deuterated lipids. J. Phys. Chem. B 118, 10460–10470.

Skolova, B., Janusova, B., Vavrova, K., 2016. Ceramides with a pentadecasphingosine chain and short acyls have strong permeabilization effects on skin and model lipid membranes. Biochim. Biophys. Acta Biomembr. 1858, 220–232.

Small, D.M., 1986. The Physical Chemistry of Lipids. Plenum Press, New York.

Sonnenberger, S., Lange, S., Langner, A., Neubert, R.H.H., Dobner, B., 2016. Synthesis of ceramides NS and NP with perdeuterated and specifically ω deuterated *N*-acyl residues. J. Label. Compd. Radiopharm. 59, 531–542.

Stahlberg, S., Skolova, B., Madhu, P.K., Vogel, A., Vavrova, K., Huster, D., 2015. Probing the role of the ceramide acyl chain length and sphingosine unsaturation in model skin barrier lipid mixtures by 2H solid-state NMR spectroscopy. Langmuir 32, 4906–4915.

Stahlberg, S., Lange, S., Dobner, B., Huster, D., 2016. Probing the role of ceramide headgroup polarity in short-chain model skin barrier lipid mixtures by ^{2}H solid-state NMR spectroscopy. Langmuir 32, 2023–2031.

Sui, B., Yeh, E.A.H., Curran, D.P., 2010. Assignment of the structure of petrocortyne A by mixture syntheses of four candidate stereoisomers. J. Org. Chem. 75, 2942–2954.

t'Kindt, R., Jorge, L., Dumont, E., Couturon, P., David, F., Sandra, P., Sandra, K., 2012. Profiling and characterizing skin ceramides using reversed-phase liquid chromatography-quadrupole time-of-flight mass spectrometry. Anal. Chem. 84, 403–411.

Takahashi, H., Imao, M., Matsushita, Y., Hatta, I., 1997. Small-angle neutron scattering study on short-chain phosphatidylcholine micelle in the presence of sorbitol. Prog. Colloid Polym. Sci. 106, 223–227.

Tulloch, A.P., 1977. Synthesis of methyl 16-trideuteriohexadecanoate. Chem. Phys. Lipids 91, 85–96.

Wertz, P.W., van den Bergh, B., 1998. The physical, chemical and functional properties of lipids in the skin and other biological barriers. Chem. Phys. Lipids 91, 85–96.
White, S.H., Mirejovsky, D., King, G.I., 1988. Structure of lamellar lipid domains and corneocyte envelopes of murine stratum corneum: an X-ray diffraction study. Biochemistry 27, 3725–3732.
Wiener, M.C., White, S.H., 1991. Fluid bilayer structure determination by the combined use of x-ray and neutron diffraction. Biophys. J. 59, 174–185.
Wisse, P., de Geus, M.A.R., Cross, G., van den Nieuwendijk, A.M.C.H., van Rooden, E.J., van den Berg, R.J.B.H.N., Aerts, J.M.F.G., van der Marel, G.A., Codée, J.D.C., Overkleeft, H.S., 2015. Synthesis of 6-hydroxysphingosine and α-hydroxy ceramide using a cross-metathesis strategy. J. Org. Chem. 80, 7258–7265.
Worchester, D.L., Franks, N.P., 1976. Structural Analysis of hydrated egg lecithin and cholesterol bilayers, II. Neutron Diffraction. J. Mol. Biol. 100, 359–378.
Yardley, H.J., Summerly, R., 1981. Lipid composition and metabolism in normal and diseased epidermis. Pharmacol. Ther. 13, 383.
Young, J.F., 1967. Humidity control in the laboratoy using salt solutions. J. Appl. Chem. 17, 241–245.

4.2 Localization of methyl-branched ceramide [EOS] species within the long-periodicity phase in stratum corneum lipid model membranes: A neutron diffraction study

Adina Eichner, Stefan Sonnenberger, Bodo Dobner, Thomas Hauß, Annett Schroeter, Reinhard H.H. Neubert, *Biochimica et Biophysica Acta- Biomembranes* (2016) **1858** p.2911-2922

Online version: http://dx.doi.org/10.1016/j.bbamem.2016.09.00

Biochimica et Biophysica Acta 1858 (2016) 2911–2922

Contents lists available at ScienceDirect

Biochimica et Biophysica Acta

journal homepage: www.elsevier.com/locate/bbamem

Localization of methyl-branched ceramide [EOS] species within the long-periodicity phase in stratum corneum lipid model membranes: A neutron diffraction study

Adina Eichner [a], Stefan Sonnenberger [a], Bodo Dobner [a], Thomas Hauß [b], Annett Schroeter [a,c], Reinhard H.H. Neubert [a,d,*]

[a] Institute of Pharmacy, Martin Luther University Halle-Wittenberg, 06120 Halle/Saale, Germany
[b] Institute of Soft Matter and Functional Materials, Helmholtz-Zentrum Berlin für Materialien und Energie, 14109 Berlin, Germany
[c] DR. KADE Pharmazeutische Fabrik GmbH, 12277 Berlin, Germany
[d] Institute of Applied Dermatopharmacy at the Martin Luther University Halle-Wittenberg, 06120 Halle/Saale, Germany

ARTICLE INFO

Article history:
Received 20 June 2016
Received in revised form 25 August 2016
Accepted 3 September 2016
Available online 07 September 2016

Keywords:
Stratum corneum
Ceramides
Lipid model membrane
Long-periodicity phase
Short- periodicity phase
Neutron diffraction

ABSTRACT

The outermost layer of the mammalian skin, the stratum corneum (SC), is a very thin structure and realizes simultaneously the main barrier properties. The penetration barrier for xenobiotica is mostly represented by a complex lipid matrix. There is great interest in the subject of getting information about the arrangement of the lipids, which are mainly ceramides (CER), free fatty acids (FFA) and cholesterol (CHOL). SC lipid model membranes containing synthetically derived lipids in a non-physiological ratio were investigated. To compare the study to a former experiment, a methyl-branched ceramide [EOS] species in presence of the ultra-long chain CER[AP], CHOL and behenic acid (23/10/33/33, wt%) was applied. The membrane structure was studied using the very versatile technique of neutron diffraction. We were able to identify a long-periodicity phase (LPP) with a size of 114 Å or 118 Å with CER[EOS]-br in a ratio of >60 wt% of the ceramides. Furthermore, we figured out two additional coexisting short-periodicity phases (SPP) with repeat distances of 48 Å and 45 Å, respectively. Partial deuterations of CER[EOS]-br and CER[AP] enabled the localization of the molecules within the multiphase system. CER[EOS]-*d3* was present in the LPP, but absent in both SPP. CER[AP]-*d3* was determined in both short phases but not localized within the LPP. Besides, we revealed influences of humidity and time with respect to the long-periodicity phase.

1. Introduction

The stratum corneum (SC), as the outermost layer of the epidermis, represents simultaneously the main barrier function of human skin [1,2]. This property is mainly connected to the SC structure where dead keratin-filled cells (corneocytes) are embedded into a complex lipid matrix [3]. Here, the multilamellar arrangement of the lipids is known to play a fundamental role in the SC barrier [4,5]. The desire to overcome the skin barrier for an optimized pharmaceutical therapy demands closer insights into the arrangement of the lipids on a nano-scaled level. The SC is the only human lipid membrane structure without phospholipids. Instead, the major lipids are ceramides (CER), free fatty acids (FFA) and cholesterol (CHOL), next to its ester cholesterol sulfate (ChS) [6–8]. Several studies revealed the quantitative lipid ratios [9–13]. Ceramides are the main compounds of the SC, however, they are also the most heterogeneous lipid fraction. They differ in their head group structure, their number of carbon atoms in the acyl chains as well as in the acyl chain structure itself, so that in total a number of 342 individual compounds was determined to this day [14]. CERs are classified into 19 subclasses, including the free and the 1-O-acyl-CER species [14–17]. Wertz and Downing initiated a simple name system based on numbers in 1983. They named the CERs after their chromatographic retention (CER1-6) [18]. Later on, the numbers were given as the CERs were detected and described. Motta et al. [19] proposed a second name system in 1993 which was complemented by Robson [20], t'Kindt [17] and Rabionet [16]. Therefore, a minimal two-letter code was used to describe the CER subspecies. The first letter represents the *N*-acetylated fatty acid, i.e. **N** stands for a **n**on-hydroxy fatty acid and **A** indicates an **α**-hydroxy fatty acid. In addition, for several subspecies, the installation of a third letter was necessary to notify an additional **e**sterified fatty acid (**E**). For the description of the sphingoid bases the following letters

Abbreviations: b_{coh}, coherent neutron scattering lengths; CER, ceramide; CHOL, cholesterol; *d*, deuterium; FFA, free fatty acid; *Fh*, structure factor (SF); LPP, long-periodicity phase; SPP, short-periodicity phase; SC, stratum corneum.

* Corresponding author at: Institute of Pharmacy, Martin Luther University Halle-Wittenberg, 06120 Halle/Saale, Germany.
E-mail address: reinhard.neubert@pharmazie.uni-halle.de (R.H.H. Neubert).

http://dx.doi.org/10.1016/j.bbamem.2016.09.002
0005-2736/

were recommended: **P** (phytosphingosine), **S** (sphingosine), **DS** (dihydrosphingosine), **H** (6-hydroxy-sphingosine) and **T** (dihydroxy-dihydrosphingosine) as the most recent one [17]. Up to date, the structure of the **T**-base is not yet completely defined.

CERs are important for the structure and perpetuation of the SC barrier properties [21]. SC membrane structure determination experiments were done using X-ray techniques [22,23], but a complete elucidation of the molecular arrangement of the SC lipids is not yet performed. Using the very versatile technique of neutron diffraction, numerous insights into this subject were possible in the last decade [24–37]. Neutrons offer a relevant advantage over X-rays as they are interacting with the atomic nuclei of biological molecules and the scattering power is given by the nuclei's coherent scattering length. Due to the different scattering lengths b of the isotopes hydrogen (^{1}H) with b = −3.74 fm and deuterium (^{2}H) with b = +6.67 fm, neutrons are able to discriminate between them. A specific deuteration is tagged to a defined position of the CER, which enables its localization in the membrane profile. However, native SC material is too complex for detailed insights into the SC membrane structure. For the current study, a simple model was applied containing certain synthetic lipids. The variability of the natural material, concerning the various chain lengths and head group structures of the lipids, can be overcome by using chemical derived lipids [38]. The lipid organization of SC lipid models and native SC can be compared as shown before [39,40].

In the present study, the long-chain CER[AP]-C18 and a modified CER based on the ultralong-chain ω-acyl CER[EOS]-C30-C18:2 were applied. With an amount of 8.8 wt% and 6.5 wt% of the CER fraction, CER[AP] and CER[EOS] are present abundantly in native SC [17]. In former neutron diffraction studies CER[AP] played an important role in the assembling process of SC lipid model membranes [25,26,29,41]. CER[EOS] is the most nonpolar CER with quantitative relevance in natural SC. The more nonpolar ceramides [EODS] (0.4 wt% [17]) and the group of 1-O-acylceramides (2.3% [16]) were present only in minor amounts. However, CER[EOS] is mandatory for the SC barrier function [42]. Decreased CER[EOS] levels were observed in several diseases like atopic dermatitis or psoriasis, where the protecting properties are limited [43,44]. As well as its shorter counterpart CER[AP], CER[EOS] is highly involved in the lipid organization within the SC [45–47]. Especially, the coexistence of two crystalline lamellar phases in native SC, was a main point of interest in experiments during the last decade [48–50]. Bouwstra et al. determined the phases in human SC, referred to as short- periodicity phase (SPP) and long- periodicity phase (LPP) [48]. The SPP is described with an approximate repeat distance of <60 Å and its structure is mostly depending on the presence of long chain CERs as [AP], [AH] or [NS] [49,51]. The existence of the LPP, with a unit cell scale of <130 Å [49,52] mainly depends on the appearance and amount of ω-esterified ultra-long chain ceramides as [EOS] [39, 53–55]. But surprisingly, a recent study on SC lipid models revealed a LPP formation in absence of any ultra-long chain CER [56]. Moreover, the LPP arrangement seems to be influenced by the surrounding humidity. Kessner et al. were able to prove that in a bulk phase, CER[EOS] needs high humidity for the formation of the LPP [57]. A current image of the LPP is a three layer unit cell [47,58], where symmetric as well as asymmetric internal structures were found [59,60]. In detail, the arrangement of the LPP forming lipids is not yet finally defined. Thus, the presence and organization of the LPP in native material and in SC model systems is highly discussed in over the last years [61,62]. Recently, Mojumdar and co-workers were able to observe the LPP in neutron diffraction studies on SC lipid model membranes for the first time. Next to the lipid-trilayer-structure, they described the position of a very long chain CER, a FFA, CHOL and even ultra-long chain ω-acyl CER[EOS] using perdeuterated lipids [34,35]. Hence, closer insights into the assembling of the here applied SC lipid mixture are necessary. The application of specifically deuterated CERs will enable their localization and give additional information about their phase behavior.

2. Experimental part of neutron diffraction study

2.1. Materials

With the aim to determine the mutual effects of the molecules to each other, only a limited number of lipids with certain chain lengths was chosen. The CER[AP]-C18 ((N-(a-hydroxyoctadecanoyl)-phytosphingosine)) was a gift of Evonik Industries AG (Essen, Germany). With a purity of 98% the diastereoisomeric mixture (DL-CER[AP]) was not further treated. The deuterated lipids CER[AP]-C18-*d3* (DL-CER[AP]-*d3*) and CER[EOS]-C30-C16-*d3* were obtained by our own synthesis, which will be published soon. The protonated ultra-long chain CER[EOS]-C30-C16-br was described earlier by Engelbrecht et al., who figured out its comparability to the native CER[EOS]-C30-C18:2 by neutron diffraction and performed further characterizations of the molecule by ^{2}H NMR and DSC experiments [36]. For the specific deuteration of the applied CER[EOS]-*d3,* it was required to esterify the CER's fatty acid with a saturated FFA, here palmitic acid (PA) instead of linoleic acid with its unsaturated bindings. Furthermore, PA got a methyl group branching at position C10. With the branched methyl group, it was possible to perform the H/D exchange to receive the partial deuterated CER. The identities of the synthesized lipids were proven by high resolution mass spectrometry (M_r CER[AP] = 599.546 g mol^{-1}; M_r CER[AP]-*d3* = 605.550 g mol^{-1}; M_r CER[EOS]-br = 1001.971 g mol^{-1}; M_r CER[EOS]-*d3* = 1005.710 g mol^{-1}. Fig. 1 illustrates the chemical structures of the SC lipids, used for this experiment.

Cholesterol (purity ≥99%), behenic acid (BA) (≥99%), D_2O (99.9%), NaBr (≥99%), and K_2SO_4 (≥99%) were purchased from Sigma Aldrich GmbH (Steinheim, Germany). The organic solvents chloroform and methanol were used in GC grade (SupraSolv®, Merck Millipore KGaA (Darmstadt, Germany)). As wafers, polished quartz slides (Spectrosil 2000, 65 × 25 × 0.3 mm) from Saint Gobain (Wiesbaden, Germany) were used. The lipids were deposited on the slides by a Hamilton syringe model 1001 RN SYR 1000 μl.

2.2. Sample preparation

For the localization of the deuteration, it was necessary to prepare samples with one of the lipids labelled and one sample completely hydrogenated, as reference sample. The native lipid composition is equimolar. Here, it is related to the lipid mass ratio, corresponding to former experiments on that mixture [25,36]. To compare the phase behavior of CER[EOS]-br and its deuterated version to the neutron diffraction study of Engelbrecht et al. [36], the lipid ratio was equal. Although the level of the ultra-long chain CER with about 60 wt% of the CER fraction was much higher than in native material (6.5 wt%) [17,63], it was intentionally chosen in order to create a LPP. With the aim to receive high ordered lipid multilayers, the samples were prepared in reference to an earlier published method [64]. The lipids were dissolved separately in chloroform/methanol (2:1; v/v), reaching a concentration of 10 mg/ml. Afterwards, they were mixed up to the desired ratio (wt%) to get the final SC lipid solution (see Table 1).

Using a Hamilton syringe, a volume of 1200 μl of the lipid mixtures I–III was deposited on quartz wafers, which had a temperature of 70 °C. The lipids covered an area of 45 × 25 mm^2, respectively. Due to a vacuum storage of 12 h, the rest of the solvents were removed. Subsequently, for a stable lipid orientation, an annealing cycle was performed, meaning a heating (75 °C) and cooling (25 °C) treatment at 100% RH for at least 4 h (2 h 75 °C, 1 h 25 °C, 1 h 75 °C, cooldown to 25 °C). Thereby the lamellar lipid layers were highly ordered [65], resulting in a higher number of structure factors [66] as the procedure is well-established in neutron scattering experiments on SC lipid model membranes [32,33,35–37,41, 66–70].

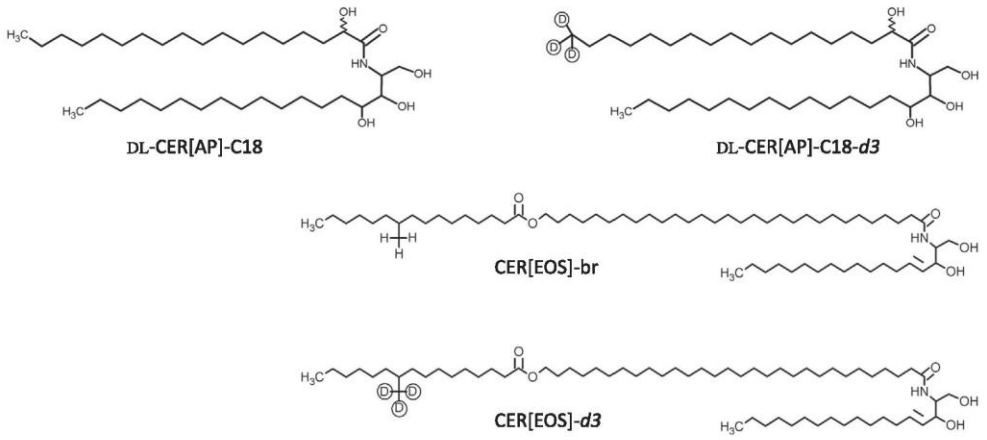

Fig. 1. Chemical structures of the applied ceramides [AP] and [EOS]-br next to their deuterated analogs.

2.3. Neutron diffraction experiment

The neutron diffraction experiment was performed at the V1 Membrane Diffractometer at the Helmholtz-Zentrum für Materialien und Energie (HZB, Berlin, Germany), located at a cold neutron source. Due to beam time allocation, the experiment was split into two parts with a break of three months in between. By the position of the pyrolytic graphite monochromator, wavelengths of $\lambda = 4.570$ Å (1st measurement) and $\lambda = 4.568$ Å (2nd measurement) were realized. Further, the distance between the sample and the two-dimensional position-sensitive ^{3}He detector (area: 20×20 cm^2; 1.5×1.5 mm^2 spatial resolution) were about 101.24 cm (1st measurement) and 101.81 cm (2nd measurement). A more detailed setup of an experiment at V1 was described earlier by Ruettinger et al. [41]. The intensities of the scattered neutrons were recorded as θ-2θ-scans, due to the resulting multiphase system and its high mosaicity. This ensured that all peaks were detected. To realize a constant and defined temperature (T) and relative humidity (RH), the samples were mounted in lockable aluminum chambers. The temperature was externally controlled and set to 32 °C, which corresponds to the skin temperature. The RH was accomplished by a saturated salt solution in the respective D_2O/H_2O contrast, where either potassium sulfate realized a constant value of 98% RH or sodium bromide a value of 57% RH [71–73]. According to former results, the high humidity was selected additionally to increase the chance for a LPP formation [57]. Every sample was measured at three different H_2O/D_2O ratios (0/100; 50/50; 92/8% (v/v)) in order to determine the phase signs of the calculated structure factors (SF). All samples needed an equilibration time of approximately 8 h after every change of D_2O contrast. It was proven before, that 8–9 h are necessary to achieve a steady level of hydration of the SC lipid model membranes [25,36,37].

During the neutron diffraction experiment, the ^{3}He detector registered the intensities I of the neutrons, which were scattered at the lattice structures of the lipid membranes. I was measured as a function of 2θ, meaning the scattering angle. Together with the wavelength λ of the incoming monochromatic neutron beam, the scattering vector Q is defined as $Q = (4\pi \sin\theta)/\lambda$. The determination of the positions of equidistant Bragg peaks (Q_n) in the diffraction pattern enabled the calculation of the lamellar periodicity d (d-spacing), using, with n as the Bragg peak's number of order. The integrated intensities of the peaks I_h of the h^{th} order were determined by Gaussian fits [74], using the software package IGOR Pro Version 6.34 A (WaveMetrics Inc., Portland, OR, USA). Further information about diffraction data treatment of lipid layer structures was described elsewhere [65,75]. The absolute value of the structure factors (SF; F_h) were calculated as $F_h = \sqrt{h \cdot A_h(\theta) \cdot I_h}$, with $A_h(\theta)$ as absorption correction and h as Lorentz factor, which related to the data collection geometry [76]. The absorption correction was performed assuming a sample thickness of 7 μm and linear absorption coefficient of 6 cm^{-1}. The determination of the F_h's phase sign - for centrosymmetric bilayers they are "+" or "−" only - was done by contrast variation, as mentioned before [66,74]. Furthermore, the calculation of neutron scattering length density (NSLD) profiles $\rho_s(x)$ was performed in order to receive insights into the lipid membrane structures on a nanoscaled level. The Fourier transformation of the SF's was calculated as [75]:

$$\rho_s(x) = a + b\frac{2}{d}\sum_{n=1}^{h_{max}} F_h \cos\left(\frac{2\pi h x}{d}\right) \quad (1)$$

with a and b as unknown variables for the relative normalization of $\rho_s(x)$ and d as the unit cell scale. The localization of the deuterium atoms is achieved by the calculation of the difference density $\rho_{diff}(x) = \rho_{deut}(x) - \rho_{prot}(x)$, with ρ_{deut} the NSLD of the specifically deuterated sample and $\rho_{prot}(x)$ the NSLD of the per-protonated sample. The resulting maxima in $\rho_{diff}(x)$ are directly connected to the presence of the labelled group at this position within the lipid unit cell.

Table 1
Composition of the investigated multilamellar membranes. For determination of the deuterated label, these systems included one deuterated lipid, in italic.

SC lipid membrane model system	Designation	Ratio wt%
I CER[AP]/CER[EOS]-br/CHOL/BA	AP_EOS-br	10/23/33/33
II CER[AP]/CER[EOS]-*d3*/CHOL/BA	AP_EOS-*d3*	10/23/33/33
III CER[AP]-*d3*/CER[EOS]-br/CHOL/BA	AP-*d3*_EOS-br	10/23/33/33

3. Results and discussion

3.1. Three-phase-system

The first approach of the study was the creation of a LPP in the applied lipid system. Therefore, the ratio of the methyl branched ultra-long chain ω-acyl CER[EOS] analog was up to >60% of the CER fraction, as ultra-long chain CERs are supposed to be necessary for the formation of a long-periodicity phase [53–55]. The neutron diffraction experiment was repeated partially after three months. Thereby, changes in the phase structure were obtained only for the LPP, in detail an increased unit cell scale. The time-depending changes of the LPP will be discussed in the section `Equilibration as a function of time`. The control sample I was characterized completely at the D_2O/H_2O contrasts at low humidity during the 2nd measurement. Differences in the peak positions for the LPP correspond to the time depending shifts and will be commented

on later. Three separated lipid phases were detected in the protonated SC lipid sample (see Fig. 2). In detail a short- periodicity phase (a) with about 48 Å, a long- periodicity phase (b) with a repeat distance of about 118 Å and a very short- periodicity phase (c) with about 45 Å were found. Thereby, for the short (a) and for the long (b) phase, highly ordered systems were obtained with diffraction peaks up to the 7th lamellar order. For the very short- periodicity phase (c), only three lamellar orders were determined. In former neutron diffraction experiments, as well as for both short phases (a) and (c), the peak intensities were decreasing from the first to the last diffraction order [24–26,28,33,41]. Here, for the long phase (b), the intensities were rising from the first to the third order and decreasing afterwards. Due to the highest peak area value for the 3rd Bragg peak order, the special structure of the NSLD profile $\rho_s(x)$ for the long- periodicity phase was reasoned, as shown before [34,35]. For the control sample, the 4th and the 6th diffraction orders of the long- periodicity phase (b) were not detected. The 5th (0.258 $Å^{-1}$) and the 7th (0.364 $Å^{-1}$) orders were only visible as shoulders of the 2nd and 3rd diffraction peaks of phase (a). Nonetheless, the integration of the signals was separately performable. Additionally, the L1 and L2 diffraction peaks of phase separated crystalline cholesterol were recorded at 0.179 $Å^{-1}$ and 0.357 $Å^{-1}$. However, as described earlier, the excessive CHOL did not affect the phase assembling process or further data treatment [77,78]. The signals at 0.536 $Å^{-1}$ and 0.718 $Å^{-1}$ could not be assigned to one of the presented lamellar orders and were not included in any further data treatment.

Compared to the SPP and LPP described in the literature, the here presented unit cell scales were smaller. With 45 Å and 48 Å, the short-periodicity phases were different from the SPP found in native SC, where a repeat distance of about 60 Å was mentioned [49]. We applied CER[AP] only with the defined chain length of C18/18 (C36), meaning 36 carbon atoms in total. In native SC, the chain length distribution of CER[AP] varies from C32 to C52 [17]. Longer alkyl chains implement higher d-spacings of the unit cells. For an all-*trans* C—C bonding a distance of 1.27 Å was determined [79,80], meaning a chain length of about 23 Å for C18 and 46 Å for a bilayer with two oppositely positioned ceramides, respectively. For CER[AP]-C24 a chain length of 30.5 Å would be assumed, with a d-spacing of 61 Å for a bilayer. However, lipid mixtures with longer chain lengths were able to form unit cell scales with dimensions of 60 Å for a SPP [32,33]. But as smaller spacings are due to shorter chain lengths, they are scientifically accepted in other SC lipid model membranes [25–28,36,37,41,81,82].

Furthermore, for the LPP a scale of 130 Å was described before in native SC [49]. Thus, with 118 Å, the obtained long- periodicity phase was smaller than previously reported. Again, this result can be explained by the shorter chain length of the applied CER[EOS]-br (C64), instead of C62 to C72, which was found as native CER[EOS] chain length distribution [17]. Nevertheless, the phase behavior and the assembling process of the applied lipid mixtures can give useful information and ideas about the native SC lipid matrix.

After the calculation of the structure factors (SF), the SF's phase signs were verified and the NSLD profiles $\rho_s(x)$ were calculated, according to Eq. (1). In the next sections, the coexisting lamellar phases will be discussed in detail.

3.2. Short-periodicity phase

With seven recorded lamellar orders, the short- periodicity phase (a) was highly ordered. From the positions of equidistant peaks, the value for the d-spacing was calculated with 48.30 ± 0.01 Å. The phase signs of the calculated structure factors (see Table 2) were proven by linear correlation of the SFs over the D_2O contrasts (see Fig. 3). The phase signs were "− + − + − + −" from the 1st to the 7th lamellar order for all contrast values.

Fig. 4 shows the NSLD profiles $\rho_s(x)$ of the control sample across one bilayer received at 8, 50, and 100% D_2O contrast at 57% RH. The profiles show positive and negative trends in their scattering length density (SLD). The distinct minima of the centered profiles were at zero. The SLD of the CH_3 groups is more negative than the SLD of CH_2 groups, based on the additional hydrogen atom and its negative b_{coh}. Thus, the minima of the profiles were a result of the accumulation of CH_3 groups as well as their interdigitation as supposed earlier [26]. Compared to that, the curves showed maxima at the left and right edges of the profile. There, the polar head groups of the lipids were dominant and due to the positive neutron scattering length of their oxygen atoms ($b_{coh} = 0.581 \times 10^{-12}$ cm [83]), the NSLD profiles had a clearly increase in that area. Overall, the profiles were equal in the middle of the membrane, indicating the absence of water. A more visible difference between the profiles was detected at the curves' maxima. There, the presence of water became apparent, due to the D_2O/H_2O exchange. The water distribution function is the difference between the NSLD profiles $\rho_s(x)$ of 100% D_2O and 8% D_2O. This function showed clearly that water was only located in the polar head group area at both profile edges.

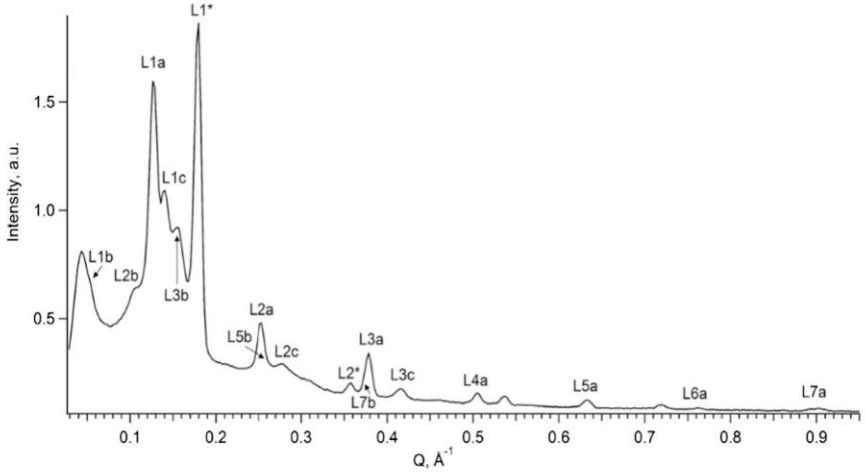

Fig. 2. Diffraction pattern of sample I, AP_EOS-br, as theta-2-theta scan, received at 100% D_2O, 98% RH and 32 °C. This scan was recorded during the first measurement of the sample. The Arabic numbers indicates the lamellar order, the letter stands for the lamellar phase. Here, 'a' stands for the short-periodicity phase, 'b' for the long-periodicity phase and 'c' for the very short-periodicity phase. The asterisk labels the diffraction peaks of phase-separated crystalline cholesterol.

Table 2
Structure factors (SF) and phase signs for phase (a) of sample I AP_EOS-br at 8% D_2O and 57% RH. The absolute values are given.

Diffraction order *h*	SF ± error
1	−1.210 ± 0.001
2	+0.803 ± 0.003
3	−1.074 ± 0.003
4	+0.604 ± 0.004
5	−0.822 ± 0.004
6	+0.349 ± 0.007
7	−0.519 ± 0.007

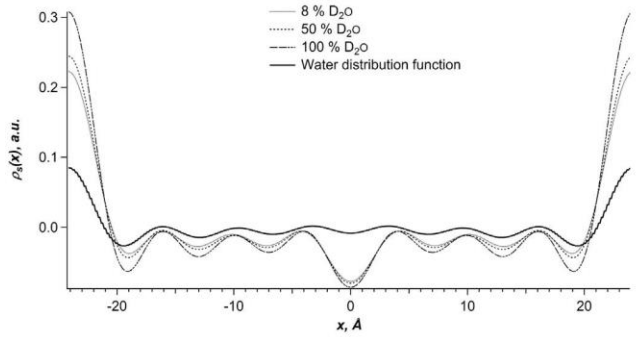

Fig. 4. NSLD Profile $\rho_s(x)$ of phase (a) of sample I, AP_EOS-br, at 57% RH and 32 °C. The profiles, received at 8, 50 and 100% D_2O are plotted. The water distribution function shows the presence of water only at the polar areas of the lipid bilayer.

3.3. Very short-periodicity phase

For the very short-periodicity phase (c) only three lamellar orders were recorded. Taking the equidistant peak positions, a d-spacing of 44.92 ± 0.07 Å was determined. The calculated structure factors (see Table 3) and their plot against the D_2O contrasts are given in Fig. 5. Again, linear trends for the lamellar orders were registered. The phase signs for the centrosymmetric lipid bilayer systems were "− + −" from the 1st to the 3rd lamellar order.

In Fig. 6 the NSLD profiles $\rho_s(x)$ of phase (c) are presented, which were received at 8, 50, and 100% D_2O contrast and 57% RH. Again, the profiles were centered at zero. Dominating minima at zero were obtained, but with broader distributions as the wider minima revealed. Compared to phase (a), the curves were not rising as steeply to the NSLD profiles maxima. The differences between minima and maxima in the scattering length densities of the profiles $\rho_s(x)$ were not as clear. This was explainable due to the lesser number of structure factors next to higher truncation errors, compared to phase (a). Furthermore, the profiles were not as equal to each other in their trends, especially in the center of the membrane. The water distribution function was fluctuating slightly beneath zero and pointed out that water was only located in the polar head group areas.

3.4. Long-periodicity phase

For the long- periodicity phase (b), in total five diffraction orders were recorded, whereby from the 1st to the 7th order the 4th and the 6th lamellar orders were not detectable. We assume that the continuous form factor was zero at both points. The equidistant peak positions were used for the calculation of the unit cell scale with 118.63 ± 2.03 Å. The calculated SFs are given in Table 4, their plot against the measured D_2O ratios is shown in Fig. 7. Based on the small intensities, the trend of the 1st, 2nd and 7th lamellar orders over the D_2O/H_2O contrasts was small, but together with the gradient of the 5th diffraction order very linear. Only for the intense 3rd order, the direct correlation was not reached. But as the trend was significant, the phase signs conformed to centrosymmetric lipid bilayers. The phase sign for the single even order ($h = 2$) was positive and negative for all odd lamellar orders [66,74].

The NSLD profiles $\rho_s(x)$ (see Fig. 8) showed comparable curves with differences in the amplitudes of their maxima and minima. It was supposable that humidity and water had an influence on that long-periodicity phase, as the contrast variation revealed changes in the profiles of the D_2O ratios over the complete bilayer structure. As we knew from the bulk phase behavior of CER[EOS] [57], hydration has an immense impact on the LPP formation. Due to both observations, we decided to take a closer look at the influence of humidity in reference to the SC model membrane system, as explained later.

The profiles were centered at zero, where for each NSLD profile $\rho_s(x)$ the distinct minimum was also present. The maxima at the edges of the profiles illustrated the area of the polar head groups. The additional broad maxima in the middle of the membrane indicated the presence of lipid head groups and, thus, two additional polar areas within the LPP unit cell.

In Fig. 8, the appearance of water was visible by the curve's maxima at the membrane corners and additionally at the inner polar areas. Furthermore, the dimensions of the intercellular part were determined. The polar head group areas at the cell borders had a scale of 7 Å, the inner ones were positioned between ± 8 Å and ± 28 Å. The inner hydrophobic area was about 16 Å, the outer ones 24 Å, respectively. Such a symmetric 3-lipid-layer formation of the LPP was described before [49] and was also apparent in recent neutron diffraction experiments [34,35]. An earlier predicted electron density profile of the LPP unit cell could be verified [22]. But it has to be noticed that this was the first time, a LPP was formed by a ultra-long chain acyl CER, which was esterified to a

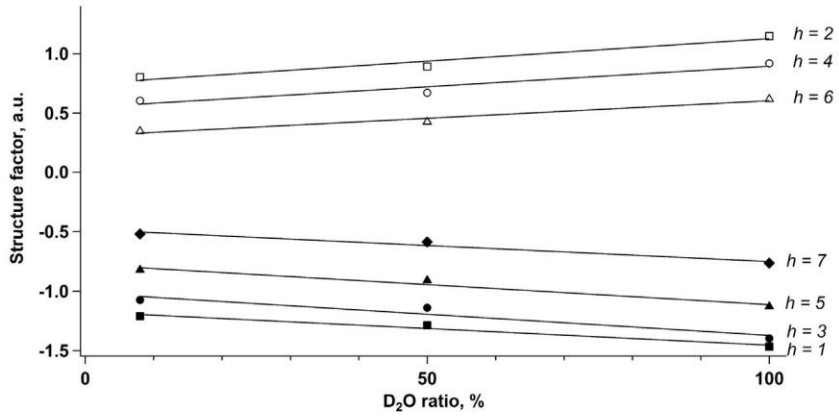

Fig. 3. Structure factors of sample I AP_EOS-br, phase (a), at 57% RH and 32 °C, plotted against the D_2O ratios. A linear correlation of the SFs was obtained.

Table 3
Structure factors (SF) and phase signs for phase (c) of sample I AP_EOS-br at 8% D_2O and 57% RH. The absolute values are given.

Diffraction order	SF ± error
1	−0.8710 ± 0.0007
2	+0.1566 ± 0.0005
3	−0.2210 ± 0.0006

saturated FFA. Former studies described the necessity of an unsaturated chain, esterified to the long chain CER, in order to form a LPP [23]. Here, the formation of the long unit cell structure was possible under the influence of CER[EOS]-br with its esterified palmitic acid. Moreover, the coexistence of SPP and LPP was described before [49,84]. These results could be verified as well, with even two short-periodicity phases, coexisting to a LPP.

The applied protonated SC lipid model membrane was investigated in a neutron diffraction experiment before [36]. However, in this earlier study, a single-phase system with dimensions of about 48 Å was recorded. This may be due to the preparation method, as the previous lipid solution was spread over the quartz surface with an airbrush pistol instead of a Hamilton syringe. The preparation with the Hamilton syringe generated reproducible Bragg peak patterns with high intensities, whereby with an airbrush pistol only minimal peak intensities with a small signal-to-noise ratio were obtained for the multiphase system. Using the syringe, we observed a slower removal of the organic solvent and explained the better lipid orientation as a function of time, as the long chains of CER[EOS]-br might need more time for the assembling process. Due to the high signal-to-noise ratio, we prepared the SC lipid model membranes containing the deuterated labels following the described method as well.

3.5. Localization of the deuterium labelled molecule part within the unit cells

The second approach of this study included the determination of the deuterium-labelled molecules within the SC lipid model membranes. Therefore, the samples II and III were prepared and measured as described above. For the sample, containing CER[AP]-*d3*, the received scattering pattern is shown in Fig. 9. It has to be noticed, that the peaks corresponding to the LPP, were not detected in sample III, besides the presence of the short and the very short-periodicity phases. Moreover, for the localization of the deuterium label position, the normalized SFs were applied. Thus, the calculated NSLD profile of the protonated sample (sample I) was compared to the NSLD profile of sample II, including the deuterated CER[AP]-C18. As mentioned above, the deuterium density distribution function $\rho_{diff}(x)$ was calculated as a difference of $\rho_{deut}(x)$ and $\rho_{prot}(x)$.The maxima of $\rho_{diff}(x)$ were directly connected to the position of the labelled groups. We were able to determine the position of

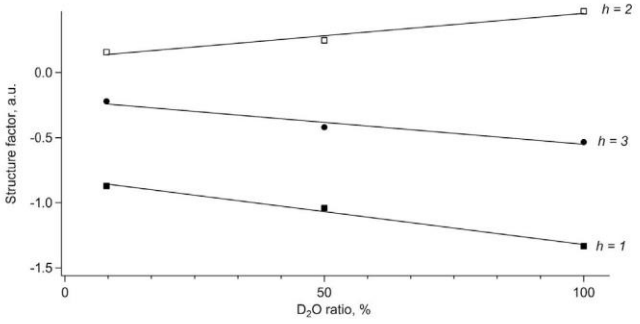

Fig. 5. Structure factors of sample I AP_EOS-br, phase (c), at 57% RH and 32 °C, plotted against the D_2O ratios. A linear correlation of the SFs was obtained.

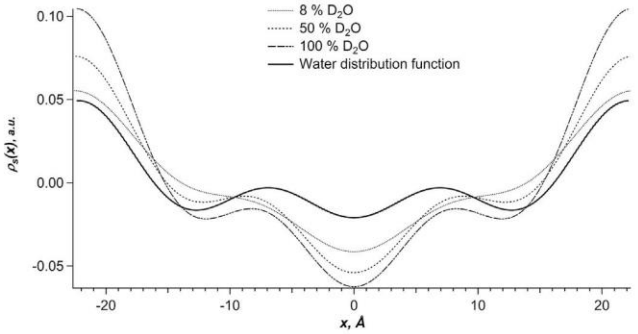

Fig. 6. NSLD Profile $\rho_s(x)$ of phase (c) of sample I, AP_EOS-br, at 57% RH and 32 °C. The profiles, received at 8, 50 and 100% D_2O are plotted. The water distribution function shows the position of water in the lipid bilayer.

Table 4
Structure factors (SF) and phase signs for phase (b) of sample I AP_EOS-br at 8% D_2O and 57% RH. The absolute values are given.

Diffraction order *h*	SF ± error
1	−0.036 ± 0.001
2	+0.054 ± 0.004
3	−0.578 ± 0.001
4	0
5	−0.255 ± 0.002
6	0
7	−0.264 ± 0.002

the long chain CER[AP]-*d3* in the short and in the very short- periodicity phase, as Figs. 10 and 11 present.

The position of the labelled CER[AP]-*d3* in the short- periodicity phase (Fig. 10) was clearly visible by the maximum of $\rho_{diff}(x)$ at the membrane center. Based on an all-*trans* C—C—C distance of 2.54 Å [79], for the C18 fatty acid chain, a maximum length of about 23 Å was assumed. Thus, including a small overlap in the membrane center, the arrangement of two oppositely positioned CER[AP]-C18 was proposed (see Fig. 10) with the CER head group in the polar regions of the bilayer and the alkyl chains directed towards the membrane center.

Additionally, the labelled CER[AP]-*d3* was detected in the very short-periodicity phase as well (Fig. 11) A significant maximum of the deuterium difference $\rho_{diff}(x)$ in the membrane center implicated the position of the labelled atoms. Here, the high difference between the protonated and deuterated NSLD profiles could be attributed to a higher quantitative amount of the long chain CER[AP] in the very short-periodicity phase compared to the 48 Å phase. Moreover, two oppositely CER[AP]-*d3* molecules were positioned with the polar head group in the corresponding unit cell parts and its alkyl chains were extended into the nonpolar membrane center. The alkyl chain ends were more

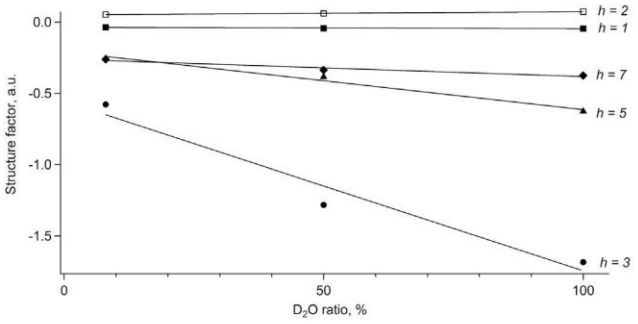

Fig. 7. Structure factors of sample I AP_EOS-br, phase (b), at 57% RH and 32 °C, plotted against the D_2O ratios.

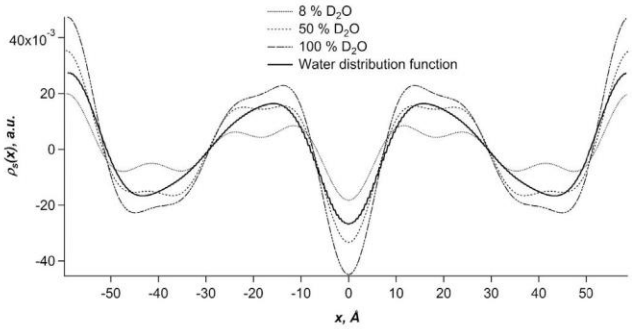

Fig. 8. NSLD Profile ρ_s (x) of phase (b) of sample I, AP_EOS-br, at 57% RH and 32 °C. The profiles, received at 8, 50 and 100% D_2O are plotted. The water distribution function shows the location of water in the lipid bilayer.

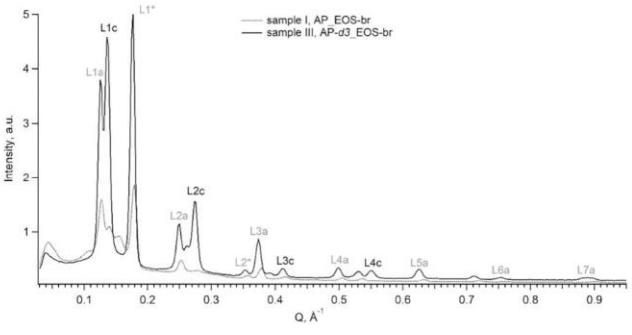

Fig. 9. Bragg peak pattern of samples I (AP_EOS-br) and sample III (AP-*d3*_EOS-br). The scattering patterns were received at 100% D_2O, 98% RH and 32 °C during the first measurement. The lamellar orders corresponding to the very short-periodicity phase (c) were colored in black, all others belonging to phase (a) and (b) were colored in grey.

overlapping in their all-*trans* conformation than for the 48 Å phase, resulting in a smaller d-spacing. In addition, the stereochemistry as another reason for the smaller spacing should be taken into account as well.

With the localization of CER[AP]-*d3* in both SPPs, the presence of the ceramide DL-enantiomeres could be an explanation for the phase separation and the existence of two short phases. It is known that the different configuration of the FFA α-hydroxy group generates different phase behaviors, concerning their hydrogen bonding, mobility and even repeat distances [85,86]. Raudenkolb et al. revealed larger dimensions of the unit cell for the natural occurring D-CER[AP] than for the unnatural L-CER[AP] [86]. They even described a V-shaped structure for L-CER[AP]. Especially the smaller unit cell scale of the very short-periodicity phase could be a result of the L-CER[AP] tilt as well. But as long as we were not able to differentiate between the enantiomers in this study, we propose the ceramide's hairpin structure as it was described as energetically more stable for CER[AP]-C18 under hydration [29], as performed here. A comparable experiment with only the natural occurring ceramide conformation is in progress.

Including former results with a SC lipid model membrane system without CER[EOS], where BA was partial deuterated [41], the understanding of the very short-periodicity phase structure became complete. In these studies, the fatty acid interdigitation in an about 45 Å phase was determined and the position of the long chain CER proposed. We were able to confirm the idea and together with the FFA and CHOL localization [24,26], the lipid phase behavior and the bilayer structure of a SPP were more revealed. As the long-periodicity phase did not exist in sample III, no CER[AP]-*d3* was detectable there. The arrangement of a very long chain CER inside a LPP, as Mojumdar et al. [33] proposed with CER[NS]-C24, could not be proven here.

The Bragg peak patterns of sample I and II are plotted in Fig. 12. As well as for the non-deuterated sample I, for the CER[EOS]-*d3* sample (II) a highly ordered multi-phase system was received. Compared to the control sample I, the intensities of all peaks were higher. Especially the signals belonging to the LPP (b) were more pronounced in the labelled sample II. Furthermore, the 6th diffraction order (0.308 $Å^{-1}$) was now recorded at 50% and 100% D_2O ratio, mainly as a result of the CER[EOS]-*d3* label and its positive b_{coh}.

Sample II was completely measured and characterized at all D_2O contrasts and humidities during the first experiment, where a unit cell scale of 114.10 ± 1.07 Å was calculated. For the localization of the deuterium label, the normalized SFs (SF_{norm}) were used. The NSLD profiles $\rho_s(x)$ of sample I and II, received during the first experiment at 8% D_2O and 57% RH, were plotted in Figs. 13 and 14. The centered profiles show the cross section of a lipid bilayer. Compared to the control sample I, the deuterated sample II showed additional maxima in the middle of the membrane. The difference of both profiles was calculated and plotted as deuterium distribution function $\rho_{diff}(x)$. The positions of the deuterated labels within the lipid bilayer were visible by the function's maxima. We assume an acyl chain length of 38.1 Å for the CER's amide bonded C30 fatty acid in its all-*trans* conformation (C30 chain) and 12.7 Å from the ester group to the deuterated methyl-branching (C16 chain with methyl-branching at C10). For the deuterium difference $\rho_{diff}(x)$, at ±36 Å two maxima were found, next to a wide

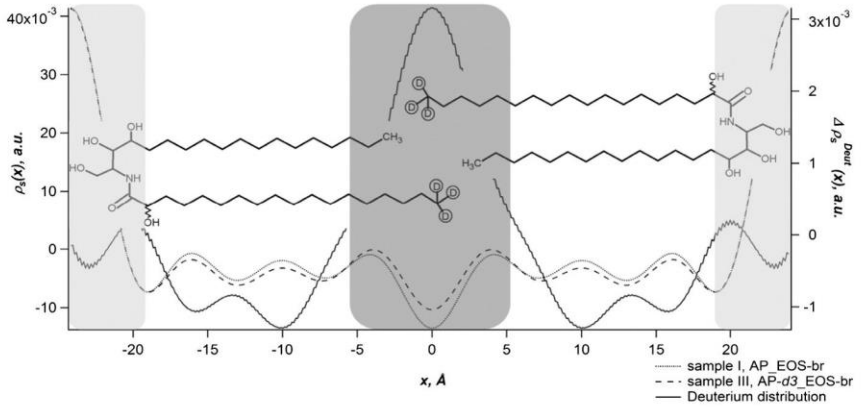

Fig. 10. Deuterium distribution function of CER[AP]-d3 in short-periodicity phase (48 Å). NSLD profiles of sample I (grey dashed line) and III (black dashed line), received at 50% D_2O, 57% RH during the 2nd experiment. The difference of both profiles $\rho_{diff}(x)$ (black bold line) marks the deuterium distribution function and the dark grey box stands for the area of deuterium positions. The polar bilayer areas are schematically highlighted as light grey boxes. Here, the inserted CER[AP]-d3 molecules propose a possible position in their hairpin conformation [29]. For the NSLD profile calculations all available SFs were included.

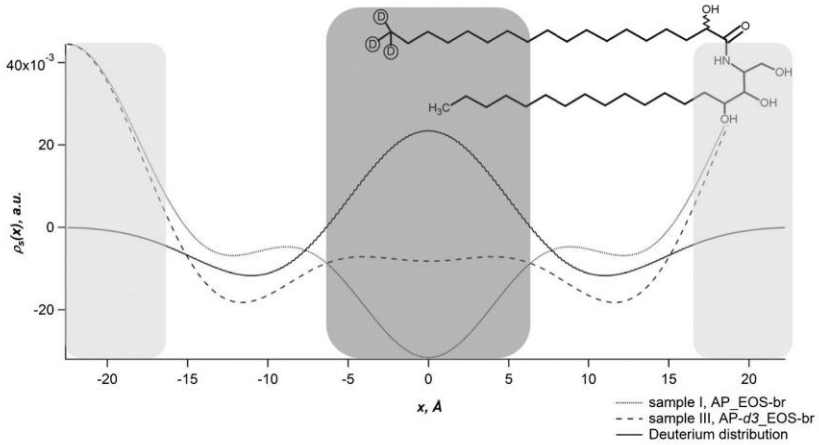

Fig. 11. Deuterium distribution function of CER[AP]-d3 in the very short-periodicity phase (45 Å). NSLD profiles of sample I (grey dashed line) and III (black dashed line), received at 50% D_2O, 57% RH during the 2nd experiment. The difference of both profiles $\rho_{diff}(x)$ (black bold line) marks the deuterium distribution function and the dark grey box stands for the area of deuterium positions. Compared to the 48 Å SPP, there is a broader area where the deuterium label was determined, visible as wider dark grey area. The polar bilayer areas are schematically highlighted as light grey boxes. Here, the inserted CER[AP]-d3 molecule proposes a possible position in its hairpin conformation [29]. Simultaneously, the molecules were located from the left side of the NSLD profile, but not pictured here in the scheme, For the NSLD profile calculations the number of SFs was 3 due to the limited number of SFs from the protonated sample.

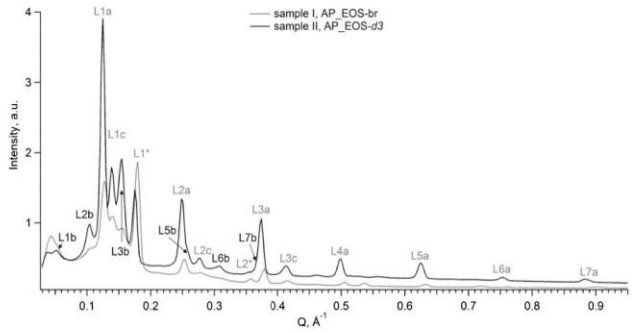

Fig. 12. Bragg peak pattern of samples I (AP_EOS-br) and sample II (AP_EOS-*d3*). The scattering patterns were received at 100% D_2O, 98% RH and 32 °C during the first measurement. The lamellar orders corresponding to the long- periodicity phase (b) were colored in black, all others belonging to phase (a) and (c) were colored in grey.

maximum between −12 to +12 Å. These maxima were mainly positioned within the non-polar parts of the unit cell, corresponding to the label position at the esterified palmitic acid. Only in the center of the bilayer, the deuterium positions and the polar parts of the LPP overlapped. Thus, several arrangements of CER[EOS]-*d3* are proposed in Figs. 13 and 14.

For the proposed positions ① and ② of the methyl-branched CER[EOS] analog we assumed its half hairpin conformation for the discussion of the here presented results. Thus, we supposed the fatty acid part as fully extended, compared to the literature [25,28,36,77,87]. With the head group in the polar area at both profile edges, the long chain of the CER was extended into the lipid bilayer (①). Thereby, its small ester group was located in the inner polar membrane segment, followed by the esterified palmitic acid in its extended conformation. Compared to the natural CER[EOS], the saturated bondings occurred no bends. Due to the partial deuteration at C10, its position could be determined in the center of the long- periodicity phase, mainly between 0 and −12 Å. In the same way, the molecule could be located mirror-

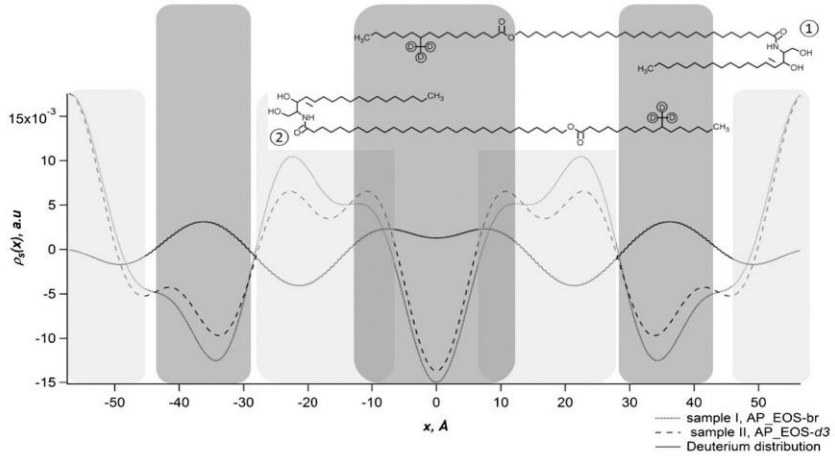

Fig. 13. Deuterium distribution function of CER[EOS]-d3. Neutron scattering length density profiles of sample I, AP_EOS-br (grey dashed line), and sample II, AP_EOS-d3 (black dashed line), received at 8% D_2O, 57% RH and 32 °C during the first measurement. The difference of both curves represented the deuterium distribution function (black bold line), showing the positions of deuterium labels within the lipid bilayer. The polar areas of the bilayer are schematically shimmed as light grey boxes, the areas where the deuterium label was detected are highlighted in dark grey. Here, the inserted CER[EOS]-d3 molecules propose their possible positions in their half hairpin conformation. The molecules were located simultaneously from the left edge of the NSLD profile, but not pictured here in the scheme.

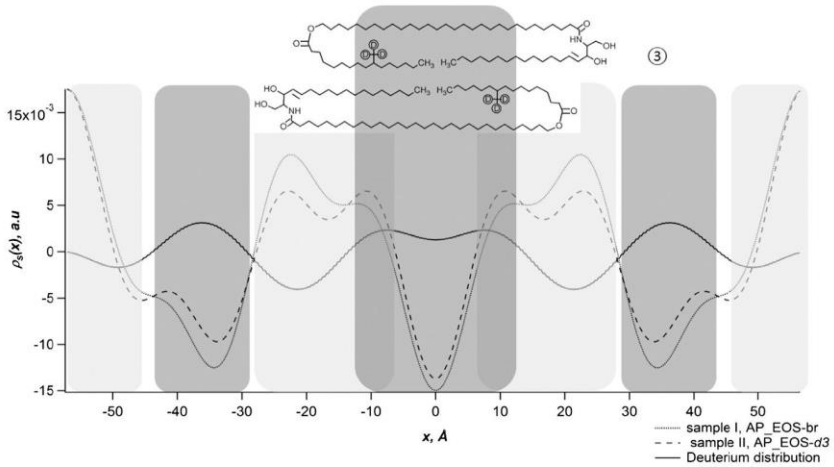

Fig. 14. Deuterium distribution function of CER[EOS]-d3. Neutron scattering length density profiles of sample I, AP_EOS-br (grey dashed line), and sample II, AP_EOS-d3 (black dashed line), received at 8% D_2O, 57% RH and 32 °C during the first measurement. The difference of both curves represented the deuterium distribution function (black bold line), showing the positions of deuterium labels within the lipid bilayer. The polar areas of the bilayer are schematically shimmed as light grey boxes, the areas where the deuterium label was detected are highlighted in dark grey. Here, the inserted CER[EOS]-d3 molecules propose possible positions in their hairpin conformation.

inverted from the left side of the bilayer, with the deuterium positioned between 0 and + 12 Å. The overlapping alkyl chains in the middle of the membrane and the intermolecular van der Waals forces could explain the stability of the LPP and its benefit to the SC barrier function. Moreover, the formation of a LPP could be supported by CER[EOS]-br in position ②. The head group of the ultra-long chain ω-acyl CER analog was supposed to be in the inner polar areas of the LPP. The ester group would be located in the second innermembranal part, so that the esterified palmitic acid could be extended into the outer non-polar part of the bilayer. Including its mirror-inverted position, that arrangement of CER[EOS]-*d3* could explain the additional maxima of the deuterium distribution function at ± 36 Å. Apart from this, the stability of the extended palmitic acid could be supported by CHOL, which was detected with its head group near the inner polar areas and its sterol backbone directed towards the outer membrane edges [34]. Moreover, the internal stability could be maximized, due to an additional interdigitation and interlocking of the alkyl chains as position ③ proposes (see Fig. 14). Therefore, a complete hairpin conformation of the CER was assumed. With a back-flipping esterified palmitic acid, the wide deuterium distribution maximum at the bilayer center could be explainable. A partial back folding of the FFA esterified to CER[EOS] was described before for linoleic acid [34]. Assuming the CER head groups were arranged into the inner polar areas, their fatty acid chains were completely extended into the bilayer middle. On the one hand, the question of the LPP stability could be answered by the interdigitation and the intermolecular interaction. On the other hand, the penetration of *exo*- and endogenic substances across a LPP would only be hardly possible due to continuous changes of polar and non-polar regions in a single unit cell. Together with a recently proposed molecular model of the LPP unit cell [34,35], the here received results give new material to the debate of the presence and structure of a long- periodicity phase.

It has to be noticed, that CER[EOS]-*d3* was not detected in both SPP. Moreover, we have to revise earlier assumed SPP models, where the ultra-long chain CER was included inside the 48 Å phase [25,36].

3.6. Influence of humidity

The impact of humidity to the applied SC model membranes was another point of interest in the presented study. As known from former experiments with bulk phase CER[EOS], the formation of a LPP was highly induced at high humidity [57]. The neutron diffraction experiments of Mojumdar et al. [34,35] were also performed at 100% RH, where a LPP was generated in a SC model membrane. Based on these results, we decided to have a closer look at possible differences in the phase behavior of the long-periodicity phase. Therefore, the sample I was measured at 57 and 98% RH at 8% D_2O and 32 °C during the second experiment. The NSLD profiles $\rho_s(x)$ of the long-periodicity phase exhibited similar basic structures at both humidities (see Fig. 15). A

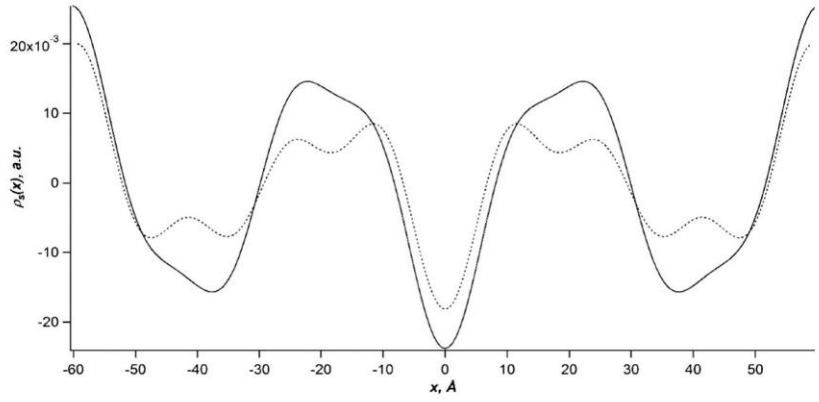

Fig. 15. Influence of humidity to sample I, AP_EOS-br, received at 8% D_2O and 32 °C during the second experiment. The NSLD profiles of the LPP (b), recorded at 57% RH (dotted line) and 98% RH (solid line) show differences, especially in the area of the polar head groups.

Table 5
Unit cell scales of sample I AP_EOS-br, received at 8% D_2O, 57% RH and 32 °C during the first and the second experiment. Over the three month in between, only the scale of the LPP changed significantly.

Measurement	d-spacing, Å		
	Phase (a)	Phase (b)	Phase (c)
1	48.42 ± 0.02	114.10 ± 0.54	44.20 ± 0.01
2	48.30 ± 0.01	118.63 ± 1.94	44.92 ± 0.02

minimal change of the d-spacing was found, meaning a swelling from 118.63 Å to 120.37 Å. Especially in the profiles maxima, where the polar head groups of the lipids were located, distinct differences were visible. At both edges of the profile, the influence of the higher humidity to the SLD was smaller, compared to both inner maxima. However, as water was present inside the polar areas of the LPP, here the differences caused by the change of humidity were plausible. It has to be pointed out, that the LPP was also formed under lower humidity but with slightly less intensities in NSLD profiles maxima. Thus, the humidity has no significant influence on the formation of a long-periodicity phase in the here presented SC lipid model membrane, but had an impact on the water absorbing parts of the bilayer and on the unit cell scale. For the shorter phases (a) and (c) no changes were obtained corresponding to results, Schröter et al. [25] presented earlier on a comparable lipid system. The high stability of the short-periodicity phases may be reasoned in the very polar head group structure of the present CER[AP] and its strong hydrogen bonding [88]. In summary, only the long-periodicity phase was able to react to humidity changes in the surrounding atmosphere.

3.7. Equilibration as a function of time

A last approach of this study were time depending changes in the phase behavior of the applied SC lipid model membranes. During the second experiment, changes of the unit cell scale were obtained for the long-periodicity phase (b). Table 5 presents the corresponding unit cell scales for sample I, AP_EOS-br, received during the first and the second measurement.

For the short-periodicity phases, a nearly constant d-spacing was recorded. The NSLD profiles $\rho_s(x)$ showed an increased d-spacing from 114.10 Å to 118.63 Å (see Fig. 16. Overall, the bilayer structure of the long-periodicity phase was stretched, as the inner maxima became wider as well. However, as the lipid trilayer structure was stable over the time, only minimal shifts of the inner maxima were visible. The longer d-spacing was further interesting, as it increased again due to the impact of humidity (see Section 3.6). Thus, although the basic organization of the bilayer was constant over time, it was still sensitive to the impact of water.

Overall, the structure of the long- periodicity phase is not as rigid as its shorter pendants. The shorter phases were more stable and fixed or already equilibrated. As only minor changes in the unit cell scale were obtained, the NSLD profiles were comparable. The presence of CER[AP] could be a possible reason for the high stability of both SPP. Its driving force during the membrane assembling process was described earlier [25,26,41]. Simultaneously, CER[EOS]-br was able to maintain the long-periodicity phase, as no long chain CER[AP] was present.

4. Summary

For the first time, a well-defined SC lipid model membrane system, containing the partially deuterated ceramides [AP]-C18 and a methyl-branched [EOS] analog, was investigated by a neutron diffraction study. Thus, we were able to determine their positions within the SC lipid bilayers. Furthermore, we observed coexisting lamellar phases, in detail two short-periodicity phases with d-spacings of about 45 Å and 48 Å and a long-periodicity phase with a d-spacing of 114 Å. We were able to detect the LPP for the first time with the applied SC lipid mixture [36]. This is very interesting as former studies figured out that a long unit cell can only be structured under the presence of an unsaturated FFA esterified to ultra-long chain CER[EOS] [23]. Here, the esterified palmitic acid supported the LPP formation.

Additionally, the influence of humidity on the applied SC lipid model membranes was analyzed, whereby only the LPP gave significant changes in its unit cell scale. Furthermore, the impact of time was investigated, meaning an increased spacing of the LPP during a second measurement.

Transparency document

The Transparency document associated with this article can be found, in the online version.

Acknowledgements

The authors would like to thank the Helmholtz-Zentrum Berlin für Materialien und Energie (HZB, Berlin, Germany) for the allocation of beam time and financial support. In addition, Evonik Industries AG (Essen, Germany) is gratefully acknowledged for the generous donation of CER[AP]-C18. The authors would like to thank the Deutsche Forschungsgemeinschaft (Projects: NE 427/30-1 and DO 463/6-1) for

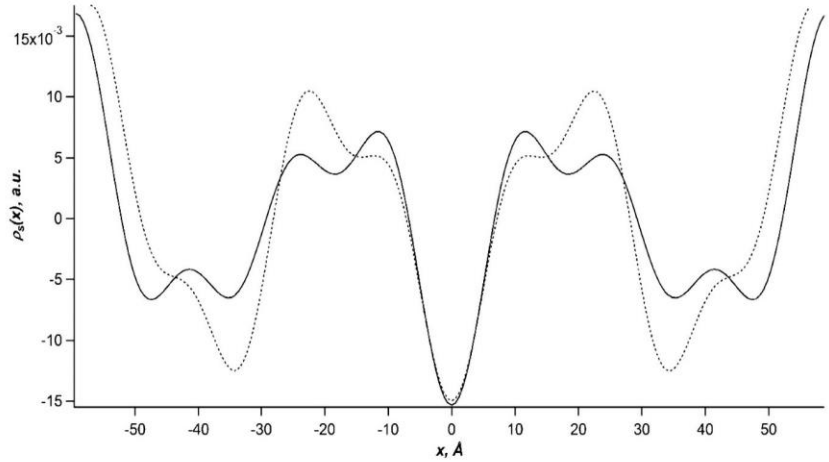

Fig. 16. Time depending changes of long-periodicity phase (b) of sample I, AP_EOS-br, received at 8% D_2O, 57% RH and 32 °C. The NSLD profile included a shift of the maxima from the first (dotted line) to the second (black line) experiment.

funding. At least, sincere thanks are given to Ms. Carolin Helmholz for her helpful annotations.

References

[1] P.W. Wertz, B. van den Bergh, The physical, chemical and functional properties of lipids in the skin and other biological barriers, Chem. Phys. Lipids 91 (2) (1998) 85–96.
[2] R.J. Scheuplin, Permeability of the skin: a review of major concepts and some new developments, J. Investig. Dermatol. 67 (5) (1976) 672–676.
[3] P.M. Elias, Epidermal lipids, barrier function and desquamation, J. Investigat. Dermatol. 80 (6) (1983) 44s–49s.
[4] P.M. Elias, D.S. Friend, The permeability barrier in mammalian epidermis, J. Cell Biol. 65 (1975) 180–191.
[5] L. Landmann, The epidermal permeability barrier, Anat. Embryol. 178 (1988) 1–13.
[6] H.J. Yardley, R. Summerly, Lipid composition and metabolism in normal and diseased epidermis, Pharmacol. Ther. 13 (2) (1981) 383.
[7] G.M. Gray, H.J. Yardley, Different populations of pig epidermal cells: isolation and lipid composition, J. Lipid Res. 16 (6) (1975) 441–447.
[8] M.A. Lampe, A.L. Burlingame, J. Whitney, M.L. Williams, B.E. Brown, E. Roitman, P.M. Elias, Human stratum corneum lipids: characterization and regional variations, J. Lipid Res. 24 (2) (1983) 120–130.
[9] Y. Masukawa, H. Narita, H. Sato, A. Naoe, N. Kondo, Y. Sugai, T. Oba, R. Homma, J. Ishikawa, Y. Takagi, T. Kitahara, Comprehensive quantification of ceramide species in human stratum corneum, J. Lipid Res. 50 (2009) 1708–1719.
[10] Y.-B. Liou, M.-T. Sheu, D.-Z. Liu, S.-Y. Lin, H.-O. Ho, Quantitation of ceramides in nude mouse skin by normal-phase liquid chromatography and atmospheric pressure chemical ionization mass spectrometry, Anal. Biochem. 401 (2010) 107–113.
[11] F.F. Sahle, S. Lange, B. Dobner, J. Wohlrab, R.H.H. Neubert, Development and validation of LC/ESI-MS method for the detection and quantification of exogenous ceramide NP in stratum corneum and other layers of the skin, J. Pharm. Biomed. Anal. 60 (2012) 7–13.
[12] H.J. Cho, B.Y. Chung, H.B. Lee, H.O. Kim, C.W. Park, C.H. Lee, Quantitative study of stratum corneum ceramides contents in patients with sensitive skin, J. Dermatol. 39 (2012) 2012.
[13] S.Y. Park, J.H. Kim, S.I. Cho, K.I. Kim, H.J. Cho, C.W. Park, C.H. Lee, H.O. Kim, Induction of a hardening phenomenon and quantitative changes of ceramides in stratum corneum, Ann. Dermatol. 26 (1) (2014) 35–42.
[14] Y. Masukawa, H. Narita, T. Kitahara, Y. Takema, K. Kita, Characterization of overall ceramide species in human stratum corneum, J. Lipid Res. 49 (7) (2008) 1466–1476.
[15] J. van Smeden, L. Hoppel, R. van der Heijden, T. Hankemeier, R.J. Vreeken, J.A. Bouwstra, LC/MS analysis of stratum corneum lipids: ceramide profiling and discovery, J. Lipid Res. 52 (6) (2011) 1211–1221.
[16] M. Rabionet, A. Bayerle, C. Marsching, R. Jennemann, H.-J. Groene, Y. Yildiz, D. Wachten, W. Shaw, J.A. Shayman, R. Sandhoff, 1-O-acylceramides are natural components of human and mouse epidermis, J. Lipid Res. 54 (2013) 3312–3321.
[17] R. t'Kindt, L. Jorge, E. Dumont, P. Couturon, F. David, P. Sandra, K. Sandra, Profiling and characterizing skin ceramides using reversed-phase liquid chromatography-quadrupole time-of-flight mass spectrometry, Anal. Chem. 84 (2012) 403–411.
[18] P.W. Wertz, D.T. Downing, Ceramides of pig epidermis: structure determination, J. Lipid Res. 24 (6) (1983) 759–765.
[19] S. Motta, M. Monti, S. Sesana, R. Caputo, S. Carelli, R. Ghidoni, Ceramide composition of the psoriatic scale, Biochim. Biophys. Acta 1182 (1993) 147–151.
[20] K.J. Robson, M.E. Stewart, S. Michelsen, N.D. Lazo, D.T. Downing, 6-hydroxy-4-sphingenine in human epidermal ceramides, J. Lipid Res. 35 (1994) 2060–2068.
[21] L. Coderch, et al., Ceramides and skin function, Am. J. Clin. Dermatol. 4 (2) (2003) 107–129.
[22] D. Groen, G.S. Gooris, J.A. Bouwstra, New insights into the stratum corneum lipid organization by X-ray diffraction analysis, Biophys. J. 97 (2009) 2242–2249.
[23] D. de Sousa Neto, G. Gorris, J. Bouwstra, Effect of the ω-acylceramides on the lipid organization of stratum corneum model membranes evaluated by X-ray diffraction and FTIR studies, Chem. Phys. Lipids 164 (2011) 184–195.
[24] D. Kessner, A. Mikhail, T. Hauss, S. Dante, S. Wartewig, R.H.H. Neubert, Localisation of partially deuterated cholesterol in quaternary SC lipid model membranes: a neutron diffraction study, Eur. Biophys. J. 37 (6) (2008) 1051–1057.
[25] A. Schroeter, D. Kessner, M.A. Kiselev, T. Hauß, S. Dante, R.H.H. Neubert, Basic nanostructure of stratum corneum lipid matrices based on ceramides [EOS] and [AP]: a neutron diffraction study, Biophys. J. 97 (2009) 1104–1114.
[26] A. Schroeter, M.A. Kiselev, T. Hauß, S. Dante, R.H.H. Neubert, Evidence of free fatty acid interdigitation in stratum corneum model membranes based in ceramide [AP] by deuterium labelling, Biochim. Biophys. Acta 1788 (10) (2009) 2194–2203.
[27] A. Schroeter, The role of ceramide (AP) for the structural assembly of stratum corneum lipid model membranes, Institute of Pharmacy, Martin Luther University Halle-Wittenberg, Halle, 2010.
[28] D. Kessner, M. Kiselev, S. Dante, T. Hauss, P. Lersch, S. Wartewig, R.H.H. Neubert, Arrangement of ceramide [EOS] in a stratum corneum lipid model matrix: new aspects revealed by neutron diffraction studies, Eur. Biophys. J. 37 (6) (2008) 989–999.
[29] M.A. Kiselev, E.V. Ermakova, A.Y. Gruzinov, A.V. Zabelin, Conformation of ceramide 6 molecules and chain-flip transitions in the lipid matrix of the outermost layer of mammalian skin, the stratum corneum, Crystallogr. Rep. 52 (3) (2007) 525–528.
[30] M.A. Kiselev, N.Y. Ryabova, A.M. Balagurov, S. Dante, T. Hauss, J. Zbytovska, S. Wartewig, R.H.H. Neubert, New insights into the structure and hydration of a stratum corneum lipid model membrane by neutron diffraction, Eur. Biophys. J. 34 (2005) 1030–1040.
[31] G.C. Charalambopoulou, T.A. Steriotis, T. Hauss, A.K. Stubos, N.K. Kanellopoulos, Structural alterations of fully hydrated human stratum corneum, Phys. B Condens. Matter 350 (1–3) (2004) e603–e606.
[32] D. Groen, G.S. Gooris, D.J. Barlow, M.J. Lawrence, J.B. van Mechelen, B. Demé, J.A. Bouwstra, Disposition of ceramide in model lipid membranes determined by neutron diffraction, Biophys. J. 100 (6) (2011) 1481–1489.
[33] E.H. Mojumdar, D. Groen, G.S. Gooris, D.J. Barlow, M.J. Lawrence, B. Demé, J.A. Bouwstra, Localization of cholesterol and fatty acid in a model lipid membrane: a neutron diffraction approach, Biophys. J. 105 (2013) 911–918.
[34] E.H. Mojumdar, G.S. Gooris, D. Groen, D.J. Barlow, M.J. Lawrence, B. Demé, J.A. Bouwstra, Stratum corneum lipid matrix: localization of acyl ceramide and cholesterol in the unit cell of the long periodicity phase, Biochim. Biophys. Acta Biomembr. 1858 (2016) 1926–1934.
[35] E.H. Mojumdar, G.S. Gooris, D.J. Barlow, M.J. Lawrence, B. Demé, J.A. Bouwstra, Skin lipids: localization of ceramide and fatty acid in the unit cell of the long periodicity phase, Biophys. J. 108 (2015) 2670–2679.
[36] T. Engelbrecht, T. Hauß, K. Süß, A. Vogel, M. Roark, S.C. Feller, R.H.H. Neubert, B. Dobner, Characterisation of a new ceramide EOS species: synthesis and investigation of the thermotropic phase behaviour and influence on the bilayer architecture of stratum corneum lipid model membranes, Soft Matter 7 (2011) 8998–9011.
[37] T.N. Engelbrecht, A. Schroeter, T. Hauß, B. Demé, H.A. Scheidt, D. Huster, R.H.H. Neubert, The impact of ceramides NP and AP on the nanostructure of stratum corneum lipid bilayer. Part I: neutron diffraction and ^{2}H NMR studies on multilamellar models based on ceramides with symmetric alkyl chain length distribution, Soft Matter 8 (2012) 2599–2607.
[38] M.W. de Jager, G.S. Gooris, I.P. Dolbnya, W. Bras, M. Ponec, J.A. Bouwstra, Novel lipid mixtures based on synthetic ceramides reproduce the unique stratum corneum lipid organization, J. Lipid Res. 45 (2004) 923–932.
[39] T.J. McIntosh, M.E. Stewart, D.T. Downing, X-ray diffraction analysis of isolated skin lipids: reconstruction of intercellular lipid domains, Biochemistry 35 (12) (1996) 3649–3653.
[40] J.A. Bouwstra, G.S. Gooris, K. Cheng, A. Weerheim, W. Bras, M. Ponec, Phase behavior of isolated skin lipids, J. Lipid Res. 37 (1996) 999–1011.
[41] A. Ruettinger, M.A. Kiselev, T. Hauss, S. Dante, A.M. Balagurov, R.H.H. Neubert, Fatty acid interdigitation in stratum corneum model membranes: a neutron diffraction study, Eur. J. Dermatol. 37 (6) (2008) 759–771.
[42] M. de Jager, G. Gooris, M. Ponec, J. Bouwstra, Acylceramide head group architecture affects lipid organization in synthetic ceramide mixtures, J. Investig. Dermatol. 123 (2004) 911–916.
[43] A. Di Nardo, P. Wertz, A. Giannetti, S. Seidenari, Ceramide and cholesterol composition of the skin of patients with atopic dermatitis, Acta Derm. Venereol. 78 (1) (1998) 27–30.
[44] S. Motta, M. Monti, S. Sesana, L. Mellesi, R. Ghidoni, R. Caputo, Abnormality of water barrier function in psoriasis. Role of ceramide fractions, Arch. Dermatol. 130 (4) (1994) 452–456.
[45] S. Wartewig, R.H.H. Neubert, Properties of ceramides and their impact on the stratum corneum structure: a review, Skin Pharmacol. Physiol. 20 (2007) 220–229.
[46] V. Schreiner, G.S. Gooris, S. Pfeiffer, G. Lanzendorfer, H. Wenck, W. Diembeck, E. Proksch, J. Bouwstra, Barrier characteristics of different human skin types investigated with X-ray diffraction, lipid analysis, and electron microscopy imaging, J. Investig. Dermatol. 114 (4) (2000) 654–660.
[47] J.A. Bouwstra, G.S. Gooris, F.E.R. Dubbelaar, A.M. Weerheim, A.P. IJzerman, M. Ponec, Role of ceramide 1 in the molecular organization of the stratum corneum lipids, J. Lipid Res. 39 (1) (1998) 186–196.
[48] J.A. Bouwstra, G.S. Gooris, J.A. van der Spek, W. Bras, The structure of human stratum corneum as determined by small angle X-ray scattering, J. Investig. Dermatol. 96 (1991) 1006–1014.
[49] J.A. Bouwstra, G.S. Gooris, J.A. van der Spek, W. Bras, Structural investigations of human stratum corneum by small-angle X-ray scattering, J. Investig. Dermatol. 97 (6) (1991) 1005–1012.
[50] N. Ohta, S. Ban, H. Tanaka, S. Nakta, I. Hatta, Swelling of intercellular lipid lamellar structure with short repeat distance in hairless mouse stratum corneum as studied by X-ray diffraction, Chem. Phys. Lipids 123 (2003) 1–8.
[51] M.W. de Jager, G.S. Gooris, I.P. Dolbnya, W. Bras, M. Ponec, J.A. Bouwstra, The phase behaviour of skin lipid mixtures based on synthetic ceramides, Chem. Phys. Lipids 125 (2) (2003) 123–134.
[52] S.H. White, D. Mirejovsky, G.I. King, Structure of lamellar lipid domains and corneocyte envelopes of murine stratum corneum. An X-ray diffraction study, Biochemistry 27 (1988) 3725–3732.
[53] J.A. Bouwstra, G.S. Gooris, F.E.R. Dubbelaar, M. Ponec, Phase behaviour of lipid mixtures based on human ceramides: coexistence of crystalline and liquid phases, J. Lipid Res. 42 (11) (2001) 1759–1770.
[54] J.A. Bouwstra, G.S. Gooris, E.R. Frank, M. Ponec, Phase behaviour of stratum corneum lipid mixtures based on human ceramides: the role of natural and synthetic ceramide 1, J. Investig. Dermatol. 118 (4) (2002) 606–617.
[55] M.A. Kiselev, E.V. Ermakova, A.Y. Gruzinov, A.V. Zabelin, Formation of the long-periodicity phase in model membranes of the outermost layer of skin (Stratum corneum), Crystallogr. Rep. 59 (1) (2014) 123–128.
[56] A. Kovacik, L. Opalka, M. Silarova, J. Roh, K. Vavrova, Synthesis of 6-hydroxyceramide using ruthenium-catalyzed hydrosilylation-protodesilylation. Unexpected formation of a long periodicity lamellar phase in skin lipid membranes, RSC Adv. 6 (77) (2016) 73343–73350.
[57] D. Kessner, G. Brezesinski, S.S. Funari, B. Dobner, R.H.H. Neubert, Impact of long chain ω-acylceramides on the stratum corneum lipid nanostructure. Part 1: thermotropic phase behaviour of CER[EOS] and CER[EOP] studied using X-ray powder diffraction and FT-Raman spectroscopy, Chem. Phys. Lipids 163 (2010) 42–50.

[58] K.C. Madison, D.C. Swartzendruber, P.W. Wertz, D.T. Downing, Presence of intact intercellular lipid lamellae in the upper layers of the stratum corneum, J. Investig. Dermatol. 88 (6) (1987) 714–718.
[59] J. Bouwstra, G. Pilgram, G. Gooris, H. Koerten, M. Ponec, New aspects of the skin barrier organization, Skin Pharmacol. Physiol. 14 (Suppl. 1) (2001) 52–62.
[60] J.R. Hill, P.W. Wertz, Molecular models of the intercellular lipid lamellae from epidermal stratum corneum, Biochim. Biophys. Acta 1616 (2) (2003) 121–126.
[61] J.A. Bouwstra, F.E.R. Dubbelaar, G.S. Gooris, M. Ponec, The lipid organization in the skin barrier, Acta Derm. Venereol. 208 (Suppl.) (2000) 23–30.
[62] T.J. McIntosh, Organization of skin stratum corneum extracellular lamellae: diffraction evidence for asymmetric distribution of cholesterol, Biophys. J. 85 (2003) 1675–1681.
[63] B. Breiden, K. Sandhoff, The role of sphingolipid metabolism in cutaneous permeability barrier formation, Biochim. Biophys. Acta 1841 (2014) 441–452.
[64] M. Seul, M.J. Sammon, Preparation of surfactant multilayer films on solid substrates by deposition from organic solution, Thin Solid Films 185 (2) (1990) 287–305.
[65] D.L. Worchester, N.P. Franks, Structural analysis of hydrated egg lecithin and cholesterol bilayers, II. Neutron diffraction, J. Mol. Biol. 100 (3) (1976) 359–378.
[66] M.C. Wiener, S.H. White, Fluid bilayer structure determination by the combined use of X-ray and neutron diffraction, Biophys. J. 59 (1991) 174–185.
[67] B.P. Schoneborn, A.C. Nunes, Neutron scattering, Annu. Rev. Biophys. Bioeng. 1 (1972) 529–552.
[68] A. Schroeter, T. Engelbrecht, R.H.H. Neubert, Influence of short chain ceramides and lipophilic penetration enhancers on the nano-structure of stratum corneum model membranes studied using neutron diffraction, Front. Chem. Sci. Eng. 7 (1) (2013) 29–36.
[69] T.N. Engelbrecht, A. Schroeter, T. Hauss, R.H.H. Neubert, Lipophilic penetration enhancers and their impact to the bilayer structure of stratum corneum lipid model membranes: neutron diffraction studies based on the example Oleic Acid, Biochim. Biophys. Acta Biomembr. 1808 (12) (2011) 2798–2806.
[70] T.N. Engelbrecht, B. Demé, B. Dobner, R.H.H. Neubert, Study of the influence of the penetration enhancer isopropyl myristate on the nanostructure of stratum corneum lipid model membranes using neutron diffraction and deuterium labelling, Skin Pharmacol. Physiol. 25 (4) (2012) 200–207.
[71] F.E.M. O'Brien, The control of humidity by saturated salt solutions, J. Sci. Instrum. 25 (1948) 73–76.
[72] J.F. Young, Humidity control in the laboratory using salt solutions, J. Appl. Chem. 17 (9) (1967) 241–245.
[73] P.W. Winston, D.H. Bates, Saturated solutions for the control of humidity in biological research, Ecology 41 (1) (1960) 232–237.
[74] N.P. Franks, W.R. Lieb, The structure of lipid bilayers and the effects of general anaesthetics, J. Mol. Biol. 133 (1979) 469–500.
[75] J.F. Nagle, S. Tristam-Nagle, Structure of lipid bilayers, Biochim. Biophys. Acta 1469 (2000) 159–195.
[76] F. Cser, About the Lorentz correction used in the interpretation of small angle X-ray scattering data of semicrystalline polymers, J. Appl. Polym. Sci. 80 (12) (2001) 2300–2308.
[77] M.W. de Jager, G.S. Gooris, M. Ponec, J.A. Bouwstra, Lipid mixtures prepared with well-defined synthetic ceramides closely mimic the unique stratum corneum lipid phase behavior, J. Lipid Res. 46 (2005) 2649–2656.
[78] M.R. Ali, K.H. Cheng, J. Huang, Ceramide drives cholesterol out of the ordered lipid bilyer phase into the crystal phase in 1-palmitoyl-2-oleoyl-sn-glycero-3-phosphocholine/cholesterol/ceramide ternary mixtures, Biochemistry 45 (2006) 12629–12638.
[79] H.I. Petrache, S.W. Dodd, M.F. Brown, Area per lipid and acyl length distribution in fluid phosphatidylcholines determined by ^{2}H NMR spectroscopy, Biophys. J. 79 (2000) 3172–3192.
[80] D.M. Small, The physical chemistry of lipids, in: D.J. Hanahan (Ed.), Handbook of Lipid Research, Plenum Press, New York, 1986.
[81] N.Y. Ryabova, M.A. Kiselev, S. Dante, T. Hauß, A.M. Balagurov, Investigation of stratum corneum lipid model membranes with free fatty acid composition by neutron diffraction, Eur. Biophys. J. 39 (2010) 1167–1176.
[82] N.Y. Ryabova, M.A. Kiselev, A.M. Balagurov, Transition processes in stratum corneum model lipid membranes with a mixture of free fatty acids, Biofizika 54 (5) (2009) 852–862.
[83] V.F. Sears, Neutron scattering lengths and cross section, Neutron News 3 (3) (1992) 26–37.
[84] J.A. Bouwstra, G.S. Gooris, W. Bras, D.T. Downing, Lipid organization in pig stratum corneum, J. Lipid Res. 35 (4) (1995) 685–695.
[85] I. Pascher, Molecular arrangements in sphingolipids. Conformation and hydrogen bonding of ceramide and their implication on membrane stability and permeability, Biochim. Biophys. Acta Biomembr. 455 (2) (1976) 433–451.
[86] S. Raudenkolb, S. Wartewig, R.H.H. Neubert, Polymorphism of ceramide 6: a vibrational spectroscopic and X-ray powder diffraction investigation of the diastereomers of N-(α-hydroxyoctadecanoyl)-phytosphingosine, Chem. Phys. Lipids 133 (2005) 89–102.
[87] D. Groen, G.S. Gooris, J.A. Bouwstra, Model membranes prepared with ceramide EOS, cholesterol and free fatty acids from a unique lamellar phase, Langmuir 26 (6) (2010) 4168–4175 Article.
[88] M.E. Rerek, H. Chen, B. Markovic, D. van Wyck, P. Garidel, R. Mendelsohn, D.J. Morre, Phytosphingosine and sphingosine ceramide headgroup hydrogen bonding: structural insights through thermotropic hydrogen/deuterium exchange, J. Phys. Chem. B 105 (2001) 9355–9362.

4.3 Influence of the penetration enhancer isopropyl myristate on stratum corneum lipid model membranes revealed by neutron diffraction and ^{2}H NMR experiments

Adina Eichner[1], Sören Stahlberg[1], Stefan Sonnenberger[1], Stefan Lange, Bodo Dobner, Andreas Ostermann, Tobias E. Schrader, Thomas Hauß, Annett Schroeter, Daniel Huster, Reinhard H.H. Neubert, *Biochimica et Biophysica Acta- Biomembranes* (2017) **1859** p.745-755

[1]These authors contributed equally to this work.

Online version: http://dx.doi.org/10.1016/j.bbamem.2017.01.029

Biochimica et Biophysica Acta 1859 (2017) 745–755

Contents lists available at ScienceDirect

Biochimica et Biophysica Acta

journal homepage: www.elsevier.com/locate/bbamem

Influence of the penetration enhancer isopropyl myristate on stratum corneum lipid model membranes revealed by neutron diffraction and ^{2}H NMR experiments

Adina Eichner [a,1], Sören Stahlberg [b,1], Stefan Sonnenberger [a,1], Stefan Lange [a,b], Bodo Dobner [a], Andreas Ostermann [c], Tobias E. Schrader [d], Thomas Hauß [e], Annett Schroeter [a], Daniel Huster [b], Reinhard H.H. Neubert [a,f,*]

[a] Institute of Pharmacy, Martin Luther University Halle-Wittenberg, 06120 Halle/Saale, Germany
[b] Institute of Medical Physics and Biophysics, University of Leipzig, 04107 Leipzig, Germany
[c] Heinz Maier-Leibnitz Zentrum (MLZ), Technische Universität München, 85748 Garching, Germany
[d] Jülich Centre for Neutron Science (JCNS) at Heinz Maier-Leibnitz Zentrum (MLZ), Forschungszentrum Jülich GmbH, 85748 Garching, Germany
[e] Institute of Soft Matter and Functional Materials, Helmholtz-Zentrum Berlin für Materialien und Energie, 14109 Berlin, Germany
[f] Institute of Applied Dermatopharmacy at the Martin Luther University Halle-Wittenberg, 06120 Halle/Saale, Germany

ARTICLE INFO

Article history:
Received 7 October 2016
Received in revised form 21 January 2017
Accepted 25 January 2017
Available online 26 January 2017

Keywords:
Stratum corneum
Lipid model membranes
Ceramides
Penetration enhancer
Neutron diffraction
^{2}H solid-state NMR spectroscopy
Phase transition
Short-periodicity phase
Long-periodicity phase

ABSTRACT

The stratum corneum (SC) provides the main barrier properties in native skin. The barrier function is attributed to the intercellular lipids, forming continuous multilamellar membranes. In this study, SC lipid membranes in model ratios were enriched with deuterated lipids in order to investigate structural and dynamical properties by neutron diffraction and ^{2}H solid-state NMR spectroscopy. Further, the effect of the penetration enhancer isopropyl myristate (IPM) on the structure of a well-known SC lipid model membrane containing synthetically derived methyl-branched ceramide [EOS], ceramide [AP], behenic acid and cholesterol (23/10/33/33 wt%) was investigated. IPM supported the formation of a single short-periodicity phase (SPP), in which we determined the molecular organization of CER[AP] and CER[EOS]-br for the first time. Furthermore, the thermotropic phase behavior of the lipid system was analyzed by additional neutron diffraction studies as well as by ^{2}H solid-state NMR spectroscopy, covering temperatures of 32 °C (physiological skin temperature), 50 °C, and 70 °C with a subsequent cooldown back to skin temperature. Both techniques revealed a phase transition and a hysteresis effect. During the cooldown, Bragg peaks corresponding to a long-periodicity phase (LPP) appeared. Additionally, ^{2}H NMR revealed that the IPM molecules are isotopic mobile at all temperatures.

Abbreviations and symbols

b_{coh}	coherent neutron scattering length
CER	ceramide
CHOL	cholesterol
$d/^2$H	deuterium
FFA	free fatty acid
F_h	structure factor, SF
IPM	isopropyl myristate
LPP	long-periodicity phase
RH	relative humidity
SC	stratum corneum
SPP	short-periodicity phase

1. Introduction

Being the outermost layer of mammalian skin, the stratum corneum (SC) maintains an important function as a diffusion barrier for penetrating substances [1,2]. Due to its complex structure, it not only protects the body from external influences but also prevents trans-epidermal water loss. Both tasks are primarily attributed to the intercellular lipids, which surround dead corneocytes and form complex multilamellar membranes [3]. It is well established that the structural organization of these layers determines the properties of the SC barrier [1], but the details of this complex structural assembly are not fully understood yet. Simultaneously, the major pathway of skin penetrating substances leads through the SC lipid matrix [3]. There, the most abundant lipids are ceramides (CER), cholesterol (CHOL) and free fatty acids (FFA) [3–5]. Among these, the very heterogeneous group of ceramides is known to play a fundamental role for the structural arrangement of the SC, and hence the

* Corresponding author.
E-mail address: reinhard.neubert@pharmazie.uni-halle.de (R.H.H. Neubert).
[1] These authors contributed equally to this work.

http://dx.doi.org/10.1016/j.bbamem.2017.01.029
0005-2736/

maintenance of the barrier function of the skin [6]. Especially the individual interactions between the CER subspecies and the lamellar lipid structure are a central point of interest.

Lipids extracted from the native SC are able to form two lamellar phases: a short-periodicity phase (SPP) with an approximated repeat spacing of 60 Å and a long-periodicity phase (LPP) with a repeat interval of 130 Å [7–9]. The SPP is known to be predominantly constructed from long-chain ceramides such as [AP] or [NP] [10,11]. The LPP formation is discussed to be highly connected to the ultra-long-chain ceramides such as CER[EOS] or CER[EOH] [12–17]. Moreover, CER[EOS] as one of the most lipophilic CER species, is mandatory for proper SC barrier function. This is in agreement with results from studies concerning atopic dermatitis or psoriasis, where the skin protection is compromised due to decreased levels of CER[EOS] [18–20].

SC lipid model membranes are very versatile tools for structural investigations and have contributed substantially to a better understanding of the lipid organization in human skin. While the SPP is well studied in SC models by neutron diffraction [10,21–24], the existence of its longer pendant, the LPP, is still under discussion. Recent studies have described the LPP structure in SC lipid model membranes at high relative humidity and determined the position of certain lipid segments in neutron diffraction experiments by deuterium labelling [25–27]. These were the first experiments, which revealed closer insights into the arrangement of the lipids within the LPP provoking additional questions regarding the LPP and its impact to the SC barrier.

For the treatment of skin diseases or disbalances, it is often desired to overcome the barrier properties and to increase the flux of pharmaceutically or cosmetically active substances through the skin temporarily. It was established that lipophilic penetration enhancers such as isopropyl myristate (IPM) induce disordering effects to the rigid SC lipid membranes and are commonly in use in different cutaneous formulations [28–31]. The liquid wax isopropyl myristate is known to increase the penetration rate of topically applied pharmaceuticals [32,33]. Although a lipophilic molecule itself, IPM features a small polar moiety at the ester group. It does not provide a clear head-to-tail polarity, which is profitable for its interaction with the membranes [34,35]. IPM is able to partially liquefy the lipids of the SC intercellular membrane [36,37]. X-ray diffraction experiments localized the ester group of the enhancer in the polar membrane region of SC models and the alkyl chain pointing towards the unit cell center [38]. Engelbrecht et al. confirmed this and further described a complete incorporation of IPM using neutron diffraction [39].

Here, we address the question whether IPM could manipulate the assembling process of a SC lipid model membrane containing a modified methyl-branched CER[EOS] (23 wt%) along with CER[AP]-C18 (10 wt%), cholesterol (CHOL) (33 wt%) and behenic acid (BA) (33 wt%), a system which showed the coexistence of SPP and LPP before [27]. We used neutron diffraction as it offers a wide range of advantages for the investigation of SC lipid models compared to X-ray diffraction. In particular, the different coherent scattering lengths for the isotopes hydrogen (^{1}H) and deuterium (^{2}H) [40–43] enabled the localization of deuterium labelled lipid segments within the model membranes on a molecular level [25,26,39,44–47]. Furthermore, we investigate the thermotropic phase behavior of this SC lipid mixture. To this end, we heated up the sample to 50 °C and 70 °C in a second neutron diffraction experiment, followed by a final cool-down to 32 °C. Former experiments with SC lipids showed phase transitions around those high temperatures [48], whereby even a recrystallization to a LPP was described [9]. The thermotropic phase behavior of the SC lipid mixture was also studied using solid-state ^{2}H NMR spectroscopy. ^{2}H solid-state NMR is a powerful tool for investigating the structure and dynamics of lipid systems [49]. It also provides identification of the phase state of a certain component in the sample as well as quantification of phase proportions in the system [50–52]. Our results show that the vast majority of the IPM formed an isotropic phase that is separated from the observed SPP.

2. Materials and methods

2.1. Materials

The enantiomeric mixture of DL-CER[AP]-C18 (*N*-(a-hydroxyoctadecanoyl)-phytosphingosine) with a purity of 98% was generously provided by Evonik Industries AG (Essen, Germany). DL-CER[AP]-C18-d_3, CER[EOS]-C30-C16-d_3 and IPM-d_3 were obtained by chemical synthesis. The IPM-d_3 synthesis was described earlier [39]. The publication presenting the synthesis of CER[EOS]-C30-C16-d_3 has been submitted [53]. The detailed description of the synthesis of DL-CER[AP]-C18-d_3 as well as perdeuterated IPM-d_{25} will be published soon. The synthesis of CER[EOS]-C30-C16-br was described in a previous publication, where the CER species were characterized by DSC and Fourier transform Raman spectroscopy studies to underline the comparability to the native CER[EOS]-C30-C18:2 [54]. The identity of the applied CERs was confirmed by high resolution mass spectrometry. Cholesterol (purity ≥99%), behenic acid (≥ 99%) and the non-deuterated IPM (> 98%) were purchased from Sigma Aldrich GmbH (Steinheim, Germany) and used as received. Fig. 1 illustrates the chemical structures of the SC lipids used in our experiments.

For the neutron diffraction experiments, quartz slides with dimensions of 65 × 25 × 0.3 mm^3 were used as sample wafers providing a low scattering cross-section for neutrons and were purchased from Saint-Gobain (Wiesbaden, Germany) as polished Spectrosil 2000.

2.2. Sample preparation

For the neutron diffraction experiments, we prepared SC lipid model membranes, containing the partially deuterated ceramides [AP]-C18-d_3 and a modified ultra-long-chain ω-acyl CER[EOS]-d_3, cholesterol (CHOL), and behenic acid (BA) (10/23/33/33 wt%). A specifically deuterated IPM variant was added in a concentration of 10 wt% as used before in comparable lipid mixtures [39]. The samples were prepared according to an established procedure to yield well oriented multilamellar lipid layers [55]. Each lipid was dissolved separately in a chloroform/methanol mixture (2:1; *v*/*v*) with a resulting concentration of 10 mg/ml. Afterwards, the lipid solutions were mixed at the desired ratios. A volume of 1.2 ml was spread on a quartz slide at a temperature of 70 °C. For a complete solvent removal, the samples were stored in a desiccator at room temperature and low vacuum for 12 h. The following annealing procedure included heating (75 °C) and cooling (25 °C) cycles of at least 4 h. The state of order and the mosaicity of the SC lipid membranes strongly depend on the annealing process [56]. Due to this procedure, higher peak intensities and less mosaicity are obtained, which is beneficial for the subsequent data analysis [57,58]. The sample preparation and treatment were described in detail before [27]. Four different samples were prepared (see Table 1).

For the ^{2}H NMR measurements, the sample either contained CER[AP18]-d_3, CER[EOS]-d_3 or IPM-d_{25} (see Table 2). For the sake of a better signal-to-noise ratio and the detection of the influence of the IPM on the model membrane, we used 20 wt% of the penetration enhancer in the ^{2}H NMR samples. For sample preparation, aliquots of each constituent were dissolved in a chloroform/methanol mixture (2:1; *v*/*v*). The solvent was evaporated using a rotary evaporator. The remaining lipid film was dissolved in cyclohexane and the sample was lyophilized overnight resulting in a fluffy powder, which was hydrated with 50 wt% deuterium-depleted water. To prevent dehydration, samples were filled into 4 mm MAS rotors and sealed for static ^{2}H NMR measurements. 24 h prior to NMR spectra acquisition, samples were homogenized by freezing them in liquid nitrogen and heating them to 80 °C. This treatment was repeated 10 times before incubating the samples at 22 °C. ^{2}H NMR spectra were acquired at three temperatures in the following order: 32 °C, 50 °C, 70 °C and 32 °C.

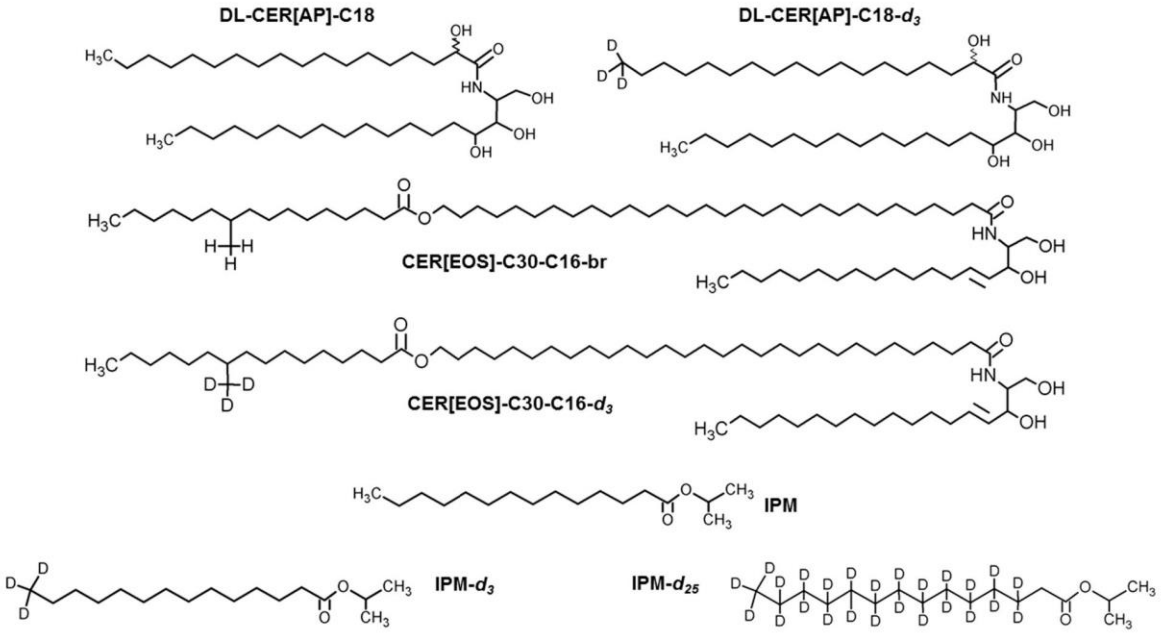

Fig. 1. Chemical structures of the ceramides and IPM molecules used in this study.

2.3. Neutron diffraction experiments

The neutron diffraction experiments at physiological skin temperature (32 °C) were performed using the instrument BIODIFF [59] at the Heinz Maier Leibnitz Zentrum (MLZ), Garching, Germany. For the first time, this instrument was used for the investigation of membrane structures, which required the installation of a modified sample environment (see Fig. (a) in the supplemental section). The experiment was performed at a wavelength of 4.72 Å with a $\Delta\lambda/\lambda$ of 2%. The detector consists of a cylindrical neutron image plate (diameter × height = $400 \times 450\ mm^2$, spatial resolution 0.5 mm × 0.5 mm), where the sample is mounted in the middle on the sample goniometer (x, y, ω) from the top [59].

To compare to in vivo conditions, the samples were measured at the skin temperature of 32 °C and a relative humidity (RH) of 98%, reached by a saturated solution of K_2SO_4 in D_2O/H_2O. The high humidity was chosen because it promotes formation of the LPP in CER[EOS] [60]. Each membrane system was measured at three different D_2O contrasts (100/0, 50/50 and 8/92% (mol/mol)) in order to vary the neutron scattering length density (NSLD) between water and lipids and to determine the structure factor phase signs (contrast matching). After each variation of the H_2O/D_2O contrast, sample equilibration was allowed for 8 h before the data acquisition started. Former experiments verified that an equilibration time of 6–8 h is sufficient to achieve an optimized hydration level of the SC lipid model membranes [10,24,54].

At BIODIFF, the measurements for the first to third Bragg peak order were performed with a sample rotation from 0° to 21°, corresponding to a 2θ range from 0° to 42° per hour (21° ω/h). Each scan was repeated five times and averaged for better statistics. For the fourth and fifth Bragg peak order a scan with an ω-range from 9° to 21°, corresponding to a 2θ range from 18° to 42° per hour (12° ω/h), was performed twice to improve the signal-to-noise ratio. Starting at a 2θ angle of 21°, the determined intensities were additionally expanded by footprint correction to compensate the sample's rotation beyond the beam. Moreover, the different rotation velocities were normalized to 21° ω/h dividing the fourth and fifth order intensities by 1.75. Additionally, a background pattern with an empty quartz slide in a sample can was recorded at each ω-range and was subtracted from the scans.

The neutron diffraction experiments to investigate the thermotropic phase behavior of the SC lipid model membranes were performed at the V1 Membrane Diffractometer of the research reactor of the Helmholtz Zentrum für Materialien und Energie (HZB, Berlin, Germany). The data

Table 1
Lipid composition of the investigated multilamellar SC models for neutron diffraction studies.

SC lipid model system	Designation	Ratio (wt%)
I CER[AP]/CER[EOS]-br/CHOL/BA + 10% IPM	AP_EOS-br_IPM	10/23/33/33
II CER[AP]/CER[EOS]-br/CHOL/BA + 10% IPM-d_3	AP_EOS-br_IPM-d_3	10/23/33/33
III CER[AP]/CER[EOS]-d_3/CHOL/BA + 10% IPM	AP_EOS-d_3_IPM	10/23/33/33
IV CER[AP]-d_3/CER[EOS]-br/CHOL/BA + 10% IPM-d_3	AP-d_3_EOS-br_IPM-d_3	10/23/33/33

Table 2
Lipid composition of the investigated SC models in the ^2H NMR studies.

SC lipid model system	Designation	Ratio (wt%)
I CER[AP]-d_3/CER[EOS]-br/CHOL/BA + 20% IPM	AP-d_3_EOS-br_IPM	10/23/33/33
II CER[AP]/CER[EOS]-d_3/CHOL/BA + 20% IPM	AP_EOS-d_3_IPM	10/23/33/33
III CER[AP]/CER[EOS]-br/CHOL/BA + 20% IPM-d_{25}	AP_EOS-br_IPM-d_{25}	10/23/33/33

were collected at a wavelength of 4.57 Å and the distance between sample and the detector was 1025.7 mm. We used a two-dimensional position-sensitive ^{3}He detector with an area of 200 × 200 mm^2 and a spatial resolution of 1.5 × 1.5 mm^2. The one-dimensional diffraction experiment was performed by a reflection setup, which is described in detail elsewhere [22].

First, the samples were measured at 8% D_2O and 98% RH at skin temperature to compare the results to those obtained at BIODIFF. Here, the comparability between the two neutron diffraction instruments was given. At 98% RH, the samples were heated up to 50 °C and 70 °C and cooled down to 32 °C. We chose a temperature below the lipid mixtures' melting point (50 °C) and a second temperature close to the melting point (70 °C), in order to prevent a displacement of the lipids from the quartz wafer due to the vertical sample setup during the measurements. Only the changes of the first Bragg peak order were investigated during the heating periods. For the thermotropic phase behavior study, the measurements were only performed at 8% D_2O, since the scattering length of water is zero at this point [61,62], hence, it is not influencing the acquired data.

2.4. Data analysis

The detector registered the intensity I of the scattered neutrons as a function of the scattering angle 2θ. From the position of a series of equidistant peaks in the diffraction pattern, the periodicity (d spacing) of the lamellar phases, was calculated using $d = (2n\pi)/Q_n$, with n as the Bragg peak's number of order. The peak positions and intensities were determined by Gaussian fitting using the software package IGOR Pro Version 6.34A (WaveMetrics Inc., Portland, OR, USA). Thereby, the particular analysis of the integrated peak intensity I_h of the hth order was performed [63]. Furthermore, using I_h, the absolute values of their correlating structure factors F_h were calculated by $F_h = \sqrt{h \cdot A_h \cdot I_h}$ with A_h as absorption correction and h as Lorentz factor, which is related to the data collection geometry [64]. To infer conclusions about the nanoscaled membrane structure from the data, NSLD profiles $\rho_s(x)$ were calculated using Fourier transformation of the structure factors F_h according to [65]:

$$\rho_s(x) = a + b\frac{2}{d}\sum_{h=1}^{h_{max}} F_h \cos\left(\frac{2\pi h x}{d}\right)$$

where a and b represent coefficients for relative normalization of $\rho_s(x)$, h the diffraction order with the associated structure factor F_h and d describes the lamellar repeat distance. The determination of the phase factor of F_h was achieved by contrast variation, which assumes "+" or "−" for centrosymmetric bilayers [58,63] as the lamellar lipid phases are supposed to be organized. A detailed description of the applied phase assignment is given in the supplement.

The localization of a ^{2}H labelled segment is possible due to the different coherent scattering length of neutrons for the isotopes hydrogen ^{1}H ($b_{coh} = -0.374 \times 10^{-12}$ cm) and deuterium ^{2}H (d) ($b_{coh} = +0.667 \times 10^{-12}$ cm) [66]. Accordingly, the structure factors of the deuterated sample F_{h_deut} as well as the corresponding factors F_{h_prot} from the protonated sample were determined and used for the Fourier transformation. By the calculation of the difference density $\rho_{diff}(x) = \rho_{deut}(x) - \rho_{prot}(x)$, with ρ_{deut} as the NSLD of the partially deuterated sample and $\rho_{prot}(x)$ as the NSLD of the protonated sample, the position of the deuterated label within the lipid unit cell is visible by the resulting maxima in $\rho_{diff}(x)$.

2.5. ^{2}H NMR experiments

All NMR spectra were acquired at a Bruker Avance 750 WB NMR spectrometer (Bruker BioSpin, Rheinstetten, Germany) using a deuterium resonance frequency of 115.1 MHz and a spectral width of ±250 kHz. In the probe, a 5 mm solenoid coil was used. Measurements were conducted applying quadrature phase detection and a phase-cycled quadrupolar echo sequence with two 2–2.3 μs π/2 pulses separated by a 30 μs delay. The time delay between two successive scans was 50 s. Samples were measured at temperatures of 32 °C, 50 °C, 70 °C and then again at 32 °C since previous studies showed that phase transitions were reversible but undergo hysteresis [67]. For further processing of the acquired spectra a self-written Mathcad (MathSoft, Cambridge, MA) script [68] and NMR WEBLAB [69] were used.

3. Results and discussion

3.1. Characterization of the single phase system by neutron diffraction

For all samples, a system with five lamellar orders in the neutron diffraction spectra was obtained (see Fig. 2). From the positions of the equidistant diffraction peaks, a d spacing of 48.4 ± 0.1 Å was calculated. The fraction of cholesterol, which could not be integrated into the membranes, gives rise to a crystalline phase, which is visible as a separated cholesterol peak at an angle of $2\theta = 8.0°$. But its presence is not affecting the data analysis [70].

The structure factor (SF) phase signs were "− + − + −" for the 1st to the 5th order (see supplemental information). By Fourier transformation, the NSLD profiles $\rho_s(x)$ for the reference sample were calculated using their absolute SFs (see Fig. 3). All NSLD profiles $\rho_s(x)$ show distinct maxima at the right and left borders of the diagram, indicating positive scattering length densities in that area. This is interpreted as the position of the polar head groups [62]. From the hydrophobic-hydrophilic boundary x_{HH} at 19.8 ± 0.4 Å (see supplemental information), we can conclude, that the hydrophobic part of the bilayer is about 39.6 ± 0.8 Å and each polar part covers 4.4 ± 0.4 Å. The water distribution function was calculated as the difference of the NSLD profiles 100% D_2O and 8% D_2O. Hence, water is only located in the polar head group region and not positioned beside the alkyl chains.

As explained in the Introduction, repeat distances of about 60 Å are associated with the SPP [9]. Clearly, the observed d spacing of about 48 Å is much shorter than that. The reason for this discrepancy is the membrane composition of native SC, as it is composed of more complex lipid mixtures including several ceramide subclasses and fatty acids with longer alkyl chain lengths [46,71]. Here, only four SC lipids with a defined chain length were chosen, in order to get further insights into the membrane assembling process with a more detailed understanding of the structures and lipid interactions. The CER[AP]-C18 is not able to form a SPP with dimensions of 60 Å. Referring to a length of 1.27 Å per C—C bond [72,73], for the amide bonded C18 fatty acid a chain length of 22.9 Å can be assumed in its all-*trans* conformation. The arrangement of two CER[AP] molecules opposite to each other would result in a maximum spacing of 45.7 Å for the fatty acid chains. This is not compatible with a 60 Å spacing. A detailed discussion referring to that topic is found elsewhere [27]. Thus, a lower d spacing was accepted and even presented in former experiments [10,21,22,24,44,54,74,75].

The lamellar spacing of 48 Å means that the applied CER[EOS]-br did not induce the formation of a LPP unit cell. In an earlier experiment on the SC lipid system without the penetration enhancer IPM, a multiphase system was obtained [27]. There, one phase showed a highly ordered ($h = 7$) SPP of 48 Å and another phase formed a LPP with a d spacing of about 118 Å [27]. We suggest that the lower number of diffraction peaks observed in the experimental neutron spectra is indicative of a larger variation in the lamellar stacking with respect to one another or a decreased order of the internal membrane structure. In principle, a fluidizing effect of the IPM on the SC membranes could be a reason for this [36,37].

Thus, IPM showed several effects to the SC lipid model membrane: Next to a decreased lamellar order, it inhibited a LPP formation. This result is of immediate importance with regard to the LPP impact to the SC barrier function.

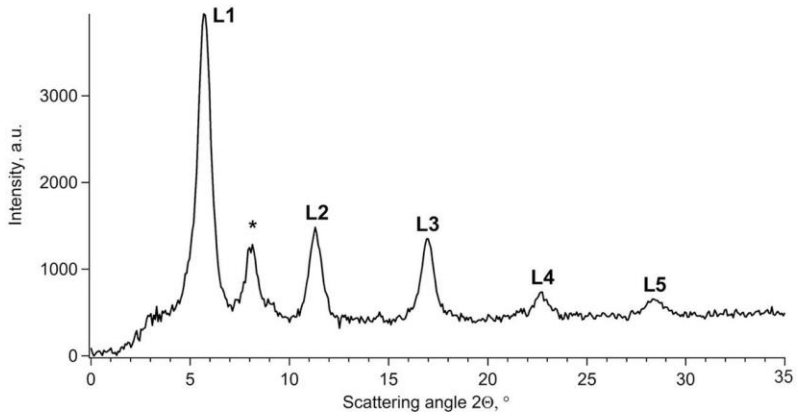

Fig. 2. Neutron diffraction spectrum of sample I, measured at 100% D_2O contrast, 98% RH and a temperature of 32 °C. The described background subtraction was performed. Next to the crystalline CHOL peak (*), the diffraction orders are labelled L1 to L5.

3.2. Localization of the deuterated lipid segments inside the SC lipid model membranes

3.2.1. CER[AP]-C18-d_3

To localize the deuterium labelled groups of CER[AP], the normalized SFs were used. The NSLD profiles and $\rho_{diff}(x)$ are illustrated in Fig. 4. The deuterated methyl group was localized between ± 7.0 Å from the bilayer center, indicated by a maximum of $\rho_{diff}(x)$.

We assume the hairpin conformation for CER[AP]-d_3, because it is energetically more stable under hydration than the extended structure [76]. Hereby, the CER head groups are located in both polar bilayer borders and the non-polar alkyl chains point towards the bilayer center. The maximum spacing of 45.7 Å for the fatty acid chains of two molecules opposite to each other is contradicting the hydrophobic thickness of the bilayer with 39.6 Å. Therefore, there has to be an alkyl chain overlap of 6.1 Å. The interdigitation of CER[AP] alkyl chain ends was suggested before for a SPP of 48 Å [23,24]. Our results are in agreement with this. But the broad deuterium distribution in the bilayer center also indicates that not all C—C bonds are in an all-*trans* conformation. In order to explain the broad deuterium distribution in that area, we have to include the possibility of shorter chain lengths than 22.9 Å, meaning less interdigitating of the deuterated methyl groups in the membrane center.

Overall, comparable results were described before for CER[NS]-C24 in a SPP of about 54 Å [71]. To the best of our knowledge, this is the first study, which localizes CER[AP]-C18 in a single SPP of about 48 Å in a SC lipid model membrane.

3.2.2. CER[EOS]-d_3

Although the preparation method was adapted from an earlier experiment [27], the high CER[EOS]-br ratio of 60 wt% of the CER fraction did not induce formation of a LPP. So the question was, if the deuterated ultra-long-chain CER could be arranged within the SPP as former experiments assumed [24,44,54]. The calculated difference in the scattering length $\rho_{diff}(x)$ (Fig. 5) shows significant maxima at ± 17 Å, which is highly correlated with the presence of the CD_3 groups. From the acquired data, we can conclude a reasonable position of the CER. The C30 alkyl chain (38.1 Å) between both polar molecule parts fits into the hydrophobic area of the bilayer, calculated with 39.6 Å. Thus, the polar head group is positioned in one polar area and the ester group in the other polar area of one unit cell. According to this, the esterified palmitic acid is suggested to extend into the next bilayer, explaining the deuterium position at ± 17 Å. At this point, the proposed arrangement of CER[EOS]-d_3 in a SPP can be used to verify earlier published ideas for the first time [24,44,54].

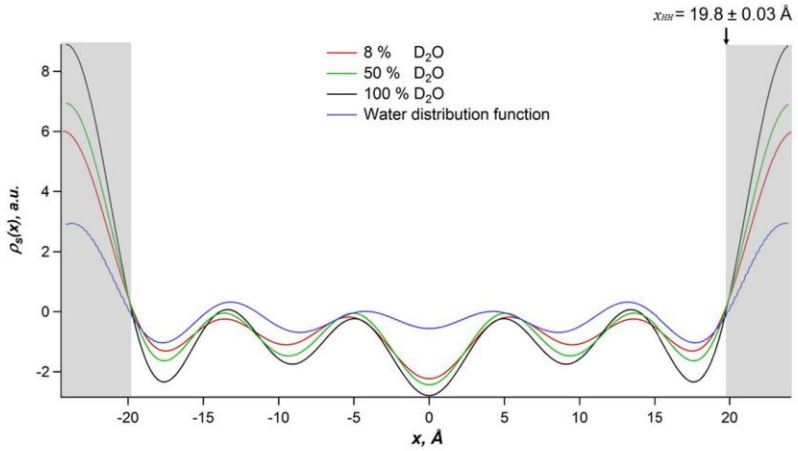

Fig. 3. The NSLD profiles for sample I, determined at 98% RH, 32 °C and all three D_2O contrasts. The blue line represents the water distribution function, plotted against the unit cell scale. The grey boxes indicate the polar head group areas.

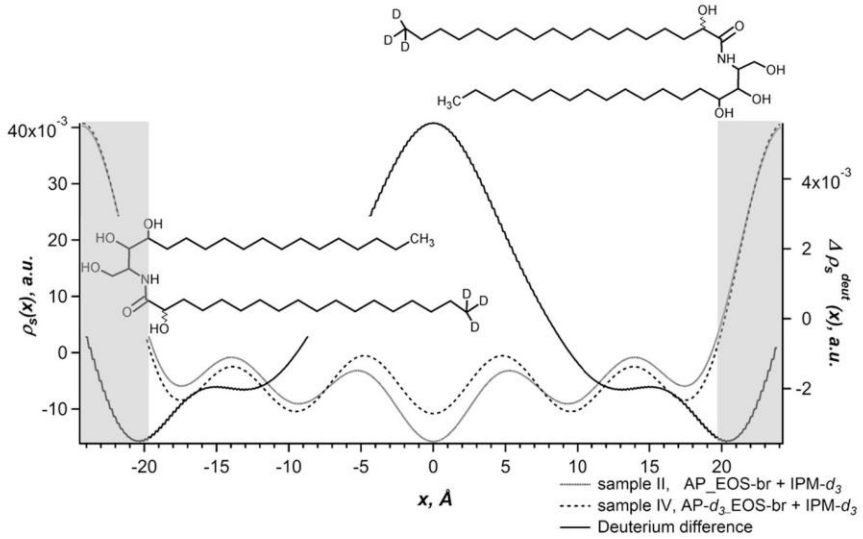

Fig. 4. The NSLD profiles of sample II (grey line) and IV (dotted line), measured at 8% D_2O, 98% RH and a temperature of 32 °C. Additionally, their difference is plotted (black line), providing an estimate of the position of the deuterated methyl group of CER[AP] in the membrane.

3.2.3. IPM-d_3

The lipophilic penetration enhancer IPM-d_3 was not detected in the SPP (see supplemental, Fig. (d) and (e)). This was surprising, as a former neutron scattering experiment of our group suggested two possible locations of IPM-d_3 [39].

One hypothesis to explain the absence of IPM in the SPP is that during sample preparation, IPM was initially homogeneously mixed with the SC lipids and detectable in the mixtures before as reported in [39]. From our current experiments, we must consider that this earlier results represent a non-equilibrium state. In our recent study, equilibration was given sufficient time to occur (i.e. 2 months) allowing the liquid wax IPM to undergo the observed phase separation into an isotropic phase. The formation of a micellar or cubic phase seems likely, as the ^2H NMR results identified IPM in an isotropic phase. A micellar or cubic phase would explain that we were not able to detect IPM in a separated phase in the diffraction study. Furthermore, an interaction of the IPM in a highly curved structure with the headgroup region of the SC membranes could be responsible for the prevention of the LPP phase.

3.3. Thermotropic phase behavior of the SC models by neutron diffraction

For closer insights into the SC lipid model membrane properties, the thermotropic phase behavior was studied. In order to investigate the effect of the penetration enhancer IPM on the phase behavior, sample II containing IPM-d_3 was selected.

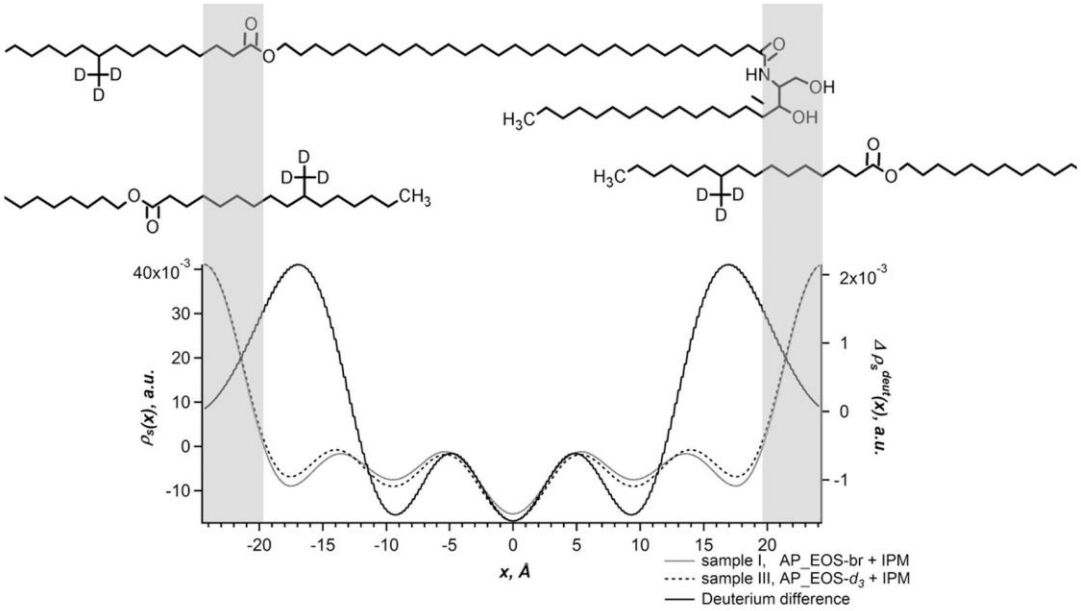

Fig. 5. NSLD profiles of sample I (grey line) and III (dotted line), measured at 8% D_2O, 98% RH and a temperature of 32 °C. Additionally, their difference is plotted (black line), providing an estimate of the position of the deuterated methyl group of CER[EOS]-br in the membrane. The polar molecule parts are positioned at the polar areas of the bilayer (grey boxes). The esterified palmitic acid extends into the next bilayer, explaining the deuterium position at ± 17 Å.

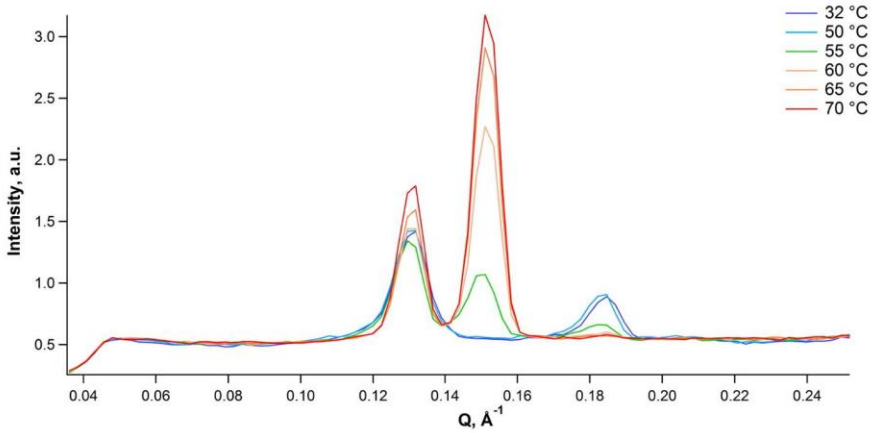

Fig. 6. Rocking curve of sample II, AP_EOS-br + IPM-d_3 during the heating period from 32 °C to 70 °C, received at 8% D_2O and 98% RH. Here, the detector position was optimized for the first lamellar order scan at 0.132 $Å^{-1}$ (L1).

The sample was heated from 32 °C to 70 °C at 98% RH (see Fig. 6). At temperatures from 32 °C to 50 °C, the 1st order Bragg peak (0.132 $Å^{-1}$) showed no changes in position or intensity. Only the peak position of crystalline cholesterol shifted slightly from 0.185 to 0.182 $Å^{-1}$ with no further meaning for the following discussion. But reaching 55 °C, an additional peak appeared at 0.151 $Å^{-1}$. Simultaneously, the 1st order Bragg peak and CHOL peak decreased in intensity. Upon further heating, the intensity of the additional peak (0.151 $Å^{-1}$) increased significantly. At 60 °C, the 1st order Bragg peak started to increase, whereby crystalline CHOL was integrated completely into the SC lipid membranes, as the corresponding signal disappeared. Both remaining peaks reached their maximum intensities at 70 °C. The increased thermal energy inside the lipid lamellae induced a phase transition and separation starting at 55 °C. Due to the application of DL-CER[AP]-C18, it is possible, that the additional phase at 0.151 $Å^{-1}$ is mainly built by a phase separated diastereomer. Assuming the 1st order Bragg peak for that peak, a *d* spacing of 41.8 Å could be calculated. Different unit cell scales for the unnatural L-CER[AP] isomer compared to the natural occurring D-CER[AP] were described before, where the V-shape conformation of L-CER[AP] turned out a smaller lamellar repeat distance [77]. A former neutron diffraction experiment on a quaternary DL-CER[AP]-C18 lipid model system detected a single SPP with ~46 Å and a second SPP with ~41 Å, appearing at 81 °C [62]. A recent study on the same SC lipid system suggested the V-shape conformation to be preferable at high temperatures [78]. From that, we can adapt the idea of the ceramide conformation change and are able to explain the presence of that newly formed 41.8 Å phase by phase separated CER[AP].

Afterwards, the phase behavior of the SC lipid model membrane under cooling was observed (see Fig. 7). With decreasing temperature, a reorganization of the lipids took place and we observed a hysteresis effect. At 65 °C, the intensity of the 1st order Bragg peak (0.132 $Å^{-1}$) increased significantly. This can be interpreted as another conformational change of CER[AP], back to the hairpin conformation. The 48 Å SPP was very stable after the phase transition. The second lamellar phase, corresponding to the 1st order Bragg peak at 0.151 $Å^{-1}$ shifted slightly towards smaller *Q* values. More interesting is its decreasing peak intensity. Referring to the recent results of Gruzinov et al. [78], a smaller peak intensity could be connected to a destabilized lamellar arrangement of CER[AP] in its V-shape conformation, back to the hairpin conformation.

A third phase appeared at 65 °C, indicated by three equidistant Bragg peak orders at 0.062 $Å^{-1}$ (L1), 0.124 $Å^{-1}$ (L2), and as a shoulder of the high crystalline CHOL peak at 0.186 $Å^{-1}$ (L3). Using the positions of these three lamellar orders and a wavelength λ of 4.57 Å, a *d* spacing of 100.8 Å was calculated. Compared to the SC lipid model membrane without IPM, where a LPP with ~114 Å was observed [27], we had distinct evidence for the appearance of a LPP here as well. With further decrease in temperature, the LPP peak intensities became smaller. At 55 °C,

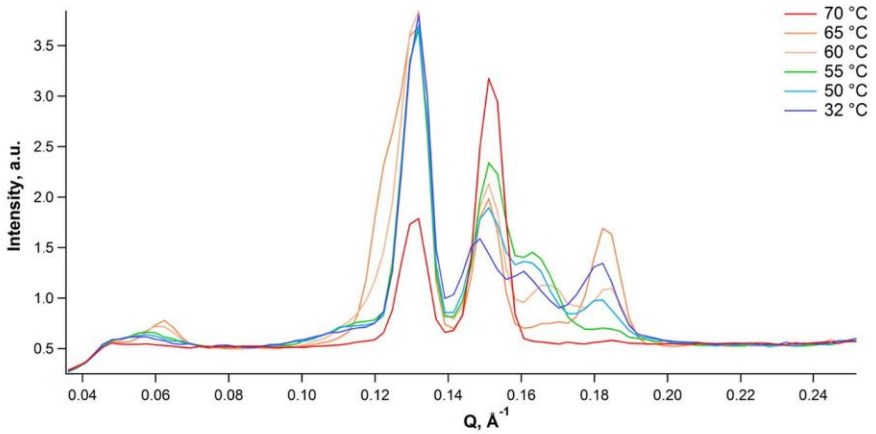

Fig. 7. Rocking curve of sample II, AP_EOS-br + IPM-d_3 during the cooling period from 70 °C to 32 °C, obtained at 8% D_2O and 98% RH. Here, the detector position was optimized for the first lamellar order scan at 0.132 $Å^{-1}$ (L1).

the 1st and 2nd lamellar orders were only visible as small signals. Simultaneously, the peaks shifted towards smaller Q values, resulting in a final *d* spacing of 111.5 Å at 32 °C.

Although a LPP appeared, this phenomenon was highly associated to the temperature. The phase transition during the cool-down enabled the formation of the long phase. This phenomenon was described before for SC lipids, extracted from native material [9]. In that case, the synthetic lipids showed a comparable phase behavior to the skin. Furthermore, the CER[EOS]-br was able to support the formation of a LPP at high relative humidity again. Former studies showed the necessity of an unsaturated FFA as an ultra-long-chain component [79]. With the present study, we are able to revise this.

Due to the phase separation of IPM, it was not able to influence the lipid phase behavior anymore and then did not inhibit the formation of a LPP during the thermal treatment. With the LPP appearance and its connection to the SC barrier function, we assume that the penetration promoting effect of IPM then was absent.

Also the intensity of the diffraction peak from the excess CHOL showed an interesting behavior during the cooling period providing insights into the membrane assembling process. The peak at 0.183 $Å^{-1}$ changed measurably indicating the partial incorporation of excess CHOL and its final recrystallization at 32 °C. But we can consider that CHOL was included in the membranes, based on the changing peak intensity of the excess sterol. We suggest it to be integrated into the newly built phases, while the lipid layers were rearranged. The necessity of cholesterol for the lamellar arrangement and a proper barrier function was described before [80,81].

3.4. Thermotropic phase behavior by ^2H NMR spectroscopy

While deuterated methyl groups represent a great tool for the localization of these molecular segments in SC lipid models using neutron diffraction, they can also be employed in ^2H NMR experiments, which help in understanding the structure and phase compositions of various SC model systems. While specifically methyl-deuterated probes in ceramides are less suited to study the phase composition of these molecules, they still represent very good probes to investigate the molecular dynamics of the ceramide acyl chains. Methyl groups undergo 3-site hopping motions, which scale the quadrupolar couplings of an otherwise rigid CH_3 group to 41.75 kHz, which is 1/3 of its maximal value. Additional motional averaging by local or more global fluctuations further decreases the observed quadrupolar splitting [82]. Thus, methyl groups can be detected with relatively high sensitivity and alterations of the detected line shape from the classic Pake doublet are indicative of motions in a broad correlation time window up to the intermediate microsecond range [82].

In the model system, we have switched the ^2H label between the terminal methyl group of CER[AP] or CER[EOS]-br, thus obtaining information about the dynamics of these molecular segments. In phospholipid membranes, the terminal methyl groups are highly disordered and undergo large amplitude motions yielding molecular order parameters smaller than 0.02. However, in SC models even the terminal methyl groups are more ordered. Fig. 8 shows the ^2H NMR spectra of CER[AP]-d_3_CER[EOS]-br_CHOL_BA + 20 wt% IPM (left) and CER[AP]_CER[EOS]-d_3_CHOL_BA + 20 wt% IPM and CER[AP]_CER[EOS]-br_CHOL_BA + 20 wt% IPM-d_{25} (right) at three temperatures. There is no indication for the presence of a rigid

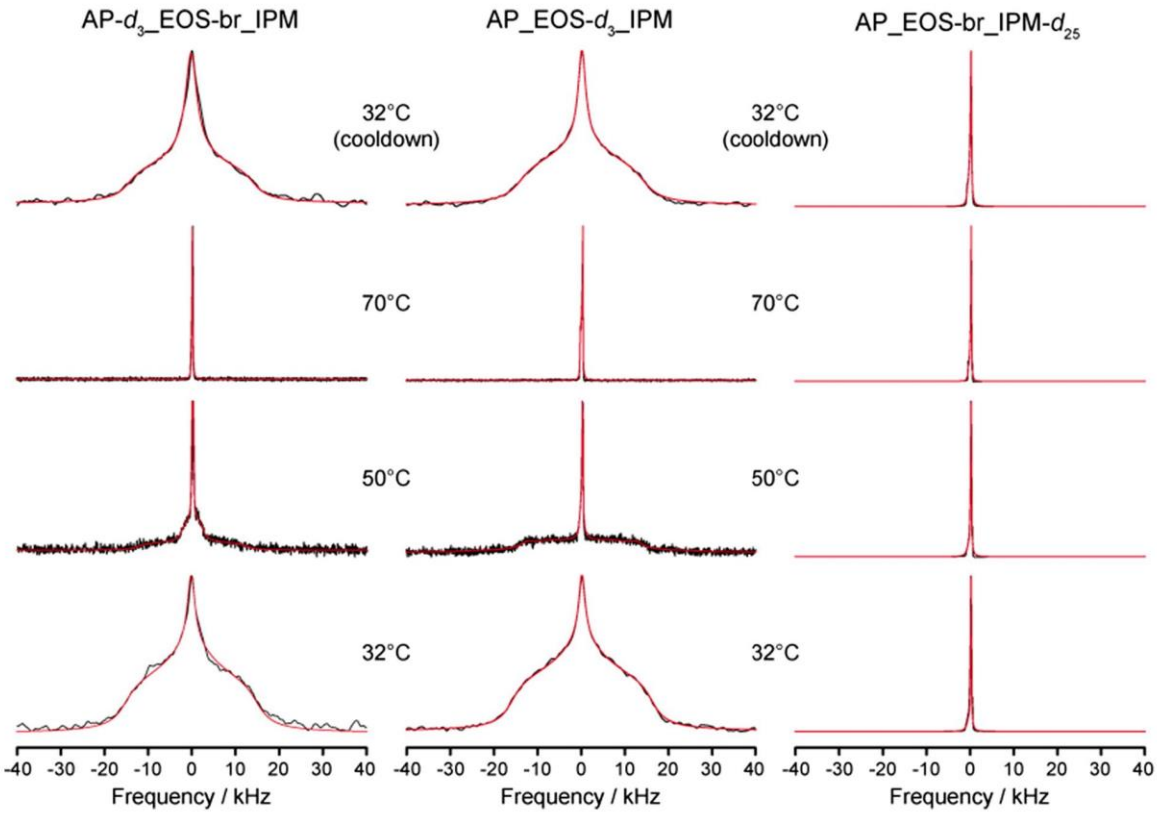

Fig. 8. ^2H NMR spectra of the mixtures given temperatures at a hydration level of 50 wt%. The left column shows the spectra of the mixture containing specifically deuterated AP-d_3, the middle column depicts spectra of the EOS-d_3 and the right column displays the spectra of IPM-d_{25}. ^2H NMR spectra were acquired using a repetition time of 50 s. The red lines represent the numerically simulated fits of the acquired spectra (black lines). Simulations were calculated assuming two-site hopping of the molecules, methyl group rotation, local fluctuations with an order parameter of 0.7–0.8, and an isotropic component.

orthorhombic or hexagonal phase, which would have manifested itself by a Pake spectrum with a quadrupolar splitting of around 40 kHz. In contrast, even at physiological skin temperature, both ceramide species show NMR spectra that are indicative of motions that can be described by a two-site hop model [83]. In this model, the —C—CH_3 bond is assumed to hop between two sites with a hopping angle of 120° [69]. This hopping appears to occur at a rate, which is faster than the inverse of the quadrupolar interaction strength, which is in the range of a few microseconds.

The simulations of the ^{2}H NMR spectra require input of the value of the motionally averaged quadrupolar coupling. As mentioned above, this value is 41.75 kHz for a rotating methyl group, but can be further averaged by motions of the chain of the ceramides. This is typically expressed by an order parameter that defines the motional amplitude of a specific bond vector of a given segment [84–86]. With these considerations, we can discuss the motions of the methyl groups of CER[AP]-C18 and CER[EOS]-br, respectively. At 32 °C, both molecules undergo the aforementioned two-site hopping but in addition, the bond vectors fluctuate expressed by an order parameter of 0.72 for CER[AP]-C18 and 0.77 for CER[EOS]-br. These results demonstrate that both CERs are part of the lamellar structure of the SC mix.

Additionally, the simulated NMR spectra feature a small isotropic component (6% for CER[AP]-C18 and 8% for CER[EOS]-br). Such behavior has been shown before for ceramides in similar SC model systems as well as for the intact SC [50–52,87,88]. At elevated temperature of 50 °C, the NMR spectra of both ceramide species become much narrower indicating large amplitude and isotropic motions (relevant for about 20% of the CER[AP]-C18 and CER[EOS]-br), the latter of which dominate the mixture at 70 °C. After cooling both samples down to skin temperature, the NMR spectra show again the two-site hopping. Nevertheless, its contribution to spectral intensity is a bit less than before heating to 50 °C. This can be interpreted as a hysteresis behavior which has already been reported for ceramide (bovine brain ceramide, Type III) containing SC model systems [67]. The line shape of the ^{2}H NMR spectra of CER[EOS]-br and CER[AP]-C18 looks alike which suggests that both species are contained within one common phase. Since an SPP could be detected at least for CER[AP]-C18, both species appear to be together in the SPP.

Very surprisingly, IPM showed isotropic ^{2}H NMR spectra at all temperatures, which means that the IPM is always highly mobile and may be organized in a structure with highly curved surfaces such as a micellar or cubic phase but possibly able to interact with the headgroups of the lipids in the lamellar phase, which could lead to a decrease in the order of the SC membrane model. Considering the signal-to-noise ratio, a possible proportion of IPM being part of a fluid phase would be <2%. However, it is not possible to distinguish between the cases where IPM is present in an isotropic phase mixed with the isotropic fluid fraction of SC lipids, and the case where IPM is present in segregated isotropic fluid outside the SC lipids.

4. Conclusion

We investigated how the penetration enhancer IPM influenced the assembling process of a well-known SC lipid model membrane containing CER[AP]-C18, ultra-long-chain CER[EOS]-br, behenic acid, and cholesterol. Using neutron diffraction, we found that IPM decreased the lamellar state of order and influenced the phase behavior of the SC model membranes possibly by interaction with the lipid headgroups. Moreover it prevented the formation of a LPP. The absence of the LPP is an interesting point with regard to a perturbed SC barrier. In fact, IPM caused effects, which disordered the rigid lamellar lipid structure and decreased the barrier properties.

Furthermore, we successfully applied partially deuterated SC lipids and were able to determine their positions within the SC lipid system for the first time. The localization of the deuterated methyl groups of CER[AP]-C18 and CER[EOS]-br generated a conclusion to the molecule positions within the lateral organization of the model membrane. Thus, our data confirmed former ideas of the CER arrangement within comparable lipid mixtures [23,24,44,54].

Although we observed a defined effect of the penetration enhancer IPM to the applied SC lipid model membrane in the neutron diffraction studies, we were not able to localize the deuterated variant inside the bilayer structure. That was unexpected as for the molecule several positions inside the SC lipid layers were described before [38,39]. A reason for this surprising behavior was found in the ^{2}H NMR spectra, which revealed IPM in an isotropic phase state at all temperatures. This suggests that IPM was not incorporated into the rigid membranes, but likely organized e.g. in a micellar phase.

The neutron scattering studies of the thermotropic phase behavior suggest a phase transition above 55 °C. Simultaneously, the ^{2}H NMR study revealed a phase transition even between 32 °C and 50 °C. Furthermore, from the ^{2}H NMR experiment we can consider that the amount of ordered lipids was only 5% at 70 °C. During the cool-down procedure, a hysteresis was found. We were able to observe several phase transitions meaning the appearance of an additional phase and the corresponding Bragg peaks. Here, especially CER[EOS]-br was involved as the first three lamellar Bragg peak orders of a LPP with a repeat distance of about 100 Å were visible. To this end, the presented results give new material to the debate of a LPP formation, the required conditions for that purpose and moreover the exact mode of action of IPM.

Transparency document

The Transparency document associated with this article can be found, in online version.

Acknowledgements

The authors are grateful to the Deutsche Forschungsgemeinschaft for the financial support (projects: HU 720/13-1, NE 427/30-1 and DO 463/6-1).

This work is based upon experiments performed at the BIODIFF instrument and membrane diffractometer V1. BIODIFF is operated by JCNS and FRM II at the Heinz Maier-Leibnitz Zentrum (MLZ), Garching, Germany. The authors gratefully acknowledge the financial support provided by JCNS to perform the neutron scattering measurements at the Heinz Maier-Leibnitz Zentrum (MLZ), Garching, Germany. Furthermore, the authors would like to thank the Helmholtz-Zentrum Berlin für Materialien und Energie (Berlin, Germany) for the allocation of neutron diffraction beam time at V1 for the thermotropic phase behavior study and the financial support. Moreover, Evonik Industries AG (Essen, Germany) is gratefully acknowledged for the generous donation of CER[AP]-C18.

Appendix A. Supplementary data

Supplementary data to this article can be found online at http://dx.doi.org/10.1016/j.bbamem.2017.01.029.

References

[1] P.W. Wertz, B. van den Bergh, The physical, chemical and functional properties of lipids in the skin and other biological barriers, Chem. Phys. Lipids 91 (1998) 85–96.
[2] R.J. Scheuplein, Permeability of the skin: a review of major concepts and some new developments, J. Invest. Dermatol. 67 (1976) 672–676.
[3] P.M. Elias, Epidermal lipids, barrier function and desquamation, J. Invest. Dermatol. 80 (1983) 44s–49s.
[4] H.J. Yardley, R. Summerly, Lipid composition and metabolism in normal and diseased epidermis, Pharmacol. Ther. 13 (1981) 383.
[5] G.M. Gray, H.J. Yardley, Different populations of pig epidermal cells: isolation and lipid composition, J. Lipid Res. 16 (1975) 441–447.
[6] L. Coderch, O. Lopez, A. de la Maza, J.L. Parra, Ceramides and skin function, Am. J. Clin. Dermatol. 4 (2003) 107–129.

[7] K.C. Madison, D.C. Swartzendruber, P.W. Wertz, D.T. Downing, Presence of intact intercellular lipid lammellae in the upper layers of the stratum corneum, J. Invest. Dermatol. 88 (1987) 714–718.

[8] S.H. White, D. Mirejovsky, G.I. King, Structure of lamellar lipid domains and Corneocyte Envelopes of murine stratum corneum. An X-ray diffraction study, Biochemistry 27 (1988) 3725–3732.

[9] J.A. Bouwstra, G.S. Gooris, J.A. van der Spek, W. Bras, Structural investigations of human stratum corneum by small-angle X-ray scattering, J. Investig. Dermatol. 97 (1991) 1005–1012.

[10] T.N. Engelbrecht, A. Schroeter, T. Hauß, B. Demé, H.A. Scheidt, D. Huster, R.H.H. Neubert, The impact of ceramides NP and AP on the nanostructure of stratum corneum lipid bilayer. Part I: neutron diffraction and ^{2}H NMR studies on multilamellar models based on ceramides with symmetric alkyl chain length distribution, Soft Matter 8 (2012) 2599–2607.

[11] M.W. de Jager, G.S. Gooris, I.P. Dolbnya, W. Bras, M. Ponec, J.A. Bouwstra, The phase behaviour of skin lipid mixtures based on synthetic ceramides, Chem. Phys. Lipids 125 (2003) 123–134.

[12] J.A. Bouwstra, G.S. Gooris, E.R. Frank, M. Ponec, Phase behaviour of stratum corneum lipid mixtures based on human ceramides: the role of natural and synthetic ceramide 1, J. Investig. Dermatol. 118 (2002) 606–617.

[13] M.A. Kiselev, E.V. Ermakova, A. Yu Gruzinov, A.V. Zabelin, Formation of the long-periodicity phase in model membranes of the outermost layer of skin (stratum corneum), Crystallogr. Rep. 59 (2014) 123–128.

[14] J.A. Bouwstra, G.S. Gooris, F.E.R. Dubbelaar, A.M. Weerheim, A.P. IJzerman, M. Ponec, Role of ceramide 1 in the molecular organization of the stratum corneum lipids, J. Lipid Res. 39 (1998) 186–196.

[15] J.A. Bouwstra, G.S. Gooris, F.E.R. Dubbelaar, M. Ponec, Phase behaviour of lipid mixtures based on human ceramides: coexistence of crystalline and liquid phases, J. Lipid Res. 42 (2001) 1759–1770.

[16] T.J. McIntosh, M.E. Stewart, D.T. Downing, X-ray diffraction analysis of isolated skin lipids: reconstruction of intercellular lipid domains, Biochemistry 35 (1996) 3649–3653.

[17] A. Kovacik, L. Opalka, M. Silarova, J. Roh, K. Vavrova, Synthesis of 6-hydroxyceramide using ruthenium-catalyzed hydrosilylation-protodesilylation. Unexpected formation of a long periodicity lamellar phase in skin lipid membranes, RSC Adv. 6 (2016) 73343–73350.

[18] A. Di Nardo, P. Wertz, A. Giannetti, S. Seidenari, Ceramide and cholesterol composition of the skin of patients with atopic dermatitis, Acta Derm. Venereol. 78 (1998) 27–30.

[19] S. Motta, M. Monti, S. Sesana, L. Mellesi, R. Ghidoni, R. Caputo, Abnormality of water barrier function in psoriasis. Role of ceramide fractions, Arch. Dermatol. 130 (1994) 452–456.

[20] S. Motta, M. Monti, S. Sesana, R. Caputo, S. Carelli, R. Ghidoni, Ceramide composition of the psoriatic scale, Biochim. Biophys. Acta 1182 (1993) 147–151.

[21] A. Schroeter, The role of ceramide (AP) for the structural assembly of stratum corneum lipid model membranes, in: Institute of Pharmacy, vol. Ph.D., Martin Luther University Halle-Wittenberg, Halle, 2010.

[22] A. Ruettinger, M.A. Kiselev, T. Hauss, S. Dante, A.M. Balagurov, R.H.H. Neubert, Fatty acid interdigitation in stratum corneum model membranes: a neutron diffraction study, Eur. J. Dermatol. 37 (2008) 759–771.

[23] A. Schroeter, M.A. Kiselev, T. Hauß, S. Dante, R.H.H. Neubert, Evidence of free fatty acid interdigitation in stratum corneum model membranes based in ceramide [AP] by deuterium labelling, Biochim. Biophys. Acta 1788 (2009) 2194–2203.

[24] A. Schroeter, D. Kessner, M.A. Kiselev, T. Hauß, S. Dante, R.H.H. Neubert, Basic nanostructure of stratum corneum lipid matrices based on ceramides [EOS] and [AP]: a neutron diffraction study, Biophys. J. 97 (2009) 1104–1114.

[25] E.H. Mojumdar, G.S. Gooris, D.J. Barlow, M.J. Lawrence, B. Demé, J.A. Bouwstra, Skin lipids: localization of ceramide and fatty acid in the unit cell of the long periodicity phase, Biophys. J. 108 (2015) 2670–2679.

[26] E.H. Mojumdar, G.S. Gooris, D. Groen, D.J. Barlow, M.J. Lawrence, B. Demé, J.A. Bouwstra, Stratum corneum lipid matrix: localization of acyl ceramide and cholesterol in the unit cell of the long periodicity phase, Biochim. Biophys. Acta Biomembr. 1858 (2016) 1926–1934.

[27] A. Eichner, S. Sonnenberger, B. Dobner, T. Hauß, A. Schroeter, R.H.H. Neubert, Localization of methyl-branched ceramide [EOS] species within the long-periodicity phase in stratum corneum lipid model membranes: a neutron diffraction study, Biochim. Biophys. Acta Biomembr. 1858 (2016) 2911–2922.

[28] V.H.W. Mak, R.O. Potts, R.H. Guy, Oleic acid concentration and effect in human stratum corneum: non-invasive determination by attenuated total reflectance infrared spectroscopy in vivo, J. Control. Release 12 (1990) 67–75.

[29] M.L. Francoeur, G.M. Golden, R.O. Potts, Oleic acid: its effects on stratum corneum in relation to (trans)dermal drug delivery, Pharm. Res. 7 (1990) 621–627.

[30] B. Ongpipattanakul, M.L. Francoeur, R.R. Burnette, R.O. Potts, Phase-separation of oleic-acid in the stratum-corneum lipids, J. Investig. Dermatol. 96 (1991) 619.

[31] B. Ongpipattanakul, R.R. Burnette, R.O. Potts, M.L. Francoeur, Evidence that oleic acid exists in a separate phase within stratum corneum lipids, Pharm. Res. 8 (1991) 350–354.

[32] S. Santoyo, A. Arellano, P. Ygartua, M. Martin, Penetration enahncer effects on the in-vitro percutaneous absorption of piroxicam through rat skin, Int. J. Pharm. 117 (1995) 219–224.

[33] K. Sato, K. Sugibayashi, Y. Morimoto, Effect and mode of action of aliphatic esters on the invitro skin permeation of nicorandil, Int. J. Pharm. 43 (1988) 31–40.

[34] B.W. Barry, Lipid-protein-partitioning theory of skin penetration enhancement, J. Control. Release 15 (1991) 237–248.

[35] Q.D. Pham, S. Björklund, J. Engblom, D. Topgaard, E. Sparr, Chemical penetration enhancers in stratum corneum — relation between molecular effects and barrier function, J. Control. Release 232 (2016) 175–187.

[36] A. Arellano, S. Santoyo, C. Martin, P. Ygartua, Influence of propylene glycol and isopropyl myristate on the in vitro percutaneous penetration of diclofenac sodium from carbopol gels, Eur. J. Pharm. Sci. 7 (1998) 129–135.

[37] C.S. Leopold, B.C. Lippold, An attempt to clarify the mechanism of the penetration enhancing effects of lipophilic vehicles with differential scanning calorimetry (DSC), J. Pharm. Pharmacol. 47 (1995) 276–281.

[38] I. Brinkmann, C.C. Mueller-Goymann, An attempt to clarify the influence of glycerol, propylene glycol, isopropyl myristate and a combination of propylene glycol and isopropyl myristate on human stratum corneum, Pharmazie 60 (2005) 215–220.

[39] T.N. Engelbrecht, B. Demé, B. Dobner, R.H.H. Neubert, Study of the influence of the penetration enhancer isopropyl myristate on the nanostructure of stratum corneum lipid model membranes using neutron diffraction and deuterium labelling, Skin Pharmacol. Physiol. 25 (2012) 200–207.

[40] T.A. Harroun, G.D. Wignall, J. Katsaras, Neutron Scattering for Biology, Springer-Verlag, Berlin Heidelberg, 2006.

[41] H. Dachs, Principles in Neutron Diffraction, Springer-Verlag, Berlin Heidelberg, 1978.

[42] B.T.M. Willis, C.J. Carlile, Neutron Properties, Oxford University Press, Oxford, Great Britain, 2009.

[43] W. Zajac, B.J. Gabrys, An Introduction to Neutron Scattering, Gordon and Breach Science Publishers, Amsterdam, Netherlands, 2000.

[44] D. Kessner, M. Kiselev, S. Dante, T. Hauss, P. Lersch, S. Wartewig, R.H.H. Neubert, Arrangement of ceramide [EOS] in a stratum corneum lipid model matrix: new aspects revealed by neutron diffraction studies, Eur. Biophys. J. 37 (2008) 989–999.

[45] D. Kessner, M. A., T. Hauss, S. Dante, S. Wartewig, R.H.H. Neubert, Localisation of partially deuterated cholesterol in quaternary SC lipid model membranes: a neutron diffraction study, Eur. Biophys. J. 37 (2008) 1051–1057.

[46] E.H. Mojumdar, D. Groen, G.S. Gooris, D.J. Barlow, M.J. Lawrence, B. Demé, J.A. Bouwstra, Localization of cholesterol and fatty acid in a model lipid membrane: a neutron diffraction approach, Biophys. J. 105 (2013) 911–918.

[47] T.N. Engelbrecht, A. Schroeter, T. Hauss, R.H.H. Neubert, Lipophilic penetration enhancers and their impact to the bilayer structure of stratum corneum lipid model membranes: neutron diffraction studies based on the example oleic acid, Biochim. Biophys. Acta Biomembr. 1808 (2011) 2798–2806.

[48] S.J. Rehfeld, P.M. Elias, Mammalian stratum corneum contains physiological lipid thermal transitions, J. Invest. Dermatol. 79 (1982) 1–3.

[49] D. Huster, Solid-state NMR spectroscopy to study protein-liquid interactions, Biochim. Biophys. Acta 1841 (2014) 1146–1160.

[50] S. Stahlberg, B. Skolova, P.K. Madhu, A. Vogel, K. Vavrova, D. Huster, Probing the role of the ceramide acyl chain length and sphingosine unsaturation in model skin barrier lipid mixtures by ^{2}H solid-state NMR spectroscopy, Langmuir 32 (2015) 4906–4915.

[51] S. Stahlberg, S. Lange, B. Dobner, D. Huster, Probing the role of ceramide headgroup polarity in short-chain model skin barrier lipid mixtures by ^{2}H solid-state NMR spectroscopy, Langmuir 32 (2016) 2023–2031.

[52] E. Brief, S. Kwak, J.T.J. Cheng, N. Kitson, J. Thewalt, Phase behavior of an equimolar mixture of *N*-palmitoyl-D-erythro-sphingosine, cholesterol, and palmitic acid, a mixture with optimized hydrophobic matching, Langmuir 25 (2009) 7523–7532.

[53] S. Sonnenberger, A. Eichner, S. Lange, A. Langner, R. Neubert, B. Dobner, Synthesis of specific deuterated derivatives of the long chained stratum corneum lipids EOS and EOP, Chemistry and Physics of Lipids, 2016.

[54] T. Engelbrecht, T. Hauß, K. Süß, A. Vogel, M. Roark, S.C. Feller, R.H.H. Neubert, B. Dobner, Characterisation of a new ceramide EOS species: synthesis and investigation of the thermotropic phase behaviour and influence on the bilayer architecture of stratum corneum lipid model membranes, Soft Matter 7 (2011) 8998–9011.

[55] M. Seul, M.J. Sammon, Preparation of surfactant multilayer films on solid substrates by deposition from organic solution, Thin Solid Films 185 (1990) 287–305.

[56] D.L. Worchester, N.P. Franks, Structural analysis of hydrated egg lecithin and cholesterol bilayers, II. Neutron diffraction, J. Mol. Biol. 100 (1976) 359–378.

[57] B.P. Schoneborn, A.C. Nunes, Neutron scattering, Annu. Rev. Biophys. Bioeng. 1 (1972) 529–552.

[58] M.C. Wiener, S.H. White, Fluid bilayer structure determination by the combined use of X-ray and neutron diffraction, Biophys. J. 59 (1991) 174–185.

[59] Heinz-Maier-Leibnitz-Zentrum, BIODIFF: diffractometer for large unit cells, J. Large Scale Res. Facil. 1 (2015) 1–4.

[60] D. Kessner, G. Brezesinski, S.S. Funari, B. Dobner, R.H.H. Neubert, Impact of long chain ω-acylceramides on the stratum corneum lipid nanostructure. Part 1: thermotropic phase behaviour of CER[EOS] and CER[EOP] studied using X-ray powder diffraction and FT-Raman spectroscopy, Chem. Phys. Lipids 163 (2010) 42–50.

[61] S. Dante, T. Hauss, N.A. Dencher, Insertion of externally administered amyloid β peptide 25–35 and perturbation of lipid bilayers, Biochemistry 42 (2003) 13667–13672.

[62] M.A. Kiselev, N.Y. Ryabova, A.M. Balagurov, S. Dante, T. Hauss, J. Zbytovska, S. Wartewig, R.H.H. Neubert, New insights into the structure and hydration of a stratum corneum lipid model membrane by neutron diffraction, Eur. Biophys. J. 34 (2005) 1030–1040.

[63] N.P. Franks, W.R. Lieb, The structure of lipid bilayers and the effects of general anaesthetics, J. Mol. Biol. 133 (1979) 469–500.

[64] F. Cser, About the Lorentz correction used in the interpretatin of small angle X-ray scattering data of semicrystalline polymers, J. Appl. Polym. Sci. 80 (2001) 2300–2308.

[65] J.F. Nagle, S. Tristam-Nagle, Structure of lipid bilayers, Biochim. Biophys. Acta 1469 (2000) 159–195.

[66] V.F. Sears, Neutron scattering lengths and cross section, Neutron News 3 (1992) 26–37.

[67] D.B. Fenske, J.L. Thewalt, M. Bloom, N. Kitson, Models of stratum corneum intercellular membranes: ^{2}H NMR of macroscopically oriented multilayers, Biophys. J. 67 (1994) 1562–1573.
[68] D. Huster, K. Arnold, K. Gawrisch, Influence of docosahexaenoic acid and cholesterol on lateral lipid organization in phospholipid membranes, Biochemistry 37 (1998) 17299–17308.
[69] V. Macho, L. Brombacher, H.W. Spiess, The NMR-WEBLAB: an internet approach to NMR lineshape analysis, Appl. Magn. Reson. 20 (2001) 405–432.
[70] M.W. de Jager, G.S. Gooris, I.P. Dolbnya, M. Ponec, J.A. Bouwstra, Modelling the stratum corneum lipid organisation with synthetic lipid mixtures: the importance of synthetic ceramide composition, Biochim. Biophys. Acta 1684 (2004) 132–140.
[71] D. Groen, G.S. Gooris, D.J. Barlow, M.J. Lawrence, J.B. van Mechelen, B. Demé, J.A. Bouwstra, Disposition of ceramide in model lipid membranes determined by neutron diffraction, Biophys. J. 100 (2011) 1481–1489.
[72] H.I. Petrache, S.W. Dodd, M.F. Brown, Area per lipid and acyl length distribution in fluid phosphatidylcholines determined by ^{2}H NMR spectroscopy, Biophys. J. 79 (2000) 3172–3192.
[73] D.M. Small, The Physical Chemistry of Lipids, Plenum Press, New York, 1986.
[74] N.Y. Ryabova, M.A. Kiselev, S. Dante, T. Hauß, A.M. Balagurov, Investigation of stratum corneum lipid model membranes with free fatty acid composition by neutron diffraction, Eur. Biophys. J. 39 (2010) 1167–1176.
[75] N.Y. Ryabova, M.A. Kiselev, A.M. Balagurov, Transition processes in stratum corneum model lipid membranes with a mixture of free fatty acids, Biofizika 54 (2009) 852–862.
[76] M.A. Kiselev, E.V. Ermakova, A.Y. Gruzinov, A.V. Zabelin, Conformation of ceramide 6 molecules and chain-flip transitions in the lipid matrix of the outermost layer of mammalian skin, the stratum corneum, Crystallogr. Rep. 52 (2007) 525–528.
[77] S. Raudenkolb, S. Wartewig, R.H.H. Neubert, Polymorphism of ceramide 6: a vibrational spectroscopic and X-ray powder diffraction investigation of the diastereomers of *N*-(α-hydroxyoctadecanoyl)-phytosphingosine, Chem. Phys. Lipids 133 (2005) 89–102.
[78] A.Y. Gruzinov, A.V. Zabelin, M.A. Kiselev, Short periodicity phase based on ceramide [AP] in the model lipid membranes of stratum corneum does not change during hydration, Chem. Phys. Lipids 202 (2017) 1–5.
[79] D. de Sousa Neto, G. Gorris, J. Bouwstra, Effect of the ω-acylceramides on the lipid organization of stratum corneum model membranes evaluated by X-ray diffraction and FTIR studies, Chem. Phys. Lipids 164 (2011) 184–195.
[80] K.R. Feingold, M. Mao-Qiang, G.K. Menon, S.S. Cho, B.E. Brown, P.M. Elias, Cholesterol synthesis is required for cutaneous barrier function in mice, J. Clin. Invest. 86 (1990) 1738–1745.
[81] G.K. Menon, K.R. Feingold, A.H. Moser, B.E. Brown, P.M. Elias, De novo sterologenesis in the skin. II. Regulation by cutaneous barrier requirements, J. Lipid Res. 26 (1985) 418–427.
[82] R.J. Wittebort, E.T. Olejniczak, R.G. Griffin, Analysis of deuterium nuclear magnetic resonance line shapes in anisotropic media, J. Phys. Chem. 86 (1987) 5411–5420.
[83] L.S. Batchelder, C.E. Sullivan, L.W. Jelinski, D.A. Torchia, Characterization of leucine side-chain reorientation in collagen-fibrils by solid-state ^{2}H NMR, Proc. Natl. Acad. Sci. U. S. A. 79 (1982) 386–389.
[84] D. Huster, Investigations of the structure and dynamics of membrane-associated peptides by magic angle spinning NMR, Prog. Nucl. Magn. Reson. Spectrosc. 46 (2005) 79–107.
[85] P. Schmidt, L. Thomas, P. Müller, H.A. Scheidt, D. Huster, The G protein-coupled neuropeptide Y receptor type 2 is highly dynamic in lipid membranes as revealed by solid-state NMR spectroscopy, Chemistry 20 (2014) 4986–4992.
[86] D. Huster, L. Xiao, M. Hong, Solid-state NMR investigation of the dynamics of soluble and membrane-bound colicin Ia channel-forming domain, Biochemistry 40 (2001) 7662–7674.
[87] X. Chen, S. Kwak, M. Lafleur, M. Bloom, N. Kitson, J. Thewalt, Fatty acids influence "solid" phase formation in models of stratum corneum intercellular membranes, Langmuir 23 (2007) 5548–5556.
[88] S. Björklund, A. Nowacka, J.A. Bouwstra, E. Sparr, D. Topgaard, Characterization of stratum corneum molecular dynamics by natural-abundance ^{13}C solid-state NMR, PLoS One 8 (2013), e61889.

5 DISCUSSION AND OUTLOOK

The barrier function of mammalian skin is highly connected to the very heterogeneous mixture of SC lipids. Besides quantitative studies [74, 76], in the last years, the structural arrangement of certain SC lipid subspecies was focused in several works [19, 22, 36-38, 118, 121]. However, the complex SC lipid membrane structure is not yet fully understood. Within this thesis, simplified SC lipid model systems with one or two CER subspecies, together with CHOL and selected FFAs, have been used. This allowed conclusions about the internal impacts of the lipids to each other. For that purpose, amongst others, neutron diffraction technique was an excellent device to gain insights into the nanoscaled structures of lipid bilayers. Especially, the application of specifically deuterated lipids facilitated the localization of the labeled compounds due to the different coherent SLs of neutrons for hydrogen and deuterium. The labeled positions also allowed conclusions referring to the molecule positions within a bilayer structure. This knowledge is important for the understanding of the SC barrier function. Moreover, the formulation and modification of dermal and transdermal drug delivery profits enormously from these findings. Often penetration enhancers are ingredients of such formulations in order to increase the flux through the SC by disordering the SC lipids. Thereby the rigid lipid arrangement is fractured and cannot maintain its delimiting effect on the penetration rate. Consequently, it is of high interest to gain information about the lipid interactions under the influence of an enhancer. Thus, barrier properties and options to overcome it temporarily can be investigated on a molecular scale.

The present thesis covers (i) the localization of partially deuterated CER[AP]-C18 variant in a SPP [164], (ii) the determination of CER[EOS]-d_3 in a LPP [165], and (iii) the influence of lipophilic penetration enhancer IPM to the applied SC lipid model membrane [166]. A final discussion of all received results and an outlook to possible future works will complete this work.

5.1 Localization of CER[AP]-C18 in a quaternary SC lipid model membrane

The influence of the very polar CER[AP] to the assembling process of quaternary SC lipid model membranes was proven earlier [21, 23, 24, 39, 116]. This CER subspecies with its phytosphingosine backbone was reported to be the driving force for the model bilayer architecture. However, these effects are highly connected to the arrangement of CER[AP] and it was difficult to further substantiate any of the propositions. Now, it was possible to describe the synthesis of a partially deuterated CER[AP] variant, which enabled the verification of the earlier ideas, concerning that SC lipid. For that purpose, the synthetically derived racemic CER[AP]-C18-d_3 was applied in a SC lipid model membrane together with CHOL, ChS, and

SA (55/25/5/15, wt%), a mixture, which was investigated earlier by Ruettinger et al. [39]. The prepared membrane was investigated using neutron diffraction. A highly-ordered system with a unit cell scale of about 44 Å was observed, whereby Ruettinger et al. identified two coexisting lamellar phases with repeat distances of 46.3 Å and 45.3 Å [39]. This finding could be a result from an additional buffer treatment prior to the measurements, which was performed here. Earlier studies showed, that this treatment helps to increase the lamellar state of order by hydration [132, 154]. Nevertheless, in native skin a very high chain lengths distribution of all lipids supports the SPP d spacing of about 60 Å. Here, the selected C18 chain lengths of CER and FFA components generated the smaller unit cell scale, as reported in comparable works [18, 24, 39, 123, 167, 168]. A detailed insight into the nanostructure of the CER[AP] based SC lipid model system was possible due to the partial deuteration of the lipid. By means of the neutron diffraction experiments and the NSLD profiles, the deuterium position in the bilayer was localizable and from that, possible molecule positions for CER[AP] have been concluded: The CER is positioned with its head group in the polar parts of the bilayer and its alkyl chains are directed towards the bilayer center. Assuming the *hairpin* conformation, the labelled ends of the parallel arranged alkyl chains of two oppositely positioned CER molecules would interdigitate in the middle of the unit cell. Compared to this, the V-shaped assembly differs, presenting no parallel arranged alkyl chains but a tilt. However, the V-shaped arrangement of CER[AP] is very supposable, as it fits perfectly into the received unit cell scale. Different phase behaviors for the DL-enantiomers of CER[AP] were described earlier [124], e.g. the L-form prefers the V-shaped assembly and showed smaller d spacings. Based on the enantiomeric ratio of 56 % for the L-form and 44 % for the D-form, the L-diastereomer has distinct influence on the bilayer arrangement. Therefore, the decreased unit cell scale in the present work is interpreted as a result of the dominating V-shape of L-CER[AP]. A recent publication presents comparable results for a SC lipid model system based on CER[AP] [123]. Additionally, they found a second lamellar phase, where the CER conformation is supposed to be fully V-shaped. For this phase, no intermembrane water was found due to contrast variation. For the most abundant CER subspecies in native skin [76], CER [NP], very the same observations were reported for its V-shaped assembly in a similar SC lipid model mixture [28]. But in the present work, the contrast variation clearly revealed the presence of water molecules alongside the polar lipid head groups. From that it was concluded, that the V-shaped conformation of CER[AP] might dominate but there has to be another arrangement of the CER, e.g. the *hairpin* conformation, as Ruettinger et al. proposed [39]. Summing up, the application of specifically deuterated CER[AP]-d_3 enabled more comprehensive insights into the membrane structure of a well-known SC lipid model system.

5.2 Influence of CER[EOS]-br variant on CER[AP]-based SC lipid model membrane

Referring to the received knowledge about the arrangement of long-chain CER[AP], it was another point of interest to investigate the impact of an ultra-long-chain CER[EOS] variant on the applied SC lipid model membrane. In detail, the CER variant was esterified with palmitic acid, which contained a methyl-branching at position C10, instead of the naturally occurring esterified unsaturated linoleic acid. This synthetically derived CER derivative, called CER[EOS]-br, was investigated intensively before and showed a similar phase behavior compared to the native subspecies [38]. Until now, all neutron diffraction approaches, concerning SC lipid model membranes based on CER[AP]-C18, CER[EOS] or CER[EOS]-br, CHOL and a FFA component showed the existence of a single SPP with unit cell dimensions of about 48 Å [19, 22, 38]. Although the presence of CER[EOS] is highly connected to a LPP formation [30, 32, 34], it was still absent in these model systems. It was discussed, that the phytosphingosine backbone, with one additional hydroxy group, has more influence on the lipid membrane assembly as the sphingosine backbone.

In the present work, the focus was placed on the identification of specifically deuterated CER[EOS]-br and CER[AP] in a SC lipid model membrane together with CHOL and BA. Thereby, it was the aim, to verify the arrangements of both CERs in a SPP with about 48 Å, which were presented in earlier works of our group [19, 38]. For that purpose, SC lipid model membranes in a ratio of 10/23/33/33 wt% (CER[AP]-C18/CER[EOS]-br/CHOL/BA) were prepared, fully protonated as well as with labelled CER[AP] or CER[EOS]-br derivatives. The formation of three coexisting lamellar phases with repeat distances of about 48 Å, 45 Å, and 118 Å was observed, with two of these unit cell scales in the dimension of a SPP and one in the dimension of a LPP. The obtained phases are smaller than found in native SC. This might be reasoned by the shorter chain lengths of CER[AP] and CER[EOS]-br, as mentioned above. Especially for CER[EOS] a native chain lengths distribution from C62 to C72 is described [76]. Consequently, the applied C64 chain length in total explains the smaller repeat distance. Moreover, the applied CER[EOS]-br variant was able to support the assembly of a LPP. This was a new finding because the literature describes an unsaturated esterified FFA component to be mandatory for a LPP formation [11]. But above all, ultra-long-chain CERs are described to be essentially for the assembly of a LPP [30, 31, 33], except from a recent study, which revealed a long unit cell structure of about 106 Å in a SC lipid mixture without any ultra-long chain CER compound [35]. Unfortunately, the authors of this work did not discussed their ideas about reasons for that finding or a possible arrangement of the applied very-long-chain 6-hydroxyceramide component. Furthermore, detailed insights into the substructure of the received long phase were missing, so that any comparison to the present work is impractically.

As the LPP appears to be essentially for proper skin barrier functions [32, 87, 112, 117], detailed knowledge about its structure is mandatory for further understanding and investigations in this regard. Thereby, especially its subunit structure is of high interest. Earlier works presented a three-lipid-layer structure, which is interrupted by two polar areas [13, 27, 106]. However, there are different descriptions of the substructure distribution of the LPP. In native materials, sublattice spacings of 50-30-50 Å [109, 169] or 46-24-46 Å [107] were found. In detail, the central hydrophobic area is much smaller than the outer ones. In neutron diffraction studies on a SC lipid model membrane, a nearly equal subspacing distribution with 44 Å-42 Å-44 Å was detected [36]. The present results identified a three-lipid-layer substructure within the received 118 Å LPP, which showed sublattice spacings of 40-38-40 Å. This is in comparable dimensions to the other neutron diffraction experiment, which presented a 130 Å LPP [36]. A confirmation of Norlén´s asymmetry model of a 110 Å phase is not given from that almost symmetric sublattice distribution.

In the present work, for the first time, the partially deuterated CER[EOS]-br variant has been applied and revealed three possible positions for the molecule in its *hairpin* and even *fully extended* conformation within the complex long unit cell. Thus, all overlapping alkyl chains and their intermolecular van der Waals forces are able to stabilize the LPP arrangement. Moreover, interdigitation and interlocking of the very rigid alkyl chains impede the intercellular pathway for external substances. Due to the successively stacked hydrophilic and hydrophobic parts of a single LPP unit cell, the penetration rate is massively limited, representing a high benefit referring to the SC barrier properties. Overall, the obtained results give new valuable insights into the substructure of a LPP together with the arrangement of the CER[EOS]-br variant. However, the CER[AP]-d_3 variant was not localizable in the LPP. The two coexisting SPPs might be a reason for that finding, as both of them are mainly composed of CER[AP]. Thus, the present deuterium level in the LPP could have been too low to be detected by neutron diffraction. But, as e.g. CER[NS]-C24 was localized in a single LPP [115], it is absolutely conceivable, that the applied CER[AP]-C18 could be arranged in comparable positions. Furthermore, the impact of humidity to the LPP has been investigated. From bulk phase experiments on CER[EOS] we know, that the LPP formation is dependent on the surrounding humidity [12]. Isolated porcine SC lipids formed a LPP, which was about 128 Å at 98% RH and only 125 Å at 32% RH [34]. Mammalian SC lipids instead formed a LPP, which showed no changes under hydration [27]. In the recent study, the received LPP of the investigated SC lipid model membrane increased from ~118 Å to ~120 Å, whereby especially the inner polar areas were very sensitive to the surrounding humidity. However, as the LPP was present at 57% RH as well, the humidity seems to have no significant impact on its stability, although its unit cell scale and inner water level changed. Moreover, changes in the LPP dimension over a time of about three months were detected. The equilibration period revealed an increasing

spacing from ~114 Å to ~118 Å, where all parts of the unit cell expanded to the same extend. This finding was very interesting, because the LPP structure was not only stable over the time of storage but also elongating. Therefore, it can be concluded, that the long unit cell is very rigid over the time even in its substructure. However, the LPP was still sensitive to water as the subsequent experiments with changing humidity figured out. This was the first time, that changes in the unit cell dimensions were detected in the CER[AP]-based SC lipid model membranes. But, the ability of equilibration in the LPP seems to be highly connected to the presence and properties of CER[EOS]-br because no significant level of CER[AP]-C18 could be detected in the present LPP. This assumption is confirmed by the existence of both SPPs, which are discussed below.

However, it was interesting, that the here applied SC lipid model system figured out three coexisting phases compared to the earlier work of Engelbrecht et al. [38] with a single main phase. This difference was interpreted as a question of divergent sample preparation and sample treatment. Hereby, especially the humidity appears to be important for the lipid assembly in a LPP, as the samples within this work were stored under high humidity directly after sample preparation prior to the measurements. Nevertheless, comparable results regarding the presence of a highly-ordered 48 Å SPP were observed. The earlier proposed arrangement of CER[AP]-C18 in this SPP [19, 38] could be confirmed by the application of the specifically deuterated derivative of the CER[AP]: The CER is arranged with its head group in the polar membrane parts and its alkyl chains pointing towards the unit cell center, supposing the CER *hairpin* conformation. For two oppositely positioned CER[AP]-C18 molecules, a small overlap in the bilayer center has been found. Differing from the idea of Engelbrecht et al. [38], the labelled CER[EOS]-br variant could not be detected in this SPP, neither in its *extended*, nor in its *hairpin* conformation. Aside from that, it is possible that the amount of CER[EOS]-br was too low to be detected. Thus, it can be assumed, that the ultra-long-chain CER variant was not significantly part of the 48 Å phase and the phase structure was mainly prescribed by the applied CER[AP]. Due to that finding, for the 48 Å phase it can be concluded, that the phytosphingosine was the dominating force regarding to the lipid assembling process. This statement is in agreement with earlier works of our group [19, 21, 22, 38]. Moreover, for this SPP no changes during the hydration were detected. Comparable results were presented earlier, too [19, 123]. As well as the humidity, the time of storage did not show any relevant influence on the 48 Å SPP. The unit cell scale was nearly constant and the NSLD profiles did not differ significantly (see supplementary data in the appendix). A reason for the very high stability of the CER[AP]-dominated phase could be the high number of polar OH groups and the corresponding hydrogen network they form [170].

The second SPP with a unit cell scale of about 45 Å showed comparable dimensions to the SPP received in the SC lipid model membrane without CER[EOS]-br [164]. Again, assuming

the CER *hairpin* conformation, the partially deuterated CER[AP]-C18 variant in this second SPP has been determined with its head group in the polar bilayer parts and its alkyl chains directed towards the unit cell center. The labelled molecule parts were located in the middle of the bilayer, overlapping further than in the 48 Å SPP. Because of the small unit cell scale and the wide area of deuterium distribution, the V-shaped CER conformation has to be taken into account as well. A reason for that assumption is the application of a racemic mixture of CER[AP]-d_3. For the DL-enantiomers different phase behaviors are known, especially concerning the hydrogen bonding, their preferred CER conformation and the repeat distances they form [62, 124]. In detail, for L-CER[AP] smaller unit cell scales were observed than for the D-enantiomer, caused by its preferential V-shaped structure [124]. Thus, for the 45 Å SPP it can be assumed, that the L-form is arranged in its favorite conformation and mainly responsible for the shorter repeat distance. However, for a complete V-shape assembly, no water was found alongside the CERs [123]. Likely to the SC lipid model membrane without CER[EOS]-br [164], here water was detected aside the polar lipid head groups. Consequently, the V-shaped CER[AP] cannot be the only conformation within the investigated model. Thus, the present D-CER[AP] has to be part of the shorter SPP in its favorite *hairpin* conformation, too. Closer insights into the phase behavior of the single CER[AP] enantiomers and their impact on the present SC lipid model system are not possible at this point. Therefore, experiments with the pure D- and L-forms are scheduled.

Nevertheless, as well as for the longer SPP, no significant impact of humidity was detected in the NSLD profiles for the 45 Å phase (see supplementary data in the appendix). Furthermore, for the influence of time, only minor changes were observed. So it can be assumed, that the second SPP is as stable and rigid as the longer SPP. This finding is a useful hint to the impact of CER[AP]-C18 on the prepared SC lipid model membranes. The long-chain CER seems to be responsible for the very high stability of the SPPs and generates its immediate formation during sample preparation. Consequently, the arrangement of CER[AP] in the short phases occurs fast and permanently, so that CER[AP] is influencing the stability of the short phase and generating the rigid bilayer structure. The immense impact on the lipid assembly was observed before [19, 20, 39]. Taking this into account, it is not surprising, that the long-chain CER was not detectable in the LPP, perhaps enabling the phase properties like being sensitive to humidity and time. Therefore, the questions arises whether the number of OH groups has an impact on the integration of the long-chain CER into the LPP. Whereas CER[NS] with only two OH groups was localized in a LPP [115], the applied CER[AP] with four OH groups was not detected the in the LPP. Possibly, an excessive hydrogen network inhibits the sensitive LPP properties and its flexibility and therefore, the very polar CER derivative was not integrated into the LPP assembling process.

5.3 Effect of penetration enhancer isopropyl myristate on applied SC lipid model membrane and its thermotropic phase behavior

Due to the new and interesting results of the previous experiment, the question came up whether a lipophilic penetration enhancer could manipulate the LPP formation and consequently reduce the SC barrier properties. For that purpose, the liquid wax IPM was added in a concentration of 10 wt% to the known SC lipid model system with CER[AP]-C18/CER[EOS]-br/CHOL/BA (10/23/33/33 wt%). The enhancer is a usual additive in cosmetic and pharmaceutical products. It was even applied in the same concentration in a SC lipid model system based on CER[AP]-C18 [132]. For the neutron diffraction experiments performed within this part of the thesis, the neutron diffractometer BIODIFF was used for the first time as device for studies on SC lipid model membranes. A single SPP with dimensions of about 48 Å was detected with only five diffraction orders. Since the previous experiment revealed seven highly ordered Bragg peaks for the 48 Å SPP, a higher variation in the lamellar stacking or decreased internal membrane order, resulting in a higher mosaicity, can be concluded for the used model system. There is a high evidence, that the fluidizing effect of IPM [133, 134], is a reason for the less ordered lipid arrangement. Moreover, the enhancer prevented the formation of a LPP. This could be interpreted as direct impact to a decreased level of barrier function because the LPP seems to be of high relevance for proper SC protection level [32, 87, 112, 117]. Hence, the enhancer affected the rigid lipid arrangement and inhibited the barrier-connected LPP arrangement. Consequently, IPM would enable a higher penetration rate for pharmaceutically active components via the intercellular pathway. Nevertheless, it has to be pointed out, that the effects of IPM on the obtained SPP are limited, as no significant changes compared to the lipid model without IPM were observed. Thus, the SPP is not only resistant to humidity and time of storage, but to the liquid wax as well. This indicates, that in the lipid packing of the SC, areas of different flexibility and stability are present. Finally, the statement that SC lipids are mainly affected by hydrophobic compounds [171], can be underlined, although the lipids of the LPP seems to be more sensible to the hydrophobic enhancer than these of the SPP.

The application of the partially deuterated CERs answered the question, where the ultra-long-chain CER[EOS]-d_3 was localized in absence of the LPP. Together with the long-chain CER[AP]-C18-d_3 it was present in the 48 Å SPP. Comparable CER arrangements were suggested before [19, 22, 38], but it now will be discussed as result of IPM impact. While the sample preparation was similar to that, where three coexisting phases were observed [165], here only the enhancer component was different. Thus, the enhancer was mainly responsible for the differences on the resulting nanostructure of the SC lipid model membrane and the corresponding CER assembly. With respect to the IPM impact, a general confirmation of the

earlier proposed ideas for the CER arrangements [19, 22, 38] can only be made with reservation. However, CER[AP]-d_3 and CER[EOS]-d_3 were detected in a single 48 Å SPP for the first time: The long-chain CER was found in its *hairpin* conformation with its head group in the polar parts of the unit cell and its alkyl chains directing towards the bilayer center, interdigitating there with oppositely arranged CER[AP] molecules. The ultra-long-chain CER[EOS]-d_3 was localized with its head group in one polar bilayer area and with the ester group in the other polar bilayer part, extending the esterified palmitic acid into the next bilayer. As mentioned before, this arrangement of both CERs was already proposed [38], but without the fluidizing effects of IPM. Therefore, it is possible to compare the obtained data with the SC lipid mixture without enhancer [165]. It was very surprising, that CER[EOS]-br was found in the SPP. Although its long and static alkyl chains would inhibit an integration into the observed SPP, it was probably the small ester group, which stabilized the stretched molecule due to its arrangement in the second polar bilayer part. However, due to the higher detected deuterium level of CER[AP]-d_3, the amount of CER[EOS]-d_3 in the SPP was probably much lower than that of the long-chain CER[AP]. Thus, the supporting ^{2}H NMR measurements revealed, that both CERs were present in the same phase. Therefore, the conclusion can be made, that again CER[AP]-C18 was dominating the SPP, even in presence of CER[EOS]-br.

The application of partially deuterated IPM-d_3 could not answer the question whether the penetration enhancer was localized within the SPP. Although two positions in a SC lipid model membrane without CER[EOS]-br were presented [132], none of them was detectable in the present experiment. An explanation is provided by the ^{2}H NMR studies, which identified a perdeuterated IPM derivative as isotropically. A reason for that result was found in phase separation, caused by the sample preparation, which was performed two month prior to the neutron diffraction studies at BIODIFF. During the preparation procedure, IPM was mixed up homogeneously with the other synthetically derived SC lipids. But until the measurements started, a complete equilibration of the samples occurred, whereby the liquid wax IPM underwent a phase separation from the rigid SC lipids. Its assembly in a cubic or micellar phase explains why the BIODIFF experiments could not detect IPM in a separated phase. Nevertheless, clear effects of the penetration enhancer to the arrangement of the applied SC lipids were observed: (i) It prevented the formation of a LPP, which could be connected to a disturbed barrier function, (ii) it supported the integration of ultra-long-chain CER[EOS]-br in a SPP, a finding which was observed for the first time and (iii) overall, due to its fluidity it was not integrated permanently into the fluid-crystalline SC lipid stacks. This is an enormous advantage regarding to the recovery of the SC lipids and the skin barrier properties, as the penetration enhancing effect is just temporarily. Moreover, IPM was not influencing the lipid model membranes during the subsequent studies of thermotropic phase behavior. It was phase separated and isotropic at all exposed temperatures.

For the investigation of the phase behavior, the sample containing IPM-d_3 was heated up to 70 °C and cooled-down to skin temperature afterwards. During the cool-down process, a hysteresis effect of the SC lipid model membrane was observed, meaning in detail the appearance of a LPP with dimensions of about 111 Å. Finally, due to the rearrangement of the SC lipids, CER[EOS]-br was able to form a long phase, independent on the enhancer or the dominating CER[AP]. Similar results were known from Bouwstra et al.[27, 105, 172, 173], who detected LPPs with repeat distances between 132-134 Å in native SC materials, which appeared during the cool-down process from 65-75 °C back to room temperature. Although the unit cell scale determined within this experimental part of the thesis was smaller than in the native material, this LPP was in comparable dimensions to the one that has been found in the SC lipid model system without IPM [165]. Hence, there is a high evidence for the presence of a LPP after the thermic treatment. Again we found a LPP, which was formed by the ultra-long-chain CER[EOS]-br, esterified with a saturated fatty acid. This finding revised earlier presented results, where only esterified unsaturated fatty acid components were able to assemble in a LPP [11]. However, the very simple model system used here might have facilitated the LPP assembly by the ultra-long-chain component CER[EOS]-br despite of the esterified PA, compared to the earlier investigated complex model system, where long-chain and very-long-chain CERs were dominating [11]. Nevertheless, until IPM was phase separated and the thermal treatment was performed, CER[EOS]-br was able to induce the LPP formation afterwards. The phase separated IPM was not able to prevent the LPP assembly anymore and thus, could not execute its penetration enhancing effects.

Besides CER[EOS]-br also CER[AP] underwent phase transitions throughout the studies of the thermotropic phase behavior. During the heating period, an additional SPP with a calculated d spacing of about 41 Å appeared, which was highly connected to the applied diastereomers of CER[AP]-C18. Again, the L-enantiomer with its favorite V-shaped conformation could be a reason for that smaller SPP [124]. This hypothesis was underlined by results of the group of Kiselev et al., who investigated a quaternary SC lipid model system based on DL-CER[AP]-C18 and observed a second SPP of about 41 Å, which appeared as a result of heating [24]. Therefore, there is a high evidence, that the here performed heating treatment caused a separation of the diastereomers of CER[AP]-C18, which rearranged in two SPPs with different unit cell scales afterwards. But again, the 48 Å SPP was very stable. Assuming that the D-form of CER[AP] is dominating that durable SPP, we can gain useful knowledge from that, concerning its presence in native SC: In all applied SC lipid model membranes the natural occurring D-CER[AP]-C18 is supporting a very rigid and stable SPP, which is persistent against heating [166], humidity and the impact of time and storage [165]. Adapting that finding to the native SC, it could be assumed, that the long-chain CER would play an important role for the SPP stability and corresponding barrier properties.

5.4 Outlook

The outcomes of the performed experiments offer further ideas concerning the investigated SC lipid model membranes. For example, studies with separated CER[AP] diastereomers will be necessary in order to gain detailed knowledge about the single phase behavior of the native D-form. Then, precise statements regarding the impact of the pure enantiomer to the lipid assembly and the corresponding phase properties are possible. Here, partially deuterated and perdeuterated D-CER[AP] variants could produce detailed insights into their molecular interaction with other synthetically derived SC lipids, e.g. in neutron diffraction, ^{2}H NMR or FTIR studies. Additionally, it would be of high interest, if, together with CER[EOS]-br, CHOL, and BA (10/23/33/33 wt%), the D-form would also support the three coexisting phases or if the 45 Å SPP would be absent. Another interesting issue for that SC lipid model system is the application of long-chain CER subspecies with different head group structures, e.g. CER[AS] or CER[AH], which would reveal the impact of the polarity to the LPP formation due to their presence inside. These experiments could help to verify, if the number of OH groups and their molecular positions impact the inclusion of the long-chain CER component in the LPP. For that purpose, the chemical synthesis of specifically deuterated derivatives of these CERs would be a first step. Moreover, there are numerous questions to answer, e.g. (i) Does the simplified SC lipid model membrane show the coexistence of SPP and LPP as well? (ii) Is CER[AP] able to incorporate in the LPP due to the reduced CER[EOS] level? (iii) Are earlier results concerning a minimal concentration of CER[EOS], necessary for the LPP assembly [112, 113], confirmable? (iv) Does the CER[EOS] level perform direct impacts to the observed LPP properties regarding its sensitivity for RH and time, if the concentration of CER[EOS]-br will be reduced to the native concentration? Although this SC lipid model composition was often investigated, in the last decade, there are still details, which have to be revealed.

For IPM, in the present thesis a defined effect was observed, followed by a separation from the SC lipids. This would enable the recovery of the SC barrier properties. Nevertheless, the exact mode of action, especially for the prevention of the LPP formation, is still unclear. It is imaginable, that an interaction with the lipid head groups was responsible for that finding. Moreover, not only the lipophilic penetration enhancers (e.g. IPM or oleic acid) and their impact on SC lipid models were investigated in the last years [132, 154], but also hydrophilic enhancers (e.g. taurine and urea) were applied to SC lipid models, in order to elucidate their impact on a molecular scale [125]. Unfortunately, the interplay of the latter with the lipid head groups is not detectable using neutron diffraction. Consequently, lipophilic enhancers should be focused in further experiments, which are comparable to the present studies. At first,

measurements directly after the sample preparation prior to the equilibrium state could reveal the time depending movements and phase separation of the liquid wax IPM. From that, conclusions concerning the velocity of the phase separation and the way of IPM through the SC lipid model membranes could be made.

Overall, in the last years, useful results were presented, which enabled a better understanding of SC lipids and the nanostructure of their molecular arrangements and interactions. Nevertheless, the high and still rising number of CER subspecies offers a wide field of experimental possibilities, which has to be explored for a complete comprehension and adaption to native SC.

6 SUMMARY

6.1 English Version

The present thesis focused on investigations of selected SC lipid model membranes with the aim of getting detailed insights into their arrangements on a molecular scale. Therefore, multilamellar model membranes, containing the most abundant SC lipid fractions CERs, CHOL, and FFA were prepared. An enormous benefit of this work was the first application of partially deuterated ceramide species in the model systems for the investigations using the sensitive technique of neutron diffraction. Due to diverging coherent SLs for hydrogen and deuterium, neutrons differentiate between the two isotopes. This enabled the localization of the deuterated lipid segment within the multilamellar model membranes and gave useful ideas about the lipid arrangement and their impact to membrane properties.

In the first part of this work, a well-defined SC lipid mixture based on CER[AP]-C18, CHOL, SA and ChS (55/25/15/5, wt%) was analyzed, whereby the CER component was selectively deuterated at the end of the amid bound fatty acid. For this system, an earlier work presented a first model idea with CER[AP]-C18 in its *hairpin* conformation [39]. The here presented scientific publication verified this result partially [164]: The received SPP was about 44 Å and the deuterium label was localized in the unit cell center. This finding underlined the idea of CER[AP] in its *hairpin* conformation but the small repeat distance indicated a V-shaped conformation as well. In detail, a racemic mixture of the very polar long-chain CER was applied, which explains the different conformational states. For both enantiomers, D- and L-CER[AP], different phase behaviors were described, covering their favorite conformation and differing unit cell scales [123, 124]. Overall, both enantiomers were present in the single SPP, meaning that none of them dominated and both were able to assemble in their particular favorite conformation. This finding is of high benefit for the understanding of the SC lipid model system, regarding the immense impact of the CER subspecies to the membrane structure in principle due to its special arrangement.

In order to gain more information about CER[AP] and its influence, in the second part of this thesis, a methyl-branched CER[EOS] analogue was added. The protonated SC lipid model system (CER[AP]-C18/CER[EOS]-br/CHOL/BA, 10/23/33/33, wt%) was investigated in an earlier neutron diffraction study [38], where the comparability of the methyl-branched analogue to the native CER[EOS] species was demonstrated. Within this thesis, three coexisting lamellar phases have been observed, in detail two SPPs with d spacings of about 45 Å and 48 Å and a LPP with a d spacing of about 118 Å. Within the applied SC lipid mixture, a LPP could be detected and the proposed three-layer substructure of the unit cell, which was presented earlier [13, 27, 106] could be verified. This is very interesting as former studies figured out that a long unit cell can only be structured under the presence of an unsaturated FFA esterified to

ultra-long chain CER[EOS] [11]. Other neutron diffraction studies on comparable SC lipid model membranes described a single SPP with a unit cell scale of about 48 Å [19, 38] in absence of any LPP. In the scientifically accepted publication, which is presented here [165], for the first time, an esterified palmitic acid induced LPP formation could be proven. Compared to the earlier neutron diffraction experiments, this finding could be a result of differences in sample preparation. It has been observed, that a very high humidity during and directly after the sample preparation supported the LPP formation. This is in agreement with results from bulk phase experiments on pure CER[EOS], where for the ultra-long-chain CER a LPP assembly was only found under hydration [12]. Moreover, investigations concerning the impact of humidity during the neutron diffraction studies revealed that the LPP was still sensitive to changing humidities. The unit cell scale raised about 4 Å, but the d spacings of the SPPs were constant. Additionally, the impact of time was investigated during a second measurement, which revealed an increased spacing of the LPP and no changes for both SPPs. Again, it was only the long phase, which was affected by external influences.

The application of specifically deuterated CER[AP]-C18 and CER[EOS]-br enabled their localization within the received lamellar phases. The long-chain CER was detected in both SPPs, but not in the LPP, whereas the ultra-long-chain CER variant was found in the LPP and not in any of the SPPs. This outcome was very interesting, as former neutron diffraction studies supposed CER[EOS]-br in a 48 Å SPP [38]. It is possible, that in the experiments performed within this thesis, the ratio of CER[EOS]-br in the SPP was below the detection level. Nevertheless, the detected assembly of CER[EOS]-br, stretched over the LPP unit cell, was very important and enabled a surplus of knowledge relating to the LPP substructure and the impact of the CER variant on it. Apart from this, CER[AP] was dominating both short phases and could not be found in the LPP. A reason for that could be the very polar head group structure of the CER, as in the literature e.g. the less polar CER[NS] was described to be localized in a LPP [115]. Overall, as far as known from the literature, for the first time, the coexistence of SPP and LPP, which was found in native SC [27, 105], could be proven due to the here performed neutron diffraction experiment on a SC lipid model membrane.

In the last part of this thesis, the impact of the lipophilic penetration IPM in a concentration of 10 wt% on the SC lipid model system, which was investigated before, was analyzed. Here, a single SPP in dimensions of 48 Å was found in absence of any LPP. Furthermore, the deuterated CERs [AP]-d_3 and [EOS]-d_3 were localized within the unit cell, but the applied enhancer IPM-d_3 was absent. Performed ^{2}H NMR studies supported this finding, as they revealed both CERs in one phase and the enhancer in a separated isotropic phase [166]. It is reasonable, that IPM influenced the lipid assembly during the sample preparation and executed its penetration stimulating properties due to the inhibition of the LPP formation, which would decrease the SC barrier properties. Continuative studies of the thermotropic phase

behavior of the SC lipid model system revealed a phase transition, where during the cool-down period a LPP of about 110 Å was generated. Since at this stage, the liquid penetration enhancer was not mixed homogeneously with the SC lipids anymore, it could not manipulate the phase behavior of the lipids, which finally enabled the LPP arrangement. Here, the observation of the temperature dependent development of the LPP provided new insights regarding the conditions, which are necessary to form a LPP in these SC lipid model membranes.

Summarizing, this thesis presented the first application of the specifically deuterated CERs [AP]-C18-d_3 and [EOS]-d_3 in neutron diffraction studies. The deuteration enabled the localization of the lipids in different SC lipid model systems, which complemented previous ideas of their arrangement. Furthermore, new phase formations were observed, which is of high profit for the understanding of the lipid models, their bilayer substructure and their adaption to native SC.

6.2 German Version

Ausgewählte Stratum corneum Lipidmodellmembranen wurden mittels Neutronendiffraktion untersucht. Im Besonderen wurden selektiv-deuterierte SC Lipide eingesetzt, um sie in den präparierten Modellmembranen lokalisieren zu können. Dies ist durch unterschiedliche Streulängendichten möglich, die Neutronen für Wasserstoff und Deuterium aufweisen. Zunächst wurde ein bereits bekanntes SC Lipidmodell untersucht, welches aus dem endständig deuterierten CER[AP], zusammen mit Cholesterol, Stearinsäure und Cholesterolsulfat in einem Massenverhältnis von 55/25/15/5 bestand. Eine frühere Publikation zeigte erste Vorstellungen davon, wie das CER in dem Modellsystem angeordnet sein könnte [39]. Dort wurde die Haarnadel-Konformation des CERs zugrunde gelegt. Diese Modellvorstellung konnte anhand der vorliegenden Arbeit in Teilen bestätigt werden [164]. In der beobachteten *short-periodicity phase* (SPP) zeigte sich die Deuterierung im Zentrum des Bilayers, was die Annahme bestätigt, dass das CER in seiner Haarnadel- Konformation vorliegt. Allerdings ist aufgrund der Dicke des Bilayers von ~44 Å auch die V-förmige CER-Konformation eine mögliche Alternative. Dies lässt den Schluss zu, dass hier beide Enantiomere in ihrer jeweils präferierten Konformation innerhalb ein und derselben Phase vorliegen. Diese Erkenntnis erweitert die bisherigen Annahmen erheblich.

Im weiteren Verlauf dieser Arbeit wurde der Einfluss eines ultra-langkettigen CERs des Sphingosin-Typs auf eine CER[AP]-basierte SC Lipidmembran untersucht [165]. Hierzu wurde eine methylverzweigte Abwandlung (-br) des CER[EOS] eingesetzt, für die bereits ein phasengleiches Verhalten zur nativen Form nachgewiesen wurde [38]. Auch hier wurde eine an der Methylverzweigung befindliche Deuterierung eingesetzt. Die Lipidmembran bestehend aus CER[AP], CER[EOS]-br, CHOL und BA in einem Massenverhältnis von 10/23/33/33 zeigte erstmals eine Koexistenz von SPP und LPP (*long-periodicity phase*). Dies war überraschend, zeigten vorangegangene Arbeiten an ähnlichen Membranen nur eine SPP im Bereich von 48 Å [19, 38]. Hier wurden zwei SPP (48 Å und 45 Å) und eine LPP (118 Å) beobachtet. Auch war es durch dieses Experiment erstmalig möglich, eine lange Phase zu detektieren, die durch ein mit einer gesättigten Fettsäure verestertes CER[EOS] entstand. Bislang wurde angenommen, dass zur Bildung einer LPP ungesättigte Fettsäuren mit dem langkettigen CER verestert sein müssen [11]. Allerdings konnten vergleichbare Eigenschaften zwischen nativem CER[EOS] und der eingesetzten CER[EOS]-br-Variante nachgewiesen werden [38], wodurch sich die hier erhaltenen Ergebnisse hinsichtlich der LPP-Formierung unterstützen lassen. Des Weiteren wurde festgestellt, dass die LPP unter dem Einfluss von hoher Luftfeuchte minimal an Schichtdicke gewinnt, was für beide SPP nicht gezeigt werden konnte. Auch wiesen beide kurzen Phasen keine signifikanten Veränderungen ihrer Schichtdicken über einen Zeitraum von drei Monaten hinweg auf. Die Einheitszelle der langen Phase hingegen wurde um 4 Å dicker. Der Einsatz der partiell-deuterierten Varianten der CER[AP] und [EOS]-br ermöglichte

die Lokalisierung Beider in den Lipidschichten. In den kurzen Phasen wurde CER[AP] nachgewiesen, allerdings kein CER[EOS]-br, was frühere Modellvorstellungen revidiert, in denen sich das ultra-langkettige CER[EOS] in die Membranstruktur der kurzen Einheitszelle von 48 Å einfügt [19, 38]. Allerdings könnte hier auch der Anteil an CER[EOS]-br in der Phase zu gering gewesen sein, um detektiert zu werden, da sich das ultra-langkettige CER vor allem in der langen Phase befand. Diese Ergebnisse sind von enormer Relevanz für das Strukturverständnis der LPP und ihrer Bedeutung für die Barrierefunktion des Stratum corneum.

Zuletzt wurde der Einfluss des lipophilen Penetrationsenhancers Isopropylmyristat (IPM) in einer Konzentration von 10 % auf die zuvor angewandte SC Lipidmembran untersucht [166]. Überraschenderweise wurde nur eine SPP im Bereich von 48 Å beobachtet und keine LPP. Des Weiteren konnten sowohl CER[AP], als auch [EOS]-br in dieser kurzen Phase nachgewiesen werden, der Enhancer jedoch nicht. Weiterführende ^{2}H-NMR-Studien konnten diese Ergebnisse bestätigen. Diese zeigten, dass sich beide CER in einer Phase befanden und dass der lipophile Penetrationsbeschleuniger phasenseparierte in isotroper Form vorlag. Folglich ist anzunehmen, dass der Enhancer während der Probenpräparation einen starken Einfluss ausübte und dabei die Bildung der barrierefördernden LPP verhinderte. Durch das Fehlen der LPP wäre die Barrierfunktion der Modellmembran gestört und die Penetrationsrate durch die Membran erhöht. Der Penetrationsbeschleuniger hätte seine Funktion erfüllt. Da IPM bei Raumtemperatur flüssig ist, ist es denkbar, dass sich das Wachs bis zur Messung von den flüssig-kristallinen Lipidschichten phasenseparierte und seine endständig deuterierte Variante daher in den Neutronenexperimenten nicht mehr in den Lipidmembranen nachweisbar war. Diese These wird durch Studien unterstützt, die das thermotrophe Phasenverhalten der Lipidmischung untersuchten. Darin konnte beim Aufheizen bis 70 °C eine Phasenseparation beobachtet werden. Während des anschließenden Abkühlens separierten sich weitere Phasen, wobei eine LPP mit ~100 Å detektiert wurde, die während des weiteren Abkühlens sogar auf ~111 Å anwuchs. Es wird angenommen, dass der phasenseparierte Enhancer nicht mehr den gleichen Einfluss auf die Lipidanordnung hatte, wie bei der Probenpräparation, wo er homogen in der Lipidmischung verteilt war. In diesem Teil der Neutronendiffraktionsstudien war es besonders interessant, erstmalig das temperaturabhängige Entstehen der LPP zu beobachten, was wiederum einen Wissenszuwachs hinsichtlich der langen Phase und ihrer Formationsbedingungen in SC-Modellsystemen darstellt.

Insgesamt ist dies die erste Arbeit, die speziell deuterierte CER-Varianten in Neutronendiffraktionsstudien einsetzte und deren Anordnung in verschiedenen SC Lipidmodellen nachwies. Die Ergebnisse zeigen eine Erweiterung des bisherigen Kenntnisstandes über die Lipidphasen, ihr Verhalten gegenüber Temperatur, Feuchtigkeit, Zeit und eines Penetrationsbeschleunigers.

7 APPENDIX

LITERATURE

1. Wertz, P. W. and van den Bergh, B., *The physical, chemical and functional properties of lipids in the skin and other biological barriers.* Chem Phys Lipids, 1998. **91**(2): p. 85-96.
2. Elias, P. M., *Epidermal lipids, barrier function and desquamation.* The Journal of Investigative Dermatology, 1983. **80**(6): p. 44s-49s.
3. Yardley, H. J. and Summerly, R., *Lipid composition and metabolism in normal and diseased epidermis.* Pharmacology & Therapeutics, 1981. **13**(2): p. 383.
4. Gray, G. M. and Yardley, H. J., *Different populations of pig epidermal cells: isolation and lipid composition.* Journal of Lipid Research, 1975. **16**(6): p. 441-447.
5. Coderch, L., Lopez, O., de la Maza, A. and Parra, J. L., *Ceramides and skin function.* Am J Clin Dermatol, 2003. **4**(2): p. 107-29.
6. Masukawa, Y., Narita, H., Sato, H., Naoe, A., Kondo, N., Sugai, Y., Oba, T., Homma, R., Ishikawa, J., Takagi, Y. and Kitahara, T., *Comprehensive quantification of ceramide species in human stratum corneum.* Journal of Lipid Research, 2009. **50**: p. 1708-1719.
7. Liou, Y.-B., Sheu, M.-T., Liu, D.-Z., Lin, S.-Y. and Ho, H.-O, *Quantitation of ceramides in nude mouse skin by normal-phase liquid chromatography and atmospheric pressure chemical ionization mass spectrometry.* Analytical Biochemistry, 2010. **401**: p. 107-113.
8. Sahle, F. F., Lange, S., Dobner, B., Wohlrab, J. and Neubert, R. H. H., *Development and validation of LC/ESI-MS method for the detection and quantification of exogenous ceramide NP in stratum corneum and other layers of the skin.* Journal of Pharmaceutical and Biomedical Anlysis, 2012. **60**: p. 7-13.
9. Cho, H. J., Chung, B. Y., Lee, H. B., Kim, H. O., Park, Ch. W. and Lee, Ch. H., *Quantitative study of stratum corneum ceramides contens in patients with senisitve skin.* Journal of Dermantology, 2012. **39**: p. 2012.
10. Park, S. Y., Kim, J. H., Cho, S. I., Kim, K. I., Cho, H. J., Park, Ch. W., Lee, Ch. H. and Kim, H. O., *Induction of a Hardening Phenomenon and Quantitative Changes of Ceramides in Stratum Corneum.* Annals of Dermatology, 2014. **26**(1): p. 35-42.
11. de Sousa Neto, D., Gorris, G. and Bouwstra, J., *Effect of the ω-acylceramides on the lipid organization of stratum corneum model membranes evaluated by X-ray diffraction and FTIR studies.* Chemistry and Physics of Lipids, 2011. **164**: p. 184-195.
12. Kessner, D., Brezesinski, G., Funari, S. S., Dobner, B. and Neubert, R. H. H., *Impact of long chain ω-acylceramides on the stratum corneum lipid nanostructure. Part 1 : Thermotropic phase behaviour of CER[EOS] and CER[EOP] studied using X-ray powder diffraction and FT-Raman spectroscopy.* Chemistry and Physics of Lipids, 2010. **163**: p. 42-50.
13. Groen, D., Gooris, G. S. and Bouwstra, J. A., *New Insights into the Stratum Corneum Lipid Organization by X-Ray Diffraction Analysis.* Biophysical Journal, 2009. **97**: p. 2242-2249.
14. Harroun, T. A., Wignall, G. D. and Katsaras, J., *Neutron Scattering for Biology*. Neutron Scattering in Biology : Techniques and Applications, ed. J. Fitter, Gutberlet, T., Katsaras, J. 2006, Berlin Heidelberg: Springer-Verlag.
15. Dachs, H., *Principles in Neutron Diffraction*. Topics in Current Physics, Neutron Diffraction, ed. H. Dachs. 1978, Berlin Heidelberg: Springer-Verlag.

16. Willis, B. T. M. and Carlile, C. J., *Neutron properties*. Experimental Neutron Scattering. Vol. 1. 2009, Oxford, Great Britain: Oxford University Press. 325.

17. Zajac, W. and Gabrys, B. J., *An introduction to neutron scattering*. Applications of neutron scattering to Soft condensed matter, ed. B.J. Gabrys. Vol. 1. 2000, Amsterdam, Netherlands: Gordon and Breach Science Publishers. 1-26.

18. Kessner, D., A., Mikhail, Hauss, T., Dante, S., Wartewig, S. and Neubert, R. H. H., *Localisation of partially deuterated cholesterol in quaternary SC lipid model membranes: a neutron diffraction study.* European Biophysics Journal, 2008. **37**(6): p. 1051-1057.

19. Schroeter, A., Kessner, D., Kiselev, M. A., Hauß, T., Dante, S. and Neubert, R. H. H., *Basic nanostructure of stratum corneum lipid matrices based on ceramides [EOS] and [AP]: a neutron diffraction study.* Biophysical Journal, 2009. **97**: p. 1104-1114.

20. Schroeter, A., Kiselev, M. A., Hauß, T., Dante, S. and Neubert, R. H. H., *Evidence of free fatty acid interdigitation in stratum corneum model membranes based in ceramide [AP] by deuterium labelling.* Biochimica et Biophysica Acta, 2009. **1788**(10): p. 2194-2203.

21. Schroeter, A. , *The role of ceramide (AP) for the structural assembly of stratum corneum lipid model membranes*, in *Institute of Pharmacy*. 2010, Martin Luther University Halle-Wittenberg: Halle.

22. Kessner, D., Kiselev, M., Dante, S., Hauss, T., Lersch, P., Wartewig, S. and Neubert, R. H. H., *Arrangement of ceramide [EOS] in a stratum corneum lipid model matrix: new aspects revealed by neutron diffraction studies.* European Biophysics Journal, 2008. **37**(6): p. 989-999.

23. Kiselev, M. A., Ermakova, E. V., Gruzinov, A. Yu. and Zabelin, A. V., *Conformation of ceramide 6 molecules and chain-flip transitions in the lipid matrix of the outermost layer of mammalian skin, the stratum corneum.* Crystallography Reports, 2007. **52**(3): p. 525-528.

24. Kiselev, M. A., Ryabova, N. Y., Balagurov, A. M., Dante, S., Hauss, T., Zbytovska, J., Wartewig, S. and Neubert, R. H. H., *New insights into the structure and hydration of a stratum corneum lipid model membrane by neutron diffraction.* European Biophysics Journal, 2005. **34**: p. 1030-1040.

25. Madison, K. C., Swartzendruber, D. C., Wertz, P.W. and Downing, D. T., *Presence of intact intercellular lipid lammellae in the upper layers of the stratum corneum.* The Journal of Investigative Dermatology, 1987. **88**(6): p. 714-718.

26. White, S. H., Mirejovsky, D. and King, G. I., *Structure of lamellar lipid domains and corneocyte envelopes of murine stratum corneum. An X-ray diffraction study.* Biochemistry, 1988. **27**: p. 3725-3732.

27. Bouwstra, J. A., Gooris, G. S., van der Spek, J. A. and Bras, W., *Structural investigations of human stratum corneum by small-angle X-ray scattering.* Journal of Investigative Dermatology, 1991. **97**(6): p. 1005-1012.

28. Engelbrecht, T. N., Schroeter, A., Hauß, T., Demé, B., Scheidt, H. A., Huster, D. and Neubert, R. H. H., *The impact of ceramides NP and AP on the nanostructure of stratum corneum lipid bilayer. Part I: neutron diffraction and ^{2}H NMR studies on multilamellar models based on ceramides with symmetric alkyl chain length distribution.* Soft Matter, 2012. **8**: p. 2599-2607.

29. de Jager, M. W., Gooris, G. S., Dolbnya, I. P., Bras, W., Ponec, M. and Bouwstra, J. A., *The phase behaviour of skin lipid mixtures based on synthetic ceramides.* Chemistry and Physics of Lipids, 2003. **125**(2): p. 123-134.

30. Bouwstra, J. A., Gooris, G. S., Frank, E. R., Ponec, M., *Phase behaviour of stratum corneum lipid mixtures based on human ceramides: The role of natural and synthetic ceramide 1.* Journal of Investigative Dermatology, 2002. **118**(4): p. 606-617.

31. Kiselev, M. A., Ermakova, E. V., Gruzinov, A. Yu. and Zabelin, A. V., *Formation of the long-periodicity phase in model membranes of the outermost layer of skin (Stratum corneum).* Crystallography Reports, 2014. **59**(1): p. 123-128.

32. Bouwstra, J. A., Gooris, G. S., Dubbelaar, F. E. R., Weerheim, A. M., IJzerman, A. P., Ponec, M., *Role of ceramide 1 in the molecular organization of the stratum corneum lipids.* Journal of Lipid Research, 1998. **39**(1): p. 186-196.

33. Bouwstra, J. A., Gooris, G. S., Dubbelaar, F. E. R. and Ponec, M., *Phase behaviour of lipid mixtures based on human ceramides: coexistence of crystalline and liquid phases.* Journal of Lipid Research, 2001. **42**(11): p. 1759-1770.

34. McIntosh, T. J., Stewart, M. E. and Downing, D. T., *X-ray diffraction analysis of isolated skin lipids: Reconstruction of intercellular lipid domains.* Biochemistry, 1996. **35**(12): p. 3649-3653.

35. Kovacik, A., Opalka, L., Silarova, M., Roh, J. and Vavrova, K., *Synthesis of 6-hydroxyceramide using ruthenium-catalyzed hydrosilylation-protodesilylation. Unexpected formation of a long periodicity lamellar phase in skin lipid membranes.* RSC Advances, 2016. **6**(77): p. 73343-73350.

36. Mojumdar, E. H., Gooris, G. S., Groen, D., Barlow, D. J., Lawrence, M. J., Demé, B. and Bouwstra, J. A., *Stratum corneum lipid matrix: localization of acyl ceramide and cholesterol in the unit cell of the long periodicity phase.* Biochimica et Biophysica Acta, Biomembranes, 2016. **1858**: p. 1926-1934.

37. Groen, D., Gooris, G. S. and Bouwstra, J. A., *Model membranes prepared with ceramide EOS, cholesterol and free fatty acids from a unique lamellar phase.* Langmuir Article, 2010. **26**(6): p. 4168-4175.

38. Engelbrecht, T., Hauß, T., Süß, K., Vogel, A., Roark, M., Feller, S. C., Neubert, R. H. H. and Dobner, B., *Characterisation of a new ceramide EOS species: synthesis and investigation of the thermotropic phase behaviour and influence on the bilayer architecture of stratum corneum lipid model membranes.* Soft Matter, 2011. **7**: p. 8998-9011.

39. Ruettinger, A., Kiselev, M. A., Hauss, T., Dante, S., Balagurov, A. M. and Neubert, R. H. H., *Fatty acid interdigitation in stratum corneum model membranes: a neutron diffraction study.* European Biophysics Journal, 2008. **37**(6): p. 759-771.

40. *The human skin*. Available from: http://www.planet-wissen.de/natur_technik/sinne/fuehlen/.

41. Kanitakis, J., *Anatomy, histology and immunohistochemistry of normal human skin.* European Journal of Dermatology: EJD, 2002. **12**(4): p. 390-399.

42. Kielty, C. M. and Shuttleworth, C. A., *Microfibrillar elements of the dermal matrix.* Microscopy Research and Technique, 1997. **38**(4): p. 413-427.

43. Silver, F. H., Freeman, J. W. and DeVore, D., *Viscoelastic properties of human skin and processed dermis.* Skinresearch and technology, 2001. **7**(1): p. 18-23.

44. Smith, L. T., Holbrokk, K. A. and Byers, P. H., *Structure of the dermal matrix during development and in the adult.* The Journal of Investigative Dermatology, 1982. **79**(Supplement 1): p. 93s-104s.

45. Scheuplein, R. J. and Blank, I. H., *Permeability of the Skin.* Physicological Reviews, 1971. **51**(4): p. 702-747.

46. Holbrook, K. A. and Odland, G. F., *Regional differences in the thickness (cell layers) of the human stratum corneum: an ultrastructural analysis.* The Journal of Investigative Dermatology, 1974. **62**(4): p. 415-422.

47. Kligman, A. M., *The biology of the stratum corneum*. The Epidermis, ed. W. Montagna, Lobitz, W. C. 1964, New York, United States of America: Academic press inc.

48. Grove, G. L. and Kligman, A. M., *Age-associated changes in human epidermal cell renewal.* Journal of Gerontology, 1983. **38**(2): p. 137-142.

49. Scheuplein, R. J. and Morgan, L. J., *"Bound water" in keratin membranes measured by microbalance technique.* Nature, 1967. **214**(5087): p. 456-458.

50. Loomans, M. E. and Hannon, D. P., *An electron microscopic study of the effects of subtilisin and detergents on human stratum corneum.* The Journal of Investigative Dermatology, 1970. **55**(2): p. 101-114.

51. Elias, P. M., Gruber, R., Crumrine, D., Menon, G., Williams, M. L., Wakefoeld, J. S., Holleran, W. M., Uchida, Y., *Formation and functions of the corneocyte lipid envelope (CLE).* Biochimica et Biophysica Acta, 2014. **1841**: p. 314-318.

52. Wertz, P. W., Swartzendruber, D. C., Kitko, D. J., Madison, K. C. and Downing, D. T., *The role of the corneocyte lipid envelopes in cohesion of the stratum corneum.* Journal of Investigative Dermatology, 1989. **93**(7): p. 169-172.

53. Smith, W. P., Christensen, M. S., Nacht, S. and Gans, E. H., *Effect of lipids on the aggregation and permeability of human stratum corneum.* The Journal of Investigative Dermatology, 1982. **78**(1): p. 7-11.

54. Malkinson, F. D., *Permeability of the stratum corneum*. The Epidermis, ed. W. Montagna, Lobitz, W. C. 1964, New York, United States of America: Academic press inc.

55. Tregear, R. T., *Relative penetrability of hair follocles and epidermis.* The Journal of Physiology, 1961. **156**(2): p. 307-313.

56. Elias, P. M. and Friend, D. S., *The permeability barrier in mammalian epidermis.* The Journal of Cell Biology, 1975. **65**: p. 180-191.

57. Elias, P. M., McNutt, N. S. and Friend, D. S., *Membrane alterations during cornification of mammalian squamous epithelia: a freeze-fracture, tracer, and thin-section study.* The Anatomical record, 1977. **189**(4): p. 577-594.

58. Elias, P. M., *Epidermal lipids: membranes and keratinization.* Journal of Investigative Dermatology, 1981. **20**: p. 1-9.

59. Landmann, L., *The epidermal permeability barrier.* Anatomy and Embryology, 1988. **178**: p. 1-13.

60. Simonetti, O., Hoogstraate, A. J., Bialik, W., Kemenaar, J. A., Schrijvers, A. H. G. J., Boddé, H. E. and Ponec, M., *Visualization of diffusion pathways across the stratum corneum of native and in-vitro-reconstructed epidermis by confocal laser scanning microscopy.* Archieves of Dermatological Research, 1995. **287**: p. 465-473.

61. Imokawa, G., Akasaki, A., Hattori, M. and Yoshizuka, N., *Selective Recovers of deranged water-holding properties by stratum corneum lipids.* Journal of Investigative Dermatology, 1986. **87**: p. 758-761.

62. Pascher, I., *Molecular arrangements in sphingolipids. Conformation and hydrogen bonding of ceramide and their implication on membrane stability and permeability.* Biochimica et Biophysica Acta, Biomembranes, 1976. **455**(2): p. 433-451.

63. Lampe, M. A., Burlingame, A. L., Whitney, J., Williams, M. L., Brown, B. E., Roitman, E. and Elias, P. M., *Human Stratum corneum lipids: characterization and regional variations.* Journal of Lipid Research, 1983. **24**(2): p. 120-130.

64. Landmann, L., *Lamellar granules in mammalian , avian, and reptilian epidermis.* Journal of Ultrastructure Research, 1980. **72**(3): p. 245-63.

65. Elias, P. M., Menon, G. K., *Structural and lipid biochemical correlates of the epidermal permeability barrier.* Advances in Lipid Research, 1991. **24**: p. 1-26.

66. Elias, P. M., *Structure and function of the stratum corneum permeability barrier.* Drug Development Research, 1988. **13**(2-3): p. 97-105.

67. Grubauer, G., Feingold, K. R., Harris, R. M. and Elias, P. M., *Lipid content and lipid type as dterminants of the epidermal permeability barrier.* Journal of Lipid Research, 1989. **30**(1): p. 89-96.

68. Wertz, P. W., Miethke, M. C., Long, A. A., Strauss, J. S. and Downing, D. T., *The composition of the ceramides from human stratum corneum and from comedones.* The Journal of Investigative Dermatology, 1985. **84**(5): p. 410-412.

69. Wertz, P. W. and van den Bergh, B., *The physical, chemical and functional properties of lipids in the skin and other biological barriers.* Chemistry and Physics of Lipids, 1998. **91**(2): p. 85-96.

70. Weerheim, A. and Ponec, M., *Determination of stratum corneum lipid profile by tape stripping in combination with high-performance thin-layer chromatography.* Archives of Dermatological Research, 2001. **293**: p. 191-199.

71. Motta, S., Sesana, S., Monti, M., Giuliani, A. and Caputo, R., *Interlamellar lipid differences between normal and psoriatic stratum corneum.* Acta dermato-venereologica- Supplementum, 1994. **186**: p. 131-132.

72. Deffond, D., Saint Leger, D., Leveque, J. L. and Agache, P., *In vivo measurement of epidermal lipids in man.* Bioengineering and the Skin, 1986. **2**(1): p. 71-85.

73. Masukawa, Y., Narita, H., Kitahara, T., Takema, Y. and Kita, K., *Characterization of overall ceramide species in human stratum corneum.* Journal of Lipid Research, 2008. **49**(7): p. 1466-1476.

74. van Smeden, J., Hoppel, L., van der Heijden, R., Hankemeier, T., Vreeken, R. J. and Bouwstra, J. A., *LC/MS analysis of Stratum corneum lipids: Ceramide profiling and discovery.* Journal of Lipid Research, 2011. **52**(6): p. 1211-1221.

75. Rabionet, M., Gorgas, K. and Sandhoff, R., *Ceramide synthesis in the epidermis.* Biochimica et Biophysica Acta, Molecular and Cell Biology of Lipids, 2014. **1841**(3): p. 422-434.

76. t´Kindt, R. , Jorge, L., Dumont, E., Couturon, P., David, F., Sandra, P. and Sandra, K., *Profiling and characterizing skin ceramides using reversed-phase liquid chromatography-quadrupole time-of-flight mass spectrometry.* Analytical Chemistry, 2012. **84**: p. 403-411.

77. Wertz, P. W. and Downing, D. T., *Ceramides of pig epidermis: structure determination.* Journal of Lipid Research, 1983. **24**(6): p. 759-765.

78. Breiden, B. and Sandhoff, K., *The role of sphingolipid metabolism in cutaneous permeability barrier formation.* Biochimica et Biophysica Acta, 2014. **1841**: p. 441-452.

79. Motta, S., Monti, M., Sesana, S., Caputo, R., Carelli, S. and Ghidoni, R., *Ceramide composition of the psoriatic scale.* Biochimica et Biophysica Acta, 1993. **1182**: p. 147-151.

80. Robson, K. J., Stewart, M. E., Michelsen, S., Lazo, N. D. and Downing, D. T., *6-hydroxy-4-sphingenine in human epidermal ceramides.* Journal of Lipid Research, 1994. **35**: p. 2060-2068.

81. van Smeden, J., Boiten, W. A., Hankemeier, T., Rissmann, R., Bouwstra, J. A. and Vreeken, R. J., *Combined LC/MS-platform for analysis of all major stratum corneum lipids, and the profiling of skin substitutes.* Biochimica et Biophysica Acta, 2014. **1841**: p. 70-79.

82. Mojumdar, E. H., Kariman, Z., van Kerckhove, L., Gooris, G. S. and Bouwstra, J. A., *The role of ceramide chain length distribution on the barrier properties of skin lipid membranes.* Biochimica et Biophysica Acta- Biomembranes, 2014. **1838**: p. 2473-2483.

83. de Jager, M., Gooris, G., Ponec, M. and Bouwstra, J., *Acylceramide head group architecture affects lipid organization in synthetic ceramide mixtures.* Journal of Investigative Dermatology, 2004. **123**: p. 911-916.

84. Di Nardo, A., Wertz, P., Giannetti, A. and Seidenari, S., *Ceramide and cholesterol compositon of the skin of patients with atopic dermatitis.* Act dermato-venereologica, 1998. **78**(1): p. 27-30.

85. Motta, S., Monti, M., Sesana, S., Mellesi, L., Ghidoni, R. and Caputo, R., *Abnormality of water barrier function in psoriasis. Role of ceramide fractions.* Archives of Dermatology, 1994. **130**(4): p. 452-456.

86. Wartewig, S. and Neubert, R. H. H., *Properties of ceramides and their impact on the stratum corneum structure: A review.* Skin Pharmacology and Physiology, 2007. **20**: p. 220-229.

87. Schreiner, V., Gooris, G. S., Pfeiffer, S., Lanzendorfer, G., Wenck, H., Diembeck, W., Proksch, E. and Bouwstra, J., *Barrier characteristics of different human skin types investigated with X-ray diffraction, lipid analysis, and electron microscopy imaging.* Journal of Investigative Dermatology, 2000. **114**(4): p. 654-660.

88. Gray, G. M. and Yardley, H. J., *Lipid composition of cells isolated from pig, human, and rat epidermis.* Journal of Lipid Research, 1975. **16**(6): p. 434-440.

89. Norlén, L., Nicander, I., Rozell, B. L., Ollmar, S. and Forslind, B., *Inter- and intra-individual differences in human stratum corneum lipid content related to physical parameters of skin barrier function in vivo.* Journal of Investigative Dermatology, 1999. **112**(1): p. 72-77.

90. Bonté, F., Saunois, A., Pinguet, P. and Meybeck A., *Existence of a lipid gradient in the upper stratum corneum and its possible biological significance.* Archieves of Dermatological Research, 1997. **289**(2): p. 78-82.

91. Yamamoto, A., Serizawa, S., Ito, M. and Sato, Y., *Stratum corneum lipid abnormalities in atopic dermatitis.* Archieves of Dermatological Research, 1991. **283**: p. 219-223.

92. Mojumdar, E. H., Groen, D., Gooris, G. S., Barlow, D. J., Lawrence, M. J., Demé, B. and Bouwstra, J. A., *Localization of cholesterol and fatty acid in a model lipid membrane: a neutron diffraction approach.* Biophysical Journal, 2013. **105**: p. 911-918.

93. Feingold, K. R., Mao-Qiang, M., Menon, G. K., Cho, S. S., Brown, B. E. and Elias, P. M., *Cholesterol synthesis in required for cutaneous barrier function in mice.* The Journal of Clinical Investigation, 1990. **86**: p. 1738-1745.

94. Menon, G. K., Feingold, K. R., Moser, A. H., Brown, B. E. and Elias, P. M., *De novo sterologenesis in the skin. II. Regulation by cutaneous barrier requirements.* Journal of Lipid Research, 1985. **26**: p. 418-427.

95. Mojumdar, E. H., Gooris, G. S. and Bouwstra, J. A., *unpublished data*, in *Mojumdar et al., Localization of cholesterol and fatty acid in a model lipid membrane: a neutron diffraction approach*. 2013: Biophysical Journal. p. 911−918.

96. Hoeltje, M., Foerster, T., Brandt, B., Engels, T., von Rybinski, W. and Hoeltja, H.-D., *Molecular dynamics simulations of stratum corneum lipid models: fatty acids and cholesterol.* Biochimica et Biophysica Acta, 2001. **1511**: p. 156-167.

97. Zbytovská, J., Kiselev, M. A., Funari, S. S., Garamus, V. M., Wartewig, S., Palát, K. and Neubert, R., *Influence of cholesterol on the structure of stratum corneum lipid model membranes.* Colloids and surfaces, A: Physicochemical and Engineering Aspects, 2008. **328**: p. 90-99.

98. de Jager, M. W., Gooris, G. S., Dolbnya, I. P., Ponec, M. and Bouwstra, J. A., *Modelling the stratum corneumlipid organisation with synthetic lipid mixtures: the importance of synthetic ceramide composition.* Biochimica et Biophysica Acta, 2004. **1684**: p. 132-140.

99. Lavrijsen, A. P., Higounenc, I. M., Weerheim, A., Oestmann, E., Tuinenburg, E. E., Boddé, H. E. and Ponec, M., *Validation of an in vivo extraction method for human stratum corneum ceramides.* Archives of Dermatological Research, 1994. **286**(8): p. 495-503.

100. Wertz, P. W., Swartzendruber, D. C., Madison, K. C. and Downing, D. T., *Composition and morphology of epidermal cyst lipids.* Journal of Investigative Dermatology, 1987. **89**(4): p. 419-425.

101. Norlén, L., Nicander, I., Lundsjö, A., Cronholm, T. and Forslind, B., *A new HPLC-based method for the quantitative analysis if inner stratum corneum lipids with special reference to the free fatty acid fraction.* Archieves of Dermatological Research, 1998. **290**: p. 508-516.

102. Breathnach, A. S., Goodman, T., Stolinski, C. and Gross, M., *Freeze-fracture replication of cells of stratum corneum of human epidermis.* Journal of Anatomy, 1973. **114**(1): p. 65-81.

103. Swartzendruber, D. C., Wertz, P. W., Kitko, D. J., Madison, K. C. and Downing, D. T., *Molecular models of the intercellular lipid lamellae in mammalian stratum corneum.* Journal of Investigative Dermatology, 1989. **92**(2): p. 251-257.

104. Bouwstra, J. A., Gooris, G. S., van der Spek, J. A., Lavrijsen, S. and Bras, W., *The lipid and protein structure of mouse stratum corneum: A wide and small angle diffraction study.* Biochimica et Biophysica Acta, 1994. **1212**: p. 183-192.

105. Bouwstra, J. A., Gooris, G. S., Bras, W. and Downing, D. T., *Lipid organization in pig stratum corneum.* Journal of Lipid Research, 1995. **35**(4): p. 685-695.

106. Bouwstra, J. A., Dubbelaar, F. E. R., Gooris, G. S. and Ponec, M., *The lipid organization in the skin barrier.* Acta Dermato- Venereologica, 2000. **208**(Suppl): p. 23-30.

107. Bouwstra, J., Gooris, G., Ponec, M., *The lipid organisation of the skin barrier: Liquid and crystalline domains coexist in lamellar phases.* Journal of Biological Physics, 2002. **28**: p. 211-223.

108. Bouwstra, J., Pilgram, G., Gooris, G., Koerten, H. and Ponec, M., *New aspects of the skin barrier organization.* Skin Pharmacology and Physiology, 2001. **14**: p. 52-62.

109. Hill, J. R. and Wertz, P. W., *Molecular models of the intercellular lipid lamellae from epidermal stratum corneum.* Biochimica et Biophysica Acta, 2003. **1616**(2): p. 121-126.

110. Iwai, I., Han, H., den Hollander, L., Svensson, St., Öfverstedt, L.-G., Anwar, J., Brewer, J., Bloksgaard, M., Laloeuf, A., Nosek, D., Masich, S., Bagatolli, L. A., Skoglund, U. and Norlén, L., *The human skin barrier is organized as stacked bilayers of fully extended ceramides with cholesterol molecules associated with the ceramide sphingoid moiety.* Journal of Investigative Dermatology, 2012. **132**: p. 2215-2225.

111. Rissmann, R., Gooris, G., Ponec, M. and Bouwstra, J., *Long periodicity phase in extracted lipids of vernix caseosa obtained with equilibration at physiological temperature.* Chemistry and Physics of Lipids, 2009. **158**(1): p. 32-38.

112. Bouwstra, J. A., Dubbelaar, F. E. R., Gooris, G. S., Weerheim, A. M. and Ponec, M., *The role of ceramide composition in the lipid organisation of the skin barrier.* Biochimica et Biophysica Acta, 1999. **1419**(2): p. 127-136.

113. Opálka, L., Kovácik, A., Maixner, J. and Vávrová, K., *Omega-O-acylceramides in skin lipid membranes: effects of concentration, sphingoid base, and model complexity on microstructure and permeability.* Langmuir, 2016. **32**: p. 12894-12904.

114. de Jager, M. W., Gooris, G. S., Ponec, M. and Bouwstra, J. A., *Lipid mixtures prepared with well-defined synthetic ceramides closely mimic the unique stratum corneum lipid phase behavior.* Journal of Lipid Research, 2005. **46**: p. 2649-2656.

115. Mojumdar, E. H., Gooris, G. S., Barlow, D. J., Lawrence, M. J., Demé, B. and Bouwstra, J. A., *Skin lipids: localization of ceramide and fatty acid in the unit cell of the long periodicity phase.* Biophysical Journal, 2015. **108**: p. 2670-2679.

116. Schroeter, A., Kiselev, M. A., Hauß, T., Dante, S. and Neubert, R. H. H., *Evidence of free fatty acid interdigitation in stratum corneum model membranes based in ceramide [AP] by deuterium labelling.* Biochimica et Biophysica Acta, 2009. **1788**: p. 2194-2203.

117. Groen, D., Gooris, G. S., Barlow, D. J., Lawrence, M. J., van Mechelen, J. B., Demé, B. and Bouwstra, J. A., *Disposition of ceramide in model lipid membranes determined by neutron diffraction.* Biophysical Journal, 2011. **100**(6): p. 1481-1489.

118. Schroeter, A., Stahlberg, S., Skolova, B., Sonnenberger, S., Eichner, A., Huster, D., Vavrova, K., Hauß, T., Dobner, B., Neubert, R. H. H. and Vogel, A., *Phase separation in ceramide[NP] containing lipid model membranes: neutron diffraction and solid-state NMR.* Soft Matter, 2017. **13**(10): p. 2107-2119.

119. Hatta, I., Ohta, N., Inoue, K. and Yagi, N., *Coexistance of two domains in intercellular lipid matrix of stratum corneum.* Biochimica et Biophysica Acta, 2006. **1758**: p. 1830-1836.

120. Norlén, L., *Skin barrier structure and function: The single gel phase model.* Journal of Investigative Dermatology, 2001. **117**: p. 830-836.

121. Skolova, B., Hudska, K., Pullmannova, P., Kovacik, A., Palat, K., Roh, J., Fleddermann, J., Estrela-Lopis, I. and Vavrova, K., *Different phase behavior and packing of ceramides with long (C16) and very long (C24) acyls in model membranes: Infrared spectroscopy using deuterated lipids.* The Journal of physical Chemistry B, 2014. **118**: p. 10460-10470.

122. Dahlén, B. and Pascher, I., *Molecular arrangements in sphingolipids. Crystals structure of N-Tetracosanoylphytosphingosine.* Acta Crystallographica Section B: Structural Crystallography and Crystal Chemistry 1972. **28**: p. 2396-2404.

123. Gruzinov, A. Yu., Zabelin, A. V. and Kiselev, M. A., *Short periodicity phase based on ceramide [AP] in the model lipid membranes of stratum corneum does not change during hydration.* Chemistry and Physics of Lipids, 2017. **202**: p. 1-5.

124. Raudenkolb, S., Wartewig, S. and Neubert, R. H. H., *Polymorphism of ceramide 6: a vibrational spectroscopic and X-ray powder diffraction investigation of the diastereomers of N-(α-hydroxyoctadecanoyl)-phytosphingosine.* Chemistry and Physics of Lipids, 2005. **133**: p. 89-102.

125. Mueller, J., Schroeter, A., Oliveira, J. S. L., Barker, R., Trapp, M., Brezesinski, G. and Neubert, R. H. H., *The effect of urea and taurine as hydrophilic penetration enhancers on stratum corneum lipid models.* Biochimica et Biophysica Acta- Biomembranes, 2016. **1858**(9): p. 2006-18.

126. Mak, V. H. W., Potts, R. O. and Guy, R. H., *Oleic acid concentration and effect in human stratum corneum: non-invasive determination by attenuated total reflectance infrared spectroscopy in vivo.* Journal of Controlled Release, 1990. **12**(1): p. 67-75.

127. Francoeur, M. L., Golden, G. M. and Potts, R. O., *Oleic acid: its effects on stratum corneum in relation to (trans)dermal drug delivery.* Pharm Res, 1990. **7**(6): p. 621-7.

128. Ongpipattanakul, B., Francoeur, M. L., Burnette, R. R. and Potts, R. O., *Phase-Separation of Oleic-Acid in the Stratum-Corneum Lipids.* Journal of Investigative Dermatology, 1991. **96**(4): p. 619-619.

129. Ongpipattanakul, B., Burnette, R. R., Potts, R. O. and Francoeur, M. L., *Evidence that oleic acid exists in a separate phase within stratum corneum lipids.* Pharm Res, 1991. **8**(3): p. 350-4.

130. Barry, B. W., *Lipid-protein-partitioning theory of skin penetration enhancement.* Journal of Controlled Release, 1991. **15**(3): p. 237-248.

131. Brinkmann, I. and Mueller-Goymann, C. C., *An attempt to clarify the influence of glycerol, propylene glycol, isopropyl myristate and a combination of propylene glycol and isopropyl myristate on human stratum corneum.* Pharmazie, 2005. **60**(3): p. 215-220.

132. Engelbrecht, T.N., Demé, B., Dobner, B. and Neubert, R. H. H., *Study of the influence of the penetration enhancer isopropyl myristate on the nanostructure of stratum corneum lipid model membranes using neutron diffraction and deuterium labelling.* Skin Pharmacology and Physiology, 2012. **25**(4): p. 200-207.

133. Arellano, A., Santoyo, S., Martin, C. and Ygartua, P., *Influence of propylene glycol and isopropyl myristate on the in vitro percutaneous penetration of diclofenac sodium from carbopol gels.* European Journal of Pharmaceutical Sciences, 1998. **7**(2): p. 129-135.

134. Leopold, C. S. and Lippold, B. C., *An attempt to clarify the mechanism of the penetration enhancing effects of lipophilic vehicles with differential scanning calorimetry (DSC).* Journal of Pharmacy and Pharmacology, 1995. **47**(4): p. 276-281.

135. Santoyo, S., Arellano, A., Ygartua, P. and Martin, M., *Penetration enahncer effects on the in-vitro percutaneous absorption of piroxicam through rat skin.* International Journal of Pharmaceutics, 1995. **117**(2): p. 219-224.

136. Sato, K., Sugibayashi, K. and Morimoto, Y., *Effect and mode of action of aliphatic esters on the invitro skin permeation of nicorandil.* international Journal of Pharmaceutics, 1988. **43**(1-2): p. 31-40.

137. Goldberg-Cettina, M., Liu, P., Nightingale, J. and Kurihara-Bergstrom, T., *Enhanced transdermal delivery of estradiol in vitro using binary vehicles of isopropoyl myristate and short-chain alkanols.* international Journal of Pharmaceutics, 1995. **114**(2): p. 237-245.

138. Chadwick, J., *Existence of a neutron.* Proceedings of the Royal Society of London, Series A: Mathematical, Physical and Engineering Sciences, 1932. **136**: p. 692-708.

139. Olive, K. A., et al., (Particle Data Group), *Review of particle physics.* Chinese Physics C, 2014. **38**(9): p. 1-1676.

140. Schreyer, A., *Physical Properties of Photons and Neutrons*. Neutrons and Synchrotron Radiation in Engineering Materials Science. Vol. 1. 2008, Weinheim, Germany: Wiley-VCH Verlag GmbH & Co. KGaA. 79-89.

141. Schoneborn, B.P. and Nunes, A.C., *Neutron Scattering.* Annual Review of Biophysics and Bioengineering, 1972. **1**: p. 529-552.

142. Hauss, T., Büldt, G., Heyn, M. P. and Dencher, N. A., *Light-induced isomerization causes an increase in the chromophore tilt in the M intermediate of bacteriorhodopsin: A neutron diffraction study.* Proceedings of the National Academy of Sciences of the United States of America, 1994. **91**(25): p. 11854-11858.

143. Dante, S., Hauss, T. and Dencher, N. A., *Insertion of externally administered amyloid β peptide 25-35 and perturbation of lipid bilayers.* Biochemistry, 2003. **42**(46): p. 13667-13672.

144. Bueldt, G., Gally, H. U., Seelig, A. and Seelig, J., *Neutron diffraction studies on selective deuterated phospholipid bilayers.* Nature, 1978. **271**(5641): p. 182-184.

145. Tomita, B., Hasegawa, T., Tsukihara, T., Miyajima, S., Nagao, M. and Sato, M., *Two concentric protein shell structure with spikes if silkworm Bombyx mori cytoplasmic polyhedrosis virus revealed by small-angle neutron scattering using contrast variation method.* Journal of Biochemistry, 1999. **125**(5): p. 916-922.

146. Bauer, R., Behan, M., Clarke, D., Hansen, S., Jones, G., Mortensen, K. and Pedersen, J. S., *Contrast variation studies of clathrin coated vesicles by small-angle neutron scattering.* European Biophysics Journal, 1992. **21**: p. 129-136.

147. van Well, A. A. and Brinkhof, R., *Protein adsorption at a static and expanding air-water interface: a neutron reflection study.* Colloids and surfaces, A: Physicochemical and Engineering Aspects, 2000. **175**(1-2): p. 17-21.

148. de Broglie, L., *The reinterpretation of wave mechanics.* Foundations of Physics, 1970. **1**(1): p. 5-15.

149. Franks, N.P. and Lieb, W.R., *The structure of lipid bilayers and the effects of general anaesthetics.* Journal of Molecular Biology, 1979. **133**: p. 469-500.

150. Cser, F., *About the Lorentz correction used in the interpretatin of small angle X-ray scattering data of semicrystalline polymers.* Journal of Applied Polymer Science, 2001. **80**(12): p. 2300-2308.

151. Wiener, M. C. and White, S. H., *Fluid bilayer structure determination by the combined use of x-ray and neutron diffraction.* Biophysical Journal, 1991. **59**: p. 174-185.

152. Worchester, D. L. and Franks, N. P., *Structural analysis of hydrated egg lecithin and cholesterol bilayers, II. Neutron diffraction.* Journal of Molecular Biology, 1976. **100**(3): p. 359-378.

153. Nagle, J.F. and Tristam-Nagle, S., *Structure of lipid bilayers.* Biochimica et Biophysica Acta, 2000. **1469**: p. 159-195.

154. Engelbrecht, T. N., Schroeter, A., Hauss, T. and Neubert, R. H. H., *Lipophilic penetration enhancers and their impact to the bilayer structure of stratum corneum lipid model membranes: neutron diffraction studies based on the example oleic acid.* Biochimica et Biophysica Acta, Biomembranes, 2011. **1808**(12): p. 2798-2806.

155. Kessner, D., Ruettinger, A., Kiselev, M. A., Wartewig, S. and Neubert, R. H. H., *Properties of ceramides and their impact on the stratum corneum structure. Part 2 : stratum cornuem lipid model systems.* Skin Pharmacology and Physiology, 2008. **21**: p. 58-74.

156. Brief, E., Kwak, S., Cheng, J. T., Kitson, N., Thewalt, J. and Lafleur, M., *Phase behavior of an equimolar mixture of N-palmitoyl-D-erythro-sphingosine, cholesterol, and palmitic acid, a mixture with optimized hydrophobic matching.* Langmuir, 2009. **25**: p. 7523-7532.

157. Seul, M. and Sammon, M. J., *Preparation of surfactant multilayer films on solid substrates by deposition from organic solution.* Thin Solid Films, 1990. **185**(2): p. 287-305.

158. Casadei, C. M., Gumiero, A., Metcalfe, C. L., Murphy, Em J., Basran, J., Concilio, M. G., Reixeira, S. C. M., Schrader, T. E., Fielding, A. J., Ostermann, A., P., Blakeley M., Raven, E. L. and Moody, P. C. E., *Neutron cryo-crystallography captures the protonation state of ferryl heme in a peroxidase.* Science, 2014. **345**(6193): p. 193-197.

159. Coates, L., Tomanicek, S., Schrader, T. E., Weiss, K. L., Ng, J. D., Juettner, P. and Ostermann, A., *Cryogenic neutron proetein crystallography: routine methods and potential benefits.* Journal of Applied Crystallography, 2014. **47**(4): p. 1431-1434.

160. Yokoyama, T., Ostermann, A., M., Mizuguchim, Niimura, N., Schrader, T. E. and Tanaka, I., *Crystallization and preliminary neutron diffraction experiment of human farnesyl pyrophosphate synthase complexed with risedronate.* Acta Crystallographica Section F: Structural Biology and Crystallization Communications, 2014. **70**(4): p. 470-472.

161. Bryan, T., Gonzalez, J. M., Bacik, J. P., DeNunio, N. J., Unkefer, C. J., Schrader, T. E., Ostermann, A., Dunaway-Mariano, D., Allen, K. N. and Fisher, S. Z., *Neutron diffraction studies towards deciphering the protonation state of catalytic residues in the bacterial KDN9P phosphatase.* Acta Crystallographica Section F: Structural Biology and Crystallization Communications, 2013. **69**(9): p. 1015-1019.

162. Ostermann, A. and Schrader, T, *BIODIFF- diffractometer for large unit cells*. Experimental facilities; Heinz Maier-Leibnitz Zentrum, ed. R. Bruchhaus, Carsughi, F., Hesse, C., Link, P., Lommatzsch, I., Neuhaus, J., Voit, A. 2013, Garching, Germany: Forschungs-Neutronenquelle Heinz Maier-Leibnitz (FRM II).

163. Ostermann, A. and Schrader, T. E., *BioDiff: The new diffractometer for crystals with large unit cells*, in *MLZ report 2011-2013*, R. Bucher, Lommatzsch, I., Editor. 2014: Garching, Germany.

164. Sonnenberger, S., Eichner, A., Hauß, T., Schroeter, A., Neubert, R. H. H. and Dobner, B., *Synthesis of specifically deuterated ceramide [AP]-C18 and its biophysical characterization using neutron diffraction.* Chemistry and Physics of Lipids, 2017. **204**: p. 15-24.

165. Eichner, A., Sonnenberger, S., Dobner, B., Hauß, T., Schroeter, A. and Neubert, R. H. H., *Localization of methyl-branched ceramide [EOS] species within the long-periodicity phase in stratum corneum lipid model membranes: a neutron diffraction study.* Biochimica et Biophysica Acta- Biomembranes, 2016. **1858**(11): p. 2911-2922.

166. Eichner, A., Stahlberg, S., Sonnenberger, S., Lange, S., Dobner, B., Ostermann, A., Schrader, T. E., Hauß, T., Schroeter, A., Huster, D. and Neubert, R. H. H., *Influence of the penetration enhancer isopropyl myristate on stratum corneum lipid model membranes revealed by neutron diffraction and ^{2}H NMR experiments.* Biochimica et Biophysica Acta- Biomembranes, 2017. **1859**(5): p. 745-755.

167. Ryabova, N. Yu., Kiselev, M. A. and Balagurov, A. M., *Transition processes in stratum corneum model lipid membranes with a mixture of free fatty acids.* Biofizika, 2009. **54**(5): p. 852-862.

168. Ryabova, N. Yu., Kiselev, M. A., Dante, S., Hauß, T. and Balagurov, A. M., *Investigation of stratum corneum lipid model membranes with free fatty acid composition by neutron diffraction.* European Biophysics Journal, 2010. **39**: p. 1167-1176.

169. Wertz, P. W., *Integral lipids of hair and stratum corneum.* EXS, 1997. **78**(Formation and Structure of Human Hair): p. 277-237.

170. Rerek, M. E., Chen, H., Markovic, B., van Wyck, D., Garidel, P., Mendelsohn, R. and Morre, D. J., *Phytosphingosine and Sphingosine Ceramide Headgroup Hydrogen Bonding: Structural Insights trough thermotropic Hydrogen/Deuterium Exchange.* The Journal of Physical Chemics B, 2001. **105**: p. 9355-9362.

171. Pham, Q. D., Björklund, S., Engblom, J., Topgaard, D. and Sparr, E., *Chemical penetration enhancers in stratum corneum- Relation between molecular effects and barrier function.* Journal of Controlled Release, 2016. **232**: p. 175-187.

172. Bouwstra, J. A., Gooris, G. S., Salomons-De Vries, M. A., van der Spek, J. A. and Bras, W., *Structure of human stratum corneum as a function of temperature and hydration: A wide-angle x-ray diffraction study.* International Journal of Pharmaceutics, 1992. **84**(3): p. 205-2016.

173. Bouwstra, J. A., Gooris, G. S., Weerheim, A., Kempenaar, J and Ponec, M., *Characterization of stratum corneum structure in reconstructed epidermis by X-ray diffraction.* Journal of Lipid Research, 1995. **36**(3): p. 496-504.

174. Sonnenberger, S., Eichner, A., Schmitt, T., Hauß, T., Lange, S., Langner, A., Neubert, R. and Dobner, B., *Synthesis of specific deuterated derivatives of the long chained stratum corneum lipids EOS and EOP and characterization using neutron scattering.* Journal of Labelled Compounds and Radiopharmaceuticals, 2017. **60**(7): p. 316-330.

LIST OF SUBSTANCES

Lipids

The lipids, which were used for the investigation of the applied SC lipid model membranes are listed below (see Tbl. (a)). DL-CER[AP]-C18 ((N-(a-hydroxyoctadecanoyl)-phytosphingosine)) was generously provided by Evonik Industries AG (Essen, Germany). Cholesterol and cholesterol sulfate, stearic acid, behenic acid and the non-deuterated IPM were acquired from Sigma Aldrich GmbH (Steinheim, Germany) and used as received. DL-CER[AP]-C18-d_3, CER[EOS]-C30-C16-d_3 and IPM-d_3 were received by chemical synthesis [132, 174]. In a comparable way, the artificial CER[EOS]-C30-C16-br synthesis was specified in former works, where the product was characterized and analyzed by DSC and ^{1}H-NMR studies to underline the comparability to the native CER[EOS]-C30-C18:2 [38].

The identity of the applied CERs and IPM-d_3 was indicated i.a. by high resolution mass spectrometry. CER[AP]-C18: 599.550 g/mol; CER[AP]-C18-d_3: 602.571 g/mol; CER[EOS]-C30-C16-br: 1001.971 g/mol, CER[EOS]-C30-C16-d_3: 1005.710 g/mol; IPM-d_3: 273.475 g/mol.

Lipid compound	formula
DL-CER[AP]-C18	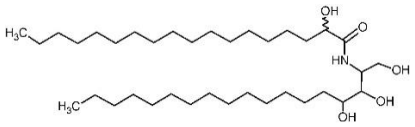
DL-CER[AP]-C18-*d*$_3$	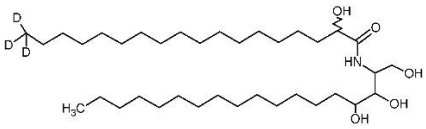
CER[EOS]-C30-C16-br	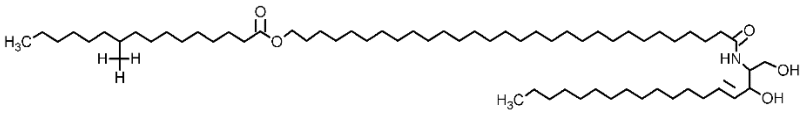
CER[EOS]-C30-C16-*d*$_3$	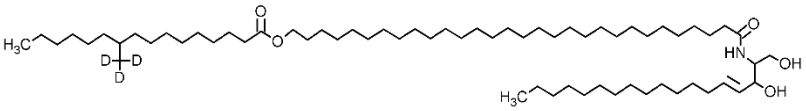
Cholesterol	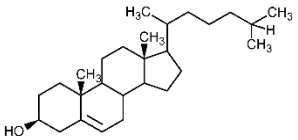
Cholesterol sulfate, Natrium salt	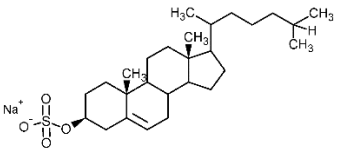
Stearic acid	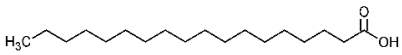
Behenic acid	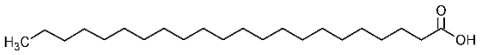
Isopropyl myristate	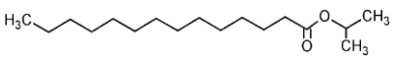
Isopropyl myristate-*d*$_3$	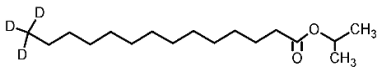

Tbl. (a): List of all applied lipid compounds and their formulas

Other chemicals

For the preparation of the SC lipid model membranes, chloroform and methanol were used for solving the lipids. Both were bought from Merck (Darmstadt, Germany) in GC-grade. During the experiments, saturated salt solutions were used to achieve a constant atmosphere around the samples. Therefore K_2SO_4 and NaBr, both received from Sigma-Aldrich (Steinheim, Germany), were applied to create the relative humidities of 98% or 57%. The salts were dissolved in D_2O (Sigma-Aldrich, Steinheim, Germany), which was used simultaneously to realize the contrast variation.

MATERIALS

For the neutron diffraction experiments quartz slides with dimensions of 65 x 25 x 0.3 mm were optimal sample wafers due to their invisibility for neutrons. They were purchased from Saint-Gobain (Wiesbaden, Germany) as polished Spectrosil 2000. For the deposition of the lipid mixtures containing CER[EOS]-br on the quartz surface, a Hamilton syringe model 1001 RN SYR with a total volume of 1000 µL was used. For the preparation of the CER[AP] system an airbrush instrument (Harder & Steenbeck, Norderstedt, Germany) was used. Furthermore a heating plate was necessary for the solvent evaporation during the sample preparation. For the annealing procedure an oven from Memmert GmbH & Co. KG (Schwabach, Germany) Type UM 500 (No. B598.0392) was chosen to achieve the desired temperatures.

APPLIED SC LIPID MODEL MEMBRANES

The applied SC lipid model membrane compositions were listed below.

1. CER[AP]

For the final characterization of the quaternary CER[AP] system, the following table includes the applied sample composition. The samples facilitated the determination of CER[AP]-C18-d_3 within the bilayer structure and confirmed earlier ideas of the CER position within the applied quaternary lipid mixture [39].

SC lipid model membrane system	Designation	Ratio wt%
I CER[AP]-C18/CHOL/SA/Chs	sample_AP	55/25/15/5
II CER[AP]-C18-d_3 /CHOL/SA/Chs	sample_AP-d_3	55/25/15/5

Tbl. (b): Compositions of sample_AP and sample_AP-d_3

2. CER[AP]_CEREOS]-br

The here presented SC lipid composition was comparable to the lipid mixture, which was applied in an earlier performed neutron diffraction experiment [38]. Here, the deuterated CER[EOS]-br variation was used, which enabled its determination in the long unit cell structure.

SC lipid membrane model system	Designation	Ratio wt%
I CER[AP]/CER[EOS]-br/CHOL/BA	AP_EOS-br	10/23/33/33
II CER[AP]/CER[EOS]-d_3/CHOL/BA	AP_EOS-d_3	10/23/33/33
III CER[AP]-d_3 /CER[EOS]z-br/CHOL/BA	AP-d_3 _EOS-br	10/23/33/33

Tbl. (c): Compositions of samples AP_EOS-br, AP_EOS-d_3, and AP-d_3_EOS-br

3. CER[AP]_CER[EOS]-br + 10% (w/w) IPM

The most complex SC lipid mixtures, which were applied within this thesis, are given in detail below. They contribute to the debate about the appearance and stability of the LPP.

SC lipid membrane model system	Designation	Ratio wt%
I CER[AP]/CER[EOS]-br/CHOL/BA+ 10% IPM	AP_EOS-br_IPM	10/23/33/33
II CER[AP]/CER[EOS]-br/CHOL/BA+ 10% IPM-d_3	AP_EOS-br_IPM-d_3	10/23/33/33
III CER[AP]/CER[EOS] -d_3 /CHOL/BA+ 10% IPM	AP_EOS-d_3 _IPM	10/23/33/33
IV CER[AP] -d_3 /CER[EOS]-br/CHOL/BA+ 10% IPM-d_3	AP-d_3 _EOS-d_3_IPM-d_3	10/23/33/33

Tbl. (d): Compositions of samples AP_EOS-br_IPM, AP_EOS-br_IPM-d_3, AP_EOS-d_3, and AP-d_3_EOS-br_IPM-d_3

SUPPLEMENTARY DATA

Synthesis of specifically deuterated ceramide [AP]-C18 and its biophysical characterization using neutron diffraction

The presented supplementing data were adapted from the appendix of the corresponding scientific publication.

Buffer treatment

A carbonate buffer (pH 9.7) was placed on the annealed samples for 30 min at room temperature and removed before a final annealing cycle at 65 °C under a water saturated atmosphere started. Due to this procedure, the increasing peak intensity is clearly visible next to a rising signal-to-noise ratio. Furthermore, the peak corresponding to crystalline CHOL (7.7 °2 θ) nearly disappeared afterwards, meaning an incorporation of CHOL in the lamellar lipid membranes.

(A) **(B)**

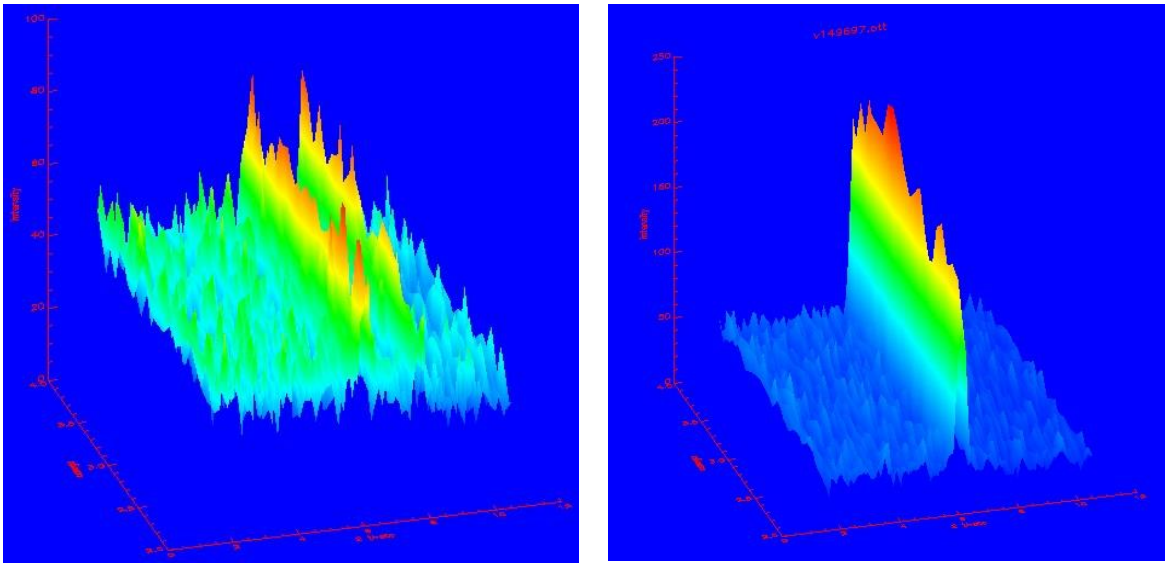

Fig. (a): Rocking scans of 1st order peak of sample_AP-d_3 before (A) and after (B) the buffer treatment.

Structure factors of the samples

	sample_AP		sample_AP-d_3	
Diffraction order h	***Q*, Å^{-1}**	**SF ± error**	***Q*, Å^{-1}**	**SF ± error**
1	0.144	-1.5814 ± 0.0016	0.145	-0.6505 ± 0.0023
2	0.288	0.4816 ± 0.0018	0.292	0.5125 ± 0.0029
3	0.431	-0.5088 ± 0.0020	0.437	-0.2111 ± 0.0030
4	0.574	0.1612 ± 0.0040	0.582	0.3329 ± 0.0039
5	0.717	-0.2278 ± 0.0037	0.722	-0.0894 ± 0.0018

Tbl. (e): Structure factors (SF) and phase signs, for the sample_AP and sample_AP-d_3 received at 8 % D_2O, 57% RH and 32 °C

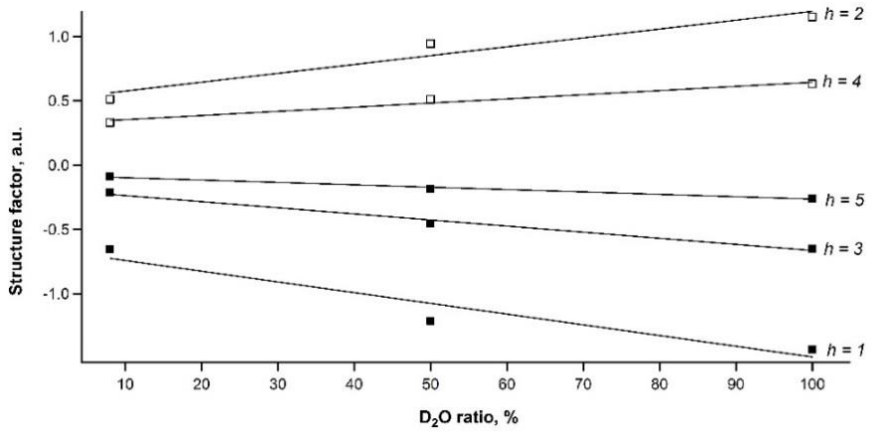

Fig. (b): Correlation between the calculated SFs of sample_AP-d_3 and the corresponding D_2O contrast, received at 57% RH and 32 °C. At least, five diffraction orders were received, which are nearly linear, plotted against the D_2O ratios.

Calculation of x_{HH}

For the calculation of x_{HH} a linear fit of the gain of the water distribution function was performed. For the linear fit following values were received: $y = a + bx$, a = -0.404 ± 0.006, b = 0.024812 ± 0.000312 was received. Assuming $y = 0$ and $x = x_{HH}$, for x_{HH} a value of (16.28 ± 0.03) Å was calculated.

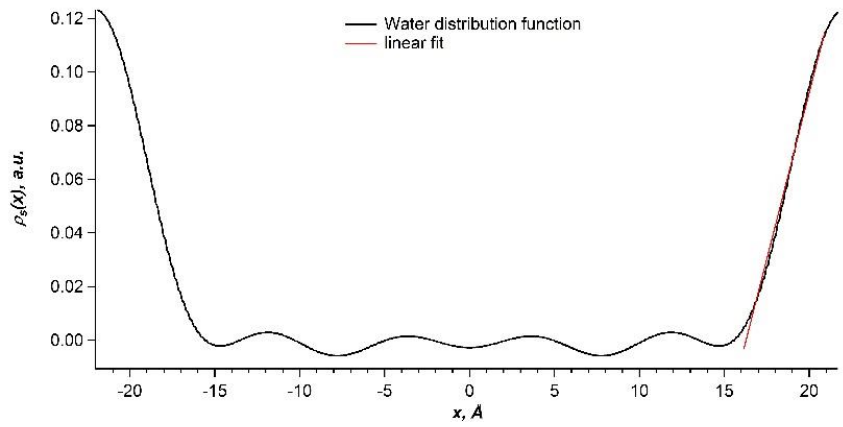

Fig. (c): Linear fit of the water distribution function´s gain.

Localization of methyl-branched ceramide [EOS] species within the long-periodicity phase in stratum corneum lipid model membranes: A neutron diffraction study

The presented supplementing data are complementary to the corresponding scientific publication.

Influence of humidity to both SPPs

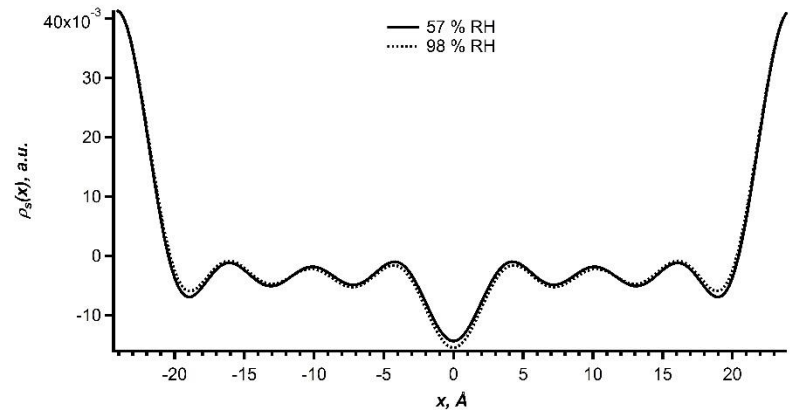

Fig. (d): Influence of humidity on 48 Å SPP of sample I, AP_EOS-br, received at 8% D2O and 32 °C during the second experiment. The curves of the NSLD profiles are very congruently.

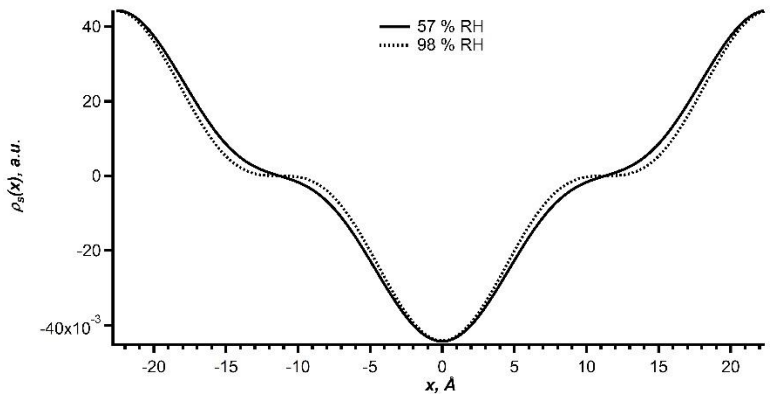

Fig. (e): Influence of humidity on 45 Å SPP of sample I, AP_EOS-br, received at 8% D2O and 32 °C during the second experiment. The curves of the NSLD profiles are very congruently.

Influence of time to both SPPs

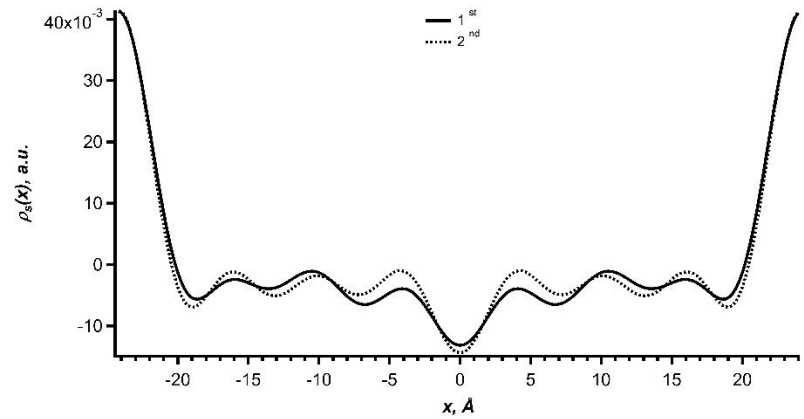

Fig. (f): Influence of time on 48 Å SPP of sample I, AP_EOS-br, received at 8% D2O, 57% RH and 32 °C. The d spacing was similar, while the intensity of the NSLD profile during the 2nd measurement was differing especially in the unit cell center with no further meaning to the stability of the SPP.

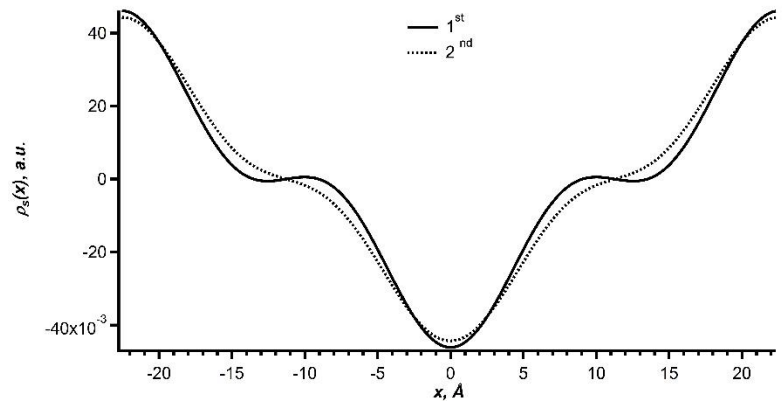

Fig. (g): Influence of time on 45 Å SPP of sample I, AP_EOS-br, received at 8% D2O, 57% RH and 32 °C. The curves of the NSLD profiles are very similar.

Influence of the penetration enhancer isopropyl myristate on stratum corneum lipid model membranes revealed by neutron diffraction and ^{2}H NMR experiments

The presented supplementing data were adapted from the appendix of the corresponding scientific publication.

Structure factors (SF, F_h) of sample I

The phase assignment of the various orders was performed by contrast matching, meaning that all samples were measured at least at three different D_2O/H_2O ratios. Table (f) presents the absolute values of F_h of all registered lamellar orders (L, *h*) and corresponding errors of the protonated control sample I at all D_2O contrasts.

Contrast	L1	L2	L3	L4	L5
8 %	-42.3728 ± 1.1822	28.8535 ± 1.3907	-34.5246 ± 1.5398	17.1992 ± 1.8274	-23.4822 ± 2.1885
50 %	-45.2581 ± 1.5772	32.8742 ± 1.4136	-36.8490 ± 1.4832	21.4707 ± 2.1417	-30.9876 ± 2.3706
100 %	-55.5356 ± 1.7049	41.1337 ± 1.1168	-47.2109 ± 1.8578	32.5949 ± 1.5597	-38.3378 ± 2.3559

Tbl. (f): Structure factors of all registered lamellar orders (L, h) and corresponding errors of the protonated control sample I at all D_2O contrasts

It is assumed, that the water layer between the lipid bilayer approximates a Gaussian distribution. With the center of the Gaussian at $x = \pm\frac{d}{2}$, its structure factors have alternating signs. The even order of the structure factors increases in amplitude with increasing D_2O ratio, whereas the odd orders decreases according to the relation $F = F_m \pm x * F_w$ with F_m structure factor of the membrane, F_w structure factor of the water layer, x is the D_2O/H_2O ratio in mol %. When plotting the measured structure factors against x, the slope should be positive (+) for even orders and negative (-) for odd orders (see Fig. h).

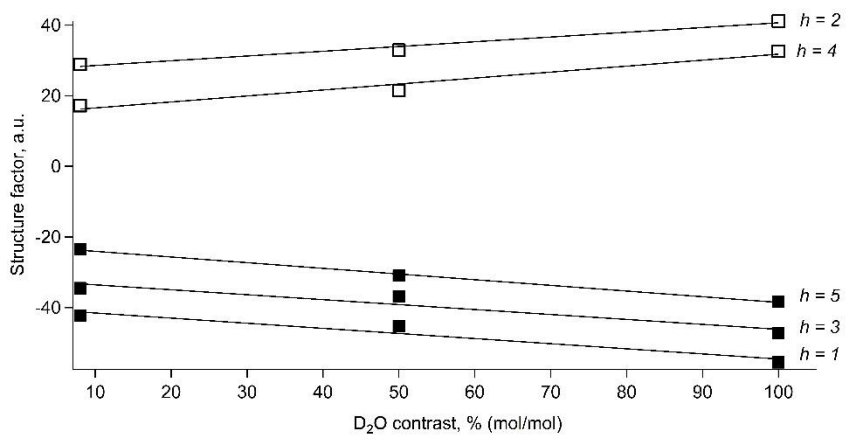

Fig. (h): Correlation between structure factors and D_2O contrast. The lamellar orders are marked with *h*. The odd-numbered orders have a negative slope, due to their phase signs.

From that, we can conclude, that the phase signs are - + - + - for the first to the fifth order. The determined phase signs were used as received.

Scaling of NSLD profiles

For the contrast variation experiments, the NSLD profiles were determined on an arbitrary scale with $a = \sum F$ and $b = 1$. This is justified by the fact that the contrast variation was done on one sample with no variation in sample mass or geometry. To determine the difference between the NSLD profiles of two different samples, the factor b was scaled to the sum of the experimental structure factors $b = \frac{1}{\sum F}$ and $a = \frac{1}{d}$.

Calculation of x_{HH}

For the calculation of the hydrophilic- hydrophobic boundary x_{HH} a linear fit of the gain of the water distribution function was performed. For the fit ($y = a + bx$) the following parameters were received: a = -19.226 ± 0.193, b = 0.9702 ± 0.0092. Assuming $y = 0$ and $x = x_{\mathrm{HH}}$, for x_{HH} a value of (19.8 ± 0.3) Å was calculated.

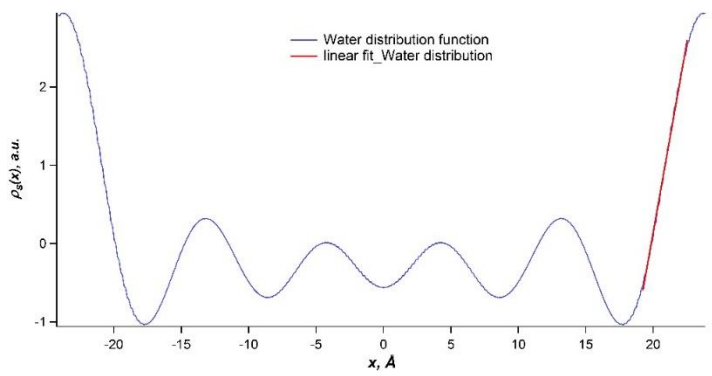

Fig. (i): Linear fit of the positive gain of the water distribution function

Absence of IPM-d_3 in SPP

For the localization of the penetration enhancer, sample II contained the d_3-labeled IPM. The presence of IPM-d_3 was tested in sample IV as well, where additionally CER[AP]-d_3 was incorporated. Fig. (j) and Fig. (k) include the corresponding NSLD profiles next to the deuterium differences. The deuterium difference curve of single IPM-d_3 in Fig. (j) indicates two maxima at ± 18 Å and a small peak at the membrane center. Based on the minimal central peak in negative dimensions for the NSLD, no position for a deuteration is localizable. More interesting are the maxima of the difference curve at ± 18 Å. Here, deuterium labels could be present but they were located at the changeover from the polar to the non-polar area of the bilayer. So they represent results from truncation errors, which was reviewed in Fig. (k). There, next to a significant central peak (corresponding to CER[AP]-C18-d_3), only very small and broad signals were found around ± 18 Å. Together with the reasonable suspicion of truncation errors in Fig. (j), the very parallel progress of both NSLD profiles at the slopes in Fig. (k) and the corresponding overlapping confidence levels around ± 18 Å allowed the conclusion that IPM-d_3 is absent in the investigated SC lipid model membranes.

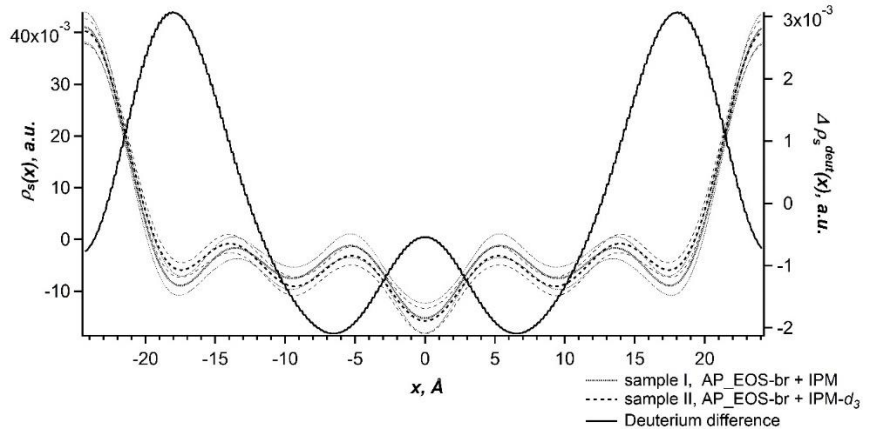

Fig. (j): The NSLD profiles of sample I (grey line) and II (dotted line), received at 8 % D_2O, 98% RH and 32 °C. Their difference is plotted (black line, axis on the right) next to their confidence levels (thin lines).

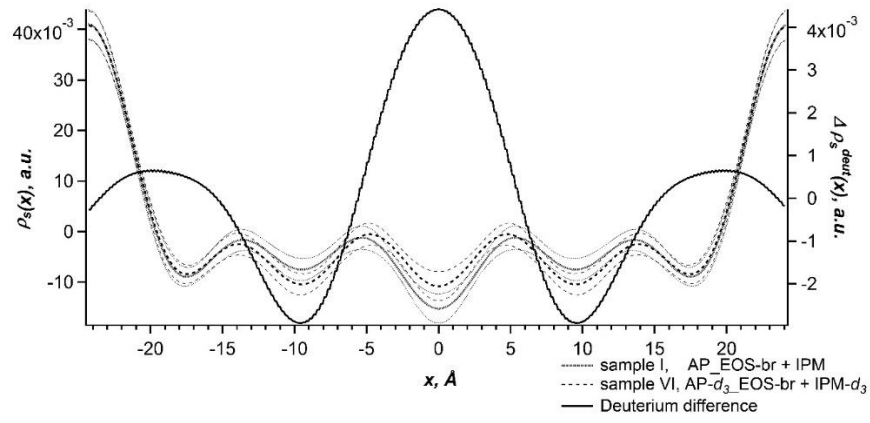

Fig. (k): The NSLD profiles of sample I (grey line) and IV (dotted line), received at 8 % D_2O, 98% RH and 32 °C. Their difference is plotted (black line, axis on the right) next to their confidence levels (thin lines). The significant maximum in the middle indicates the presence of the d_3-segment of CER[AP]-C18.

PUBLICATIONS

Research articles

Eichner, Adina; Sonnenberger, Stefan; Dobner, Bodo; Hauß, Thomas; Schroeter, Annett, Neubert, Reinhard H.H.: *Localization of methyl-branched ceramide [EOS] species within the long-periodicity phase in stratum corneum lipid model membranes: A neutron diffraction study*, Biochimica et Biophysica Acta- Biomembranes 1858 (2016) 2911–2922

Eichner, Adina; Stahlberg, Sören; Sonnenberger, Stefan; Lange, Stefan; Dobner, Bodo; Ostermann, Andreas; Schrader, Tobias E.; Hauß, Thomas; Schroeter, Annett; Huster, Daniel; Neubert, Reinhard H. H.: *Influence of the penetration enhancer isopropyl myristate on stratum corneum lipid model membranes revealed by neutron diffraction and ^{2}H NMR experiments*, Biochimica et Biophysica Acta- Biomembranes 1859 (2017) 745-755

Sonnenberger, Stefan; Eichner, Adina; Hauß, Thomas; Schroeter, Annett; Neubert, Reinhard H. H.; Dobner, Bodo: *Synthesis of specifically deuterated ceramide [AP]-C18 and its biophysical characterization using neutron diffraction*, Chemistry and Physics of Lipids 204 (2017) 15-24

Stahlberg, Sören; Eichner, Adina; Sonnenberger; Stefan; Kovacik, Andrej; Lange, Stefan; Schmitt, Thomas; Demé Bruno; Hauss, Thomas; Dobner, Bodo; Neubert, Reinhard H.H.; Huster, Daniel: The influence of a novel dimeric ceramide molecules on the nanostructure and the thermotropic phase behavior of a stratum corneum model mixture, Langmuir (just accepted manuscript, 18th of August 2017), DOI: 10.1021/acs.langmuir.7b01227

Sonnenberger, Stefan; Eichner, Adina; Schmitt, Thomas; Hauß, Thomas; Lange, Stefan; Langner, Andreas; Neubert, Reinhard H. H.; Dobner, Bodo: Synthesis of specific deuterated derivatives of the long chained stratum corneum lipids EOS and EOP and characterization using neutron scattering, Journal of Labelled Compounds and Radiopharmaceuticals 60 (2017) 316-330

Schroeter, Annett; Stahlberg, Sören; Školová, Barbora; Sonnenberger, Stefan, Eichner, Adina; Huster, Daniel; Vávrová, Kateřina; Hauß, Thomas; Dobner, Bodo; Neubert, Reinhard H.H.; Vogel, Alexander, *Phase separation in ceramide[NP] containing lipid model membranes: Neutron diffraction and solid-state NMR,* Soft Matter 13 (2017) 2107-2119

Review articles

Engelke, Verena; Rocher, Adina; Imming, Peter, *Paradoxon Kohlenmonoxid*, Pharmazeutische Zeitung, 2010; 33; 3020-3026

Schroeter, Annett; Eichner, Adina; Mueller, Josefin; Neubert, Reinhard H. H., *The Importance of Stratum Corneum Lipid Organization for Proper Barrier Function*, Percutaneous Penetration Enhancers- Chemical Methods in Penetration Enhancement, Drug Manipulation Strategies and Vehicle Effects, Springer-Verlag Berlin Heidelberg 2015, p. 19-38

Schroeter, Annett; Eichner, Adina; Mueller, Josefin; Neubert, Reinhard H. H., *Penetration Enhancers and their Mechanism studied on a Molecular Level*, Percutaneous Penetration Enhancers- Chemical Methods in Penetration Enhancement, Modification of the Stratum Corneum, Springer-Verlag Berlin Heidelberg 2015, p. 29-37

Poster presentations

Bogan, Reinhard; Eichner, Adina; Zimmermann, Thomas; Plößl, Florian; Klaubert, Bernd, *Stability testing of Paromomycin in aqueous* solution, DPhG Annual Meeting, Drug Discovery inspired by Nature, University of Freiburg, Freiburg, Germany, 2013

Eichner, Adina; Hauß, Thomas; Neubert, Reinhard H. H.; Schroeter, Annett, *Influence of the long-chain ω-acyl Ceramide [EOS] on the structure of Stratum corneum lipid membrane models*, Neutrons in Biology and Biotechnology, Institute Laue-Langevin, Grenoble, France, 2014

Eichner, Adina; Sonnenberger, Stefan; Dobner, Bodo; Ostermann, Andreas; Schrader, Tobias, E.; Hauß, Thomas; Neubert, Reinhard H. H.; Schroeter, Annett, *Presentation of a new application for biological investigations: Introducing BIODIFF for Stratum corneum structure determination*, Trends in Neutron Science –MLZ User Meeting, Ismaning, Germany, 2015

Eichner, Adina; Sonnenberger, Stefan; Dobner, Bodo; Ostermann, Andreas; Schrader, Tobias, E.; Hauß, Thomas; Neubert, Reinhard H. H.; Schroeter, Annett, *Presentation of a new application for biological investigations: Introducing BIODIFF for Stratum corneum structure determination*, Gordon Research Conference- Barrier Function of mammalian skin, Waterville Valley, NH, USA, 2015

Oral presentations

Bedeutung der langkettigen ω-acyl-Ceramide EOS und EOP in Anwesenheit der kurzkettigen Ceramide AP und AS, Opening event for recent project of Deutsche Forschungsgemeinschaft (DFG), Martin Luther University Halle-Wittenberg, Halle, Germany, 2013

Impact of Ceramide [EOS] on the lipid membrane organization of the Stratum corneum – A neutron diffraction study, 5th Joint BER II and Bessy II User Meeting, Helmholtz-Zentrum für Materialien und Energie, Berlin, Germany, 2013

Der Einfluss des Enhancers IPM auf die Struktur von SC Modellmembranen, untersucht am BIODIFF, DFG-Meeting, GOLM, Potsdam, Deutschland, 2015

New Insights into the Structure-Function Relationship of Long-Chain Omega-Acyl Ceramides to the Nanostructure of Stratum Corneum Lipid Model Membranes, Gordon Research Conference- Barrier Function of mammalian skin, Waterville Valley, NH, USA, 2015

Reports

Helmholtz-Zentrum für Materialien und Energie Berlin (HZB), Berlin, Germany

Eichner, Adina; Mueller, Josefin; Schroeter, Annett; Hauß, Thomas; Neubert, Reinhard, *Impact of specifically deuterated long-chain- ω-acyl ceramide CER[EOS] to the nanostructure of stratum corneum model membranes*, 2013

Eichner, Adina; Hauß, Thomas; Neubert, Reinhard
Impact of the long chain omega-acyl ceramide [EOS] to the thermotropic phase behavior and nanostructure of Stratum corneum lipid matrices, 2015

Heinz Maier-Leibnitz Zentrum (MLZ), Garching, Germany

Eichner, Adina; Schroeter, Annett; Ostermann, Andreas; Schrader, Tobias E.; Neubert, Reinhard, *Impact of lipophilic penetration accelerator on deuterated ω-acyl ceramide [EOS]-based Stratum corneum lipid model membranes*, 2015

Eichner, Adina; Ostermann, Andreas; Schrader, Tobias E.; Neubert, Reinhard,
Insights into the phase behaviour of Stratum corneum lipid model membranes based on specific deuterated long-chain ω-acyl ceramide [EOP, 2015

Institut Laue-Langevin (ILL), Grenoble, France

Eichner, Adina; Schroeter, Annett; Demé, Bruno.; Neubert, Reinhard,
Studying the localization of long-chain ω-acyl ceramide [EOS] in Stratum corneum lipid model membranes and its temperature depending phase behavior using specifically deuterated lipids, 2015

ACKNOWLEDGEMENTS

First of all I want to express my gratitude to Prof. Dr. Dr. h.c. Reinhard H. H. Neubert for his stunning support during the time in his group. Especially his continuous readiness to discuss the results and the permanent input of ideas were impressive and very helpful for finishing this thesis.

Furthermore, my thanks are addressed to Dr. Annett Schroeter, who was supervising this project directly. Due to her immense experiences in the world of SC lipid investigations using neutron diffraction it was possible for me to benefit from that in every sense.

My dear Dr. Thomas Hauß, without all of your knowledge about neutron scattering and the belonging theoretical and practical background, this project would not be finished yet. Thanks a lot for all your ideas and their implementation, your skills in computer sciences and your omnipresent attendance during this work.

Additionally my thanks are addressed to Prof. Dr. Bodo Dobner and Stefan Sonnenberger, who gave an immense benefit to this unique project due to the chemical synthesis of the specifically deuterated lipids, applied within this thesis.

Moreover, I would like to thank Prof. Dr. Daniel Huster, Dr. Alexander Vogel and Sören Stahlberg for the intensive collaboration regarding the ^{2}H NMR studies, which complemented the given results fruitfully.

Dr. Andreas Ostermann and Dr. Tobias E. Schrader are the best local contacts, BIODIFF could ever have. Due to their high technical knowledge and stunning support, it was possible to introduce the neutron diffraction instrument for the investigation of SC lipid model membranes for the first time. It was always great to spend time with you in Garching! And I have to express my gratitude to Harald, who was indispensable for the installation of the new sample environment.

Further thanks are addressed to Dr. Christoph Wagner for the possibility to perform X-ray scattering measurements for sample testing and the enjoyable cooperation. Not at last, your recommendation of Djerassi´s `Cantor`s Dilemma` supported this work remarkable.

My acknowledgements are also targeted to Evonik Industries AG for the resourcing of the protonated ceramides.

Special thanks are addressed to Prof. Dr. Joke A. Bouwstra and Gert Gooris for their willingness concerning the discussion of the presented LPP results. Our talks and the lab collaboration were of high benefit for this thesis. Gert: Thank you so much for opening my daily horizon!

Especially, I have to be ungrudging to the biopharmaceutical group of Prof. Neubert for all the support and in detail to Mrs. Elfi Sommer, Dr. Sandy Naumann and Ms. Sophie Steinbach for being mainly friends but critical colleagues at once. It was always great to spend time with you working, laughing, go in for running and having some wine afterwards.

My dear Josi: Thank you so much for being a friend and a wonderful partner in the hard field of ceramides and neutron sciences. Over the last years, our talks and mutual support during the hard days and nights of beamtime made this thesis to something special. I will never forget the time we spent together all over the world.

And finally I would like to thank my family, all my friends, and my cloverleaf for their amazing backing. In particular, I´m very grateful for my lovely husband for his stunning support and appreciation for all of my physical and psychological time of absence during the last years. You are my light in the darkness.

CURRICULUM VITAE

Der Lebenslauf wurde aus datenschutzrechtlichen Gründen entfernt.

EIDESTATTLICHE ERKLÄRUNG

Hiermit erkläre ich gemäß § 5 Absatz 2b der Promotionsordnung der Naturwissenschaftlichen Fakultät I (Biowissenschaften) der Martin-Luther-Universität Halle-Wittenberg, dass ich die Ergebnisse der vorliegenden Dissertationsarbeit

New insights into the nanoscaled structure of stratum corneum model membranes applying specifically deuterated lipids in neutron diffraction studies

am Institut für Pharmazeutische Technologie und Biopharmazie der Martin-Luther-Universität Halle-Wittenberg selbständig und ohne fremde Hilfe erarbeitet und verfasst habe. Ferner habe ich nur die in der Dissertation angegebenen Literaturstellen und Hilfsmittel verwendet und die entnommenen und benutzten Literaturstellen auch als solche kenntlich gemacht. Weiterhin habe ich die vorliegende Arbeit bisher keiner anderen Prüfungsbehörde vorgelegt.

Halle (Saale), im August 2017 Adina Eichner